LUNAR THERMAL MEASUREMENTS IN CONJUNCTION WITH PROJECT APOLLO

by

Sydney P. Clark, Jr.

Final Report

September 1973

Grant No. NGR-07-004-039

Yale University

New Haven, Connecticut 06520

NATIONAL AERONAUTICS AND SPACE ADMINISTRATION

This grant funded feasibility studies and development work on the lunar heat flow experiment (HFE). The first task was performed under a previous grant (NSG-400), and it consisted, among other things, of the investigation of a novel method of measuring heat flow which has the advantage of not requiring a drilled hole. The method was found not to be feasible, however, and the requirement that a drill be developed for lunar use was established. These early results are incorporated in Appendix I for convenience.

Once the necessity of drilling a hole in the moon became clear, it became desirable to develop an in situ method of measuring lunar thermal conductivity. The alternative, to measure conductivity on a returned core, suffers from the disadvantages that the volume available for investigation is much smaller than that sampled by the in situ method and the physical properties of the lunar material may be permanently altered by the coring operation. The temperature field surrounding a heater with the geometry of a cylinder of finite length was therefore investigated. The results were presented in an interim report dated January, 1967 (Appendix II). The calculations reported there formed the basis of the design of the downhole part of the HFE, which was developed and fabricated by A. D. Little, Inc.

During the final six years of the grant's duration the main activity was travel and consultation with colleagues associated with planning and fabricating the HFE. Places most frequently visited were Lamont-Doherty Geological Observatory and A. D. Little, Inc.

Probably the best measure of the success of a research program is its results. Four HFE's have been flown and two of these are in place on the

moon and returning data of high quality. They have achieved and even surpassed their design objectives, and they have proven themselves to be rugged, reliable instruments. They are described in the Apollo 15 and Apollo 17 Preliminary Science Reports, attached as Appendix III. The two instruments that failed to return data were victimized by circumstances that were unrelated to the HFE itself. One was lost as a consequence of the abort of the Apollo 13 landing. On the Apollo 16 mission, the HFE was successfully emplaced, but it was silenced when an astronaut inadvertently tripped and broke the cable connecting it to ALSEP.

APPENDIX I

Some Early Feasibility Studies

*N66-15434

SOME CALCULATIONS PERTAINING TO THE FEASIBILITY OF MEASURING LUNAR HEAT FLOW

by Sydney P. Clark, Jr.

Final Report*

September 1965

Prepared under Contract No. NsG-400*

Yale University

New Haven, Connecticut

NATIONAL AERONAUTICS AND SPACE ADMINISTRATION

Contents

Illustrations

ABSTRACT

A number of problems related to the feasibility of measuring lunar heat flow at the lunar surface or in a shallow hole have been investigated with the following results. Study of the steady periodic temperatures in the lunar material will give unambiguous information about its properties only if the surface material alone has an appreciable effect on the amplitude and phase of the thermal wave. Layering tends to reduce the amplitude of the fluctuation at a given depth. High-amplitude fluctuations near a place where the poorly conducting surface layer is missing do not penetrate far and pose no difficulty. Large perturbations of heat flow may be caused by irregularities in thickness of the surface layer, and a number of closely spaced measurements at a given landing site will be required to minimize this source of error. The "blanket" method of measuring lunar heat flow is not considered feasible because of the necessity of very closely matching the local albedo with the blanket, and because a blanket with properties such that an easily measured gradient free from periodic fluctuations can be set up by the lunar flux requires a prohibitively long time to come to thermal equilibrium. Conversely a blanket with a suitable time constant will yield only a small, seriously disturbed gradient that will be difficult to measure.

1. INTRODUCTION

A measurement of lunar heat flow will be interesting for a number of scientific reasons. Heat flow gives more direct evidence about the internal thermal regime of a planet than any other measurement that can be made at the surface. Limits to the total amount of radioactive elements in the planet's interior can be set, as well as limits to its initial temperature. In the case of the moon, a determination of heat flow will help to decide just how "dead" it is, since the source of volcanism and mountain building must ultimately be thermal energy, most of which is leaked to the surface to appear as heat flow. The small size of the moon makes it especially interesting from the thermal point of view. Cooling from the surface has affected some 70% of the volume of the moon compared with about 20% of the earth, assuming the two bodies are of the same age. As a consequence the relative importance of initial heat and radiogenic heat may be very different on the moon as compared with the earth, a possibility which makes a comparison of heat flow from the two bodies all the more interesting.

But granting the desirability of a measurement of lunar heat flow, a number of obstacles remain in the way. On the terrestrial land surface heat flow is measured in boreholes, mines or tunnels reaching depths up to several thousand feet. Considerable depths are necessary in order to avoid disturbances which occur near the surface. There is no prospect of drilling a deep hole in the moon in the foreseeable future, and any measurement of heat flow must be made at the surface or in a shallow hole. The temperatures near the lunar surface are in the first place affected by the large monthly variation in surface temperature, and secondly by

thermal refraction due to variability in the thickness of the lunar surface material, which is known to be of very low thermal conductivity compared to solid rock. The goal of the present study is to assess the seriousness of these difficulties.

In the calculations which follow, the assumption that the lunar situation can be adequately represented by a linear model, i.e. a model in which the thermal properties of the lunar material are treated as independent of temperature, is made. This assumption is probably very wrong for materials near the lunar surface under ambient lunar conditions. Temperatures are below the Debye temperatures of common rock-forming minerals, implying a temperature-dependent specific heat. Radiative transfer is presumably an important contributor to the thermal conductivity of the porous surface material, and it is strongly dependent on temperature. Both factors argue for treatment of nonlinear models, but the additional complication is hardly warranted in view of the remaining uncertainties in the details of the properties of the lunar surface material. Thus the present study represents a first approach to the problem, aimed more at recognizing difficulties than at removing them.

Four problems are considered in detail in the following sections. The first is the case of one-dimensional steady periodic heat flow in a stratified medium consisting of two layers of differing thermal properties, resting on a substratum of infinite thickness which has a third set of thermal constants. An exact solution is obtained for the case of semisoidally varying surface temperature.

A second problem again concerns steady periodic temperatures, this time in a two-layered medium with the upper layer absent within a circular

region. Numerical results are obtained for this model of a hole in the moon's poorly conducting surface layer. Perturbations of heat flow due to variable thickness of the surface layer are investigated under steady-state conditions, and finally results are extended to calculations of the disturbances associated with the emplacement of a blanket-type thermal fluxmeter on the lunar surface.

2. STEADY PERIODIC TEMPERATURES IN A 3-LAYERED MEDIUM

A. Theory

Mathematically the problem can be expressed in the following way. The region $0 \leq \underline{x} \leq \underline{X}_1$ contains material with properties $\underline{K}_1$, [illegible] etc. (see table 1 for notation), the region $\underline{X}_1 \leq \underline{x} \leq \underline{X}_3$ contains material with properties $\underline{K}_2$, etc., and the region $\underline{x} \geq \underline{X}_3$ contains material with properties $\underline{K}_3$, etc. At the boundaries $\underline{X}_1$ and $\underline{X}_3$ both temperature and thermal flux $(= K \frac{\partial \underline{T}}{\partial x})$ are continuous, $\underline{T} \to 0$ as $x \to \infty$, and $\underline{T} = \underline{A}_o \sin \omega t$ when $\underline{x} = 0$, where A_o is the constant surface amplitude. Within each region T must satisfy the equation of heat conduction, $\frac{\partial^2 T}{\partial x^2} = \frac{1}{\alpha} \frac{\partial T}{\partial t}$

This problem is most conveniently solved by the Laplace transform method described by Carslaw and Jaeger (1959). Further details about this particular problem are given by Lachenbruch (1959), who obtained the solution for the special case $\underline{x} = \underline{X}_3$. If we write $\overline{\underline{T}}$ for the Laplace transform of $\underline{T}$, and use subscripts to identify the three regions, we have (Lachenbruch, 1959):

$$\overline{\underline{T}}_1 = F\exp(q_1 x) + G\exp(-q_1 x), \tag{1}$$

$$\overline{\underline{T}}_2 = H\exp(q_2 x) + J\exp(-q_2 x), \tag{2}$$

$$\overline{\underline{T}}_3 = R\exp(-q_3 x), \tag{3}$$

where F, G, H, J, and R are constants, independent of $\underline{X}$. The two boundary conditions at each interface, $\underline{x} = \underline{X}_1$ and $\underline{x} = \underline{X}_3$, plus the condition at $\underline{x} = 0$, provide 5 equations which determine the 5 unknown quantities F, G, H, J, and R.

Table 1. Definitions of Symbols

T	Temperature
t	Time
x	Depth variable
X_1	Depth to base of upper layer
X_2	Depth beneath base of upper layer
X_3	Depth to top of substratum, $=X_1 + X_2$
ω	Angular frequency, $= 2.66 \times 10^{-6}$ sec^{-1} for 1 lunar day
K_i	Thermal conductivity of the ith layer
ρ_i	Density of the ith layer
c_i	Heat capacity of the ith layer
α_i	Thermal diffusivity of the ith layer, $= K_i/\rho_i c_i$
β_i	Thermal inertia of the ith layer, $= (K_i \rho_i c_i)^{\frac{1}{2}}$
p	Parameter of the Laplace Transform, $\overline{T} = \int_0^\infty \exp(-pt)T\,dt$
q_i	$(p/\alpha_i)^{\frac{1}{2}}$
Q	Heat flow
L	Thickness of blanket
b	Subscript denoting properties of blanket

We find

$$F = \frac{A_o \omega \exp(-q_3 X_3 - q_1 X_1)}{(p^2+\omega^2)\Delta}[(-\beta_2\beta_3 - \beta_1\beta_3 + \beta_2^2 + \beta_2\beta_1)\exp(-q_2 X_2) + (-\beta_2\beta_3 + \beta_1\beta_3 - \beta_2^2 + \beta_2\beta_1)\exp(q_2 X_2)] \quad (4)$$

$$G = \frac{A_o \omega \exp(q_1 X_1 - q_3 X_3)}{(p^2+\omega^2)\Delta}[(-\beta_2\beta_3 + \beta_1\beta_3 + \beta_2^2 - \beta_1\beta_2)\exp(-q_2 X_2) + (-\beta_2\beta_3 - \beta_1\beta_3 - \beta_2^2 - \beta_1\beta_2)\exp(q_2 X_2)] \quad (5)$$

$$H = \frac{2A_o \omega \exp(-q_2 X_3 - q_3 X_3)}{(p^2+\omega^2)\Delta}(\beta_1\beta_2 - \beta_1\beta_3) \quad (6)$$

$$J = \frac{2A_o \omega \exp(q_2 X_3 - q_3 X_3)}{(p^2+\omega^2)\Delta}(\beta_1\beta_2 + \beta_1\beta_3) \quad (7)$$

$$R = \frac{A_o \omega \exp(-q_1 X_1 - q_2 X_2 + q_3 X_3)}{(p^2+\omega^2)\Delta}(4\beta_1\beta_2), \quad (8)$$

where

$$\Delta = (-\beta_2\beta_3 - \beta_1\beta_3 + \beta_2^2 + \beta_2\beta_1)\exp(-2q_2 X_2 - 2q_1 X_1) + (-\beta_2\beta_3 + \beta_1\beta_3 - \beta_2^2 + \beta_2\beta_1)\exp(-2q_1 X_1) + (\beta_2\beta_3 - \beta_1\beta_3 - \beta_2^2 + \beta_2\beta_1)\exp(-2q_2 X_2) + (\beta_2\beta_3 + \beta_1\beta_3 + \beta_2^2 + \beta_2\beta_1) \quad (9)$$

and $X_2 = X_3 - X_1$.

The transforms of equations (1)-(3) can be inverted by the contour integration method. Lachenbruch (1959) has already shown that the line integrals involved in the inversion contribute only to the initial transient state and have nothing to do with steady periodic temperatures. Hence for present purposes we need consider only the residues at the poles of the transforms. Poles are located at $p = \pm i\omega$, following Lachenbruch, we assume that the quantity Δ (equation 9) has no zeros in the complex plane. It can be shown that the solution given below does indeed satisfy all of the conditions of the problem, which constitutes proof that either Δ has no zeros or that the residues at the resulting poles contribute nothing to the steady periodic part of the solution.

The residues at $p = \pm i\omega$ lead to the following expressions for the temperatures.

$$T_1 = \frac{A_o}{D}\{\exp(-\sqrt{\omega/2\alpha_1}x)\sin(\omega t-\sqrt{\omega/2\alpha_1}x)+$$

$$+ P_2[\exp(-2\sqrt{\omega/2\alpha_1}X_1-2\sqrt{\omega/2\alpha_2}X_2+\sqrt{\omega/2\alpha_1}x)\sin(\omega t-2\sqrt{\omega/2\alpha_1}X_1-2\sqrt{\omega/2\alpha_2}X_2+\sqrt{\omega/2\alpha_1}x)+$$

$$+ \exp(-2\sqrt{\omega/2\alpha_1}X_1-2\sqrt{\omega/2\alpha_2}X_2-\sqrt{\omega/2\alpha_1}x)\sin(\omega t+2\sqrt{\omega/2\alpha_1}X_1+2\sqrt{\omega/2\alpha_2}X_2-\sqrt{\omega/2\alpha_1}x)]+$$

$$+ P_3[\exp(-2\sqrt{\omega/2\alpha_1}X_1+\sqrt{\omega/2\alpha_1}x)\sin(\omega t-2\sqrt{\omega/2\alpha_1}X_1+\sqrt{\omega/2\alpha_1}x)+$$

$$+ \exp(-2\sqrt{\omega/2\alpha_1}X_1-\sqrt{\omega/2\alpha_1}x)\sin(\omega t+2\sqrt{\omega/2\alpha_1}X_1-\sqrt{\omega/2\alpha_1}x)]+$$

$$+ P_4[\exp(-2\sqrt{\omega/2\alpha_2}X_2-\sqrt{\omega/2\alpha_1}x)\sin(\omega t-2\sqrt{\omega/2\alpha_2}X_2-\sqrt{\omega/2\alpha_1}x)+$$

$$+ \exp(-2\sqrt{\omega/2\alpha_2}X_2-\sqrt{\omega/2\alpha_1}x)\sin(\omega t+2\sqrt{\omega/2\alpha_2}X_2-\sqrt{\omega/2\alpha_1}x)]+$$

$$+ P_2P_3[\exp(-4\sqrt{\omega/2\alpha_1}X_1-2\sqrt{\omega/2\alpha_2}X_2+\sqrt{\omega/2\alpha_1}x)\sin(\omega t+2\sqrt{\omega/2\alpha_2}X_2+\sqrt{\omega/2\alpha_1}x)+$$

$$+ \exp(-4\sqrt{\omega/2\alpha_1}X_1-2\sqrt{\omega/2\alpha_2}X_2+\sqrt{\omega/2\alpha_1}x)\sin(\omega t-2\sqrt{\omega/2\alpha_2}X_2+\sqrt{\omega/2\alpha_1}x)]+$$

$$+ P_2P_4[\exp(-2\sqrt{\omega/2\alpha_1}X_1-4\sqrt{\omega/2\alpha_2}X_2+\sqrt{\omega/2\alpha_1}x)\sin(\omega t-2\sqrt{\omega/2\alpha_1}X_1+\sqrt{\omega/2\alpha_1}x)+$$

$$+ \exp(-2\sqrt{\omega/2\alpha_1}X_1-4\sqrt{\omega/2\alpha_2}X_2-\sqrt{\omega/2\alpha_1}x)\sin(\omega t+2\sqrt{\omega/2\alpha_1}X_1-\sqrt{\omega/2\alpha_1}x)]+$$

$$+ P_3P_4[\exp(-2\sqrt{\omega/2\alpha_1}X_1-2\sqrt{\omega/2\alpha_2}X_2+\sqrt{\omega/2\alpha_1}x)\sin(\omega t-2\sqrt{\omega/2\alpha_1}X_1+2\sqrt{\omega/2\alpha_2}X_2+\sqrt{\omega/2\alpha_1}x)+$$

$$+ \exp(-2\sqrt{\omega/2\alpha_1}X_1-2\sqrt{\omega/2\alpha_2}X_2-\sqrt{\omega/2\alpha_1}x)\sin(\omega t+2\sqrt{\omega/2\alpha_1}X_1-2\sqrt{\omega/2\alpha_2}X_2-\sqrt{\omega/2\alpha_1}x)]+$$

$$+ P_2^2[\exp(-4\sqrt{\omega/2\alpha_1}X_1 - 4\sqrt{\omega/2\alpha_2}X_2 + \sqrt{\omega/2\alpha_1}x)\sin(\omega t + \sqrt{\omega/2\alpha_1}x)] +$$

$$+ P_3^2[\exp(-4\sqrt{\omega/2\alpha_1}X_1 + \sqrt{\omega/2\alpha_1}x)\sin(\omega t + \sqrt{\omega/2\alpha_1}x)] +$$

$$+ P_4^2[\exp(-4\sqrt{\omega/2\alpha_2}X_2 - \sqrt{\omega/2\alpha_1}x)\sin(\omega t - \sqrt{\omega/2\alpha_1}x)]\} \quad (10)$$

$$T_2 = \frac{A_o}{D}(P_2+P_4)\exp[-\sqrt{\omega/2\alpha_1}X_1 - \sqrt{\omega/2\alpha_2}(X_2+X_3-x)]\{\sin[\omega t - \sqrt{\omega/2\alpha_1}X_1 - \sqrt{\omega/2\alpha_2}(X_2+X_3-x)] +$$

$$+ P_2\exp[-2\sqrt{\omega/2\alpha_1}X_1 - 2\sqrt{\omega/2\alpha_2}X_2]\sin[\omega t + \sqrt{\omega/2\alpha_1}X_1 - \sqrt{\omega/2\alpha_2}(X_1-x)] +$$

$$+ P_3\exp[-2\sqrt{\omega/2\alpha_1}X_1]\sin[\omega t + \sqrt{\omega/2\alpha_1}X_1 - \sqrt{\omega/2\alpha_2}(X_2+X_3-x)] +$$

$$+ P_4\exp[-2\sqrt{\omega/2\alpha_2}X_2]\sin[\omega t - \sqrt{\omega/2\alpha_1}X_1 - \sqrt{\omega/2\alpha_2}(X_1-x)]] +$$

$$+ \frac{A_o}{D}(1+P_3)\exp[-\sqrt{\omega/2\alpha_1}X_1 - \sqrt{\omega/2\alpha_2}(X_1-x)]\{\sin[\omega t - \sqrt{\omega/2\alpha_1}X_1 + \sqrt{\omega/2\alpha_2}(X_1-x] +$$

$$+ P_2\exp[-2\sqrt{\omega/2\alpha_1}X_1 - 2\sqrt{\omega/2\alpha_2}X_2]\sin(\omega t + \sqrt{\omega/2\alpha_1}X_1 + \sqrt{\omega/2\alpha_2}(X_2+X_3-x)] +$$

$$+ P_3\exp[-2\sqrt{\omega/2\alpha_1}X_1]\sin[\omega t + \sqrt{\omega/2\alpha_1}X_1 + \sqrt{\omega/2\alpha_2}(X_1-x)] +$$

$$+ P_4\exp[-2\sqrt{\omega/2\alpha_2}X_2]\sin[\omega t - \sqrt{\omega/2\alpha_1}X_1 + \sqrt{\omega/2\alpha_2}(X_2+X_3-x)]\} \quad (11)$$

$$T_3 = \frac{A_o P_1}{D}\exp[-\sqrt{\omega/2\alpha_1}X_1 - \sqrt{\omega/2\alpha_2}X_2 + \sqrt{\omega/2\alpha_3}(X_3-x)]\{\sin(\omega t - \sqrt{\omega/2\alpha_1}X_1 - \sqrt{\omega/2\alpha_2}X_2 + \sqrt{\omega/2\alpha_3}(X_3-x)] +$$

$$+ P_2\exp[-2\sqrt{\omega/2\alpha_1}X_1 - 2\sqrt{\omega/2\alpha_2}X_2]\sin[\omega t + \sqrt{\omega/2\alpha_1}X_1 + \sqrt{\omega/2\alpha_2}X_2 + \sqrt{\omega/2\alpha_3}(X_3-x)] +$$

$$+ P_3\exp[-2\sqrt{\omega/2\alpha_1}X_1]\sin[\omega t + \sqrt{\omega/2\alpha_1}X_1 - \sqrt{\omega/2\alpha_2}X_2 + \sqrt{\omega/2\alpha_3}(X_3-x)] +$$

$$+ P_4\exp[-2\sqrt{\omega/2\alpha_2}X_2]\sin[\omega t - \sqrt{\omega/2\alpha_1}X_1 + \sqrt{\omega/2\alpha_2}X_2 + \sqrt{\omega/2\alpha_3}(X_3-x)]\} \quad (12)$$

where

$$D = 1 + 2P_2\exp(-2\sqrt{\omega/2\alpha_1}X_1 - 2\sqrt{\omega/2\alpha_2}X_2)\cos(2\sqrt{\omega/2\alpha_1}X_1 + 2\sqrt{\omega/2\alpha_2}X_2) +$$

$$+ 2P_3\exp(-2\sqrt{\omega/2\alpha_1}X_1)\cos(2\sqrt{\omega/2\alpha_1}X_1) + 2P_4\exp(-2\sqrt{\omega/2\alpha_2}X_2)\cos(2\sqrt{\omega/2\alpha_2}X_2)$$

$$+ 2P_2P_3\exp(-4\sqrt{\omega/2\alpha_1}X_1 - 2\sqrt{\omega/2\alpha_2}X_2)\cos(2\sqrt{\omega/2\alpha_2}X_2) +$$

$$+ 2P_2P_4\exp(-2\sqrt{\omega/2\alpha_1}X_1 - 4\sqrt{\omega/2\alpha_2}X_2)\cos(2\sqrt{\omega/2\alpha_1}X_1) +$$

$$+ 2P_3P_4\exp(-2\sqrt{\omega/2\alpha_1}X_1 - 2\sqrt{\omega/2\alpha_2}X_2)\cos(2\sqrt{\omega/2\alpha_1}X_1 - 2\sqrt{\omega/2\alpha_2}X_2)$$

$$+ P_2^2\exp(-4\sqrt{\omega/2\alpha_1}X_1 - 4\sqrt{\omega/2\alpha_2}X_2) + P_3^2\exp(-4\sqrt{\omega/2\alpha_1}X_1) + P_4^2\exp(-4\sqrt{\omega/2\alpha_2}X_2) \quad (13)$$

and

$$P_1 = \frac{4\beta_1\beta_2}{\beta_2\beta_3+\beta_1\beta_2+\beta_2^2+\beta_1\beta_3}$$

$$P_2 = \frac{-\beta_2\beta_3+\beta_1\beta_2+\beta_2^2-\beta_1\beta_3}{\beta_2\beta_3+\beta_1\beta_2+\beta_2^2+\beta_1\beta_3}$$

$$P_3 = \frac{-\beta_2\beta_3+\beta_1\beta_2-\beta_2^2+\beta_1\beta_3}{\beta_2\beta_3+\beta_1\beta_2+\beta_2^2+\beta_1\beta_3}$$

$$P_4 = \frac{\beta_2\beta_3+\beta_1\beta_2-\beta_2^2-\beta_1\beta_3}{\beta_2\beta_3+\beta_1\beta_2+\beta_2^2+\beta_1\beta_3} \qquad (14)$$

The temperature is a sinusoidal function of time at all depths. It is useful to have the solutions in the form $T = A \sin(\omega t + \ )$, i.e. in terms of the amplitude and phase of the fluctuations. We write $A = \frac{A_o}{D}\sqrt{B_i^2+C_i^2}$ and $\ = -\tan^{-1}(B_i/C_i)$, and find that the B_i and C_i are given by the following expressions.

$$\begin{aligned}
B_1 = {} & \exp(-\sqrt{\omega/2\alpha_1}x)\sin(\sqrt{\omega/2\alpha_1}x)+P_2[\exp(-2\sqrt{\omega/2\alpha_1}X_1-2\sqrt{\omega/2\alpha_2}X_2+\sqrt{\omega/2\alpha_1}x)- \\
& -\exp(-2\sqrt{\omega/2\alpha_1}X_1-2\sqrt{\omega/2\alpha_2}X_2-\sqrt{\omega/2\alpha_1}x)]\sin(2\sqrt{\omega/2\alpha_1}X_1+2\sqrt{\omega/2\alpha_2}X_2-\sqrt{\omega/2\alpha_1}x)+ \\
& +P_3[\exp(-2\sqrt{\omega/2\alpha_1}X_1+\sqrt{\omega/2\alpha_1}x)-\exp(-2\sqrt{\omega/2\alpha_1}X_1-\sqrt{\omega/2\alpha_1}x)]\sin(2\sqrt{\omega/2\alpha_1}X_1-\sqrt{\omega/2\alpha_1}x)+ \\
& +2P_4\exp(-2\sqrt{\omega/2\alpha_2}X_2-\sqrt{\omega/2\alpha_1}x)\cos(2\sqrt{\omega/2\alpha_2}X_2)\sin\sqrt{\omega/2\alpha_1}x \\
& -2P_2P_3\exp(-4\sqrt{\omega/2\alpha_1}X_1-2\sqrt{\omega/2\alpha_2}X_2+\sqrt{\omega/2\alpha_1}x)\cos(2\sqrt{\omega/2\alpha_2}X_2)\sin\sqrt{\omega/2\alpha_1}x \\
& +P_2P_4[\exp(-2\sqrt{\omega/2\alpha_1}X_1-4\sqrt{\omega/2\alpha_2}X_2+\sqrt{\omega/2\alpha_1}x)-\exp(-2\sqrt{\omega/2\alpha_1}X_1-4\sqrt{\omega/2\alpha_2}X_2-\sqrt{\omega/2\alpha_1}x)]x \\
& x\sin(2\sqrt{\omega/2\alpha_1}X_1-\sqrt{\omega/2\alpha_1}x)+P_3P_4[\exp(-2\sqrt{\omega/2\alpha_1}X_1-2\sqrt{\omega/2\alpha_2}X_2+\sqrt{\omega/2\alpha_1}x)- \\
& -\exp(-2\sqrt{\omega/2\alpha_1}X_1-2\sqrt{\omega/2\alpha_2}-\sqrt{\omega/2\alpha_1}x)]\sin(2\sqrt{\omega/2\alpha_1}X_1-2\sqrt{\omega/2\alpha_2}X_2-\sqrt{\omega/2\alpha_1}x) \\
& -P_2^2\exp(-4\sqrt{\omega/2\alpha_1}X_1-4\sqrt{\omega/2\alpha_2}X_2+\sqrt{\omega/2\alpha_1}x)\sin\sqrt{\omega/2\alpha_1}x \\
& -P_3^2\exp(-4\sqrt{\omega/2\alpha_1}X_1+\sqrt{\omega/2\alpha_1}x)\sin\sqrt{\omega/2\alpha_1}x+P_4^2\exp(-4\sqrt{\omega/2\alpha_2}X_2-\sqrt{\omega/2\alpha_1}x)\sin\sqrt{\omega/2\alpha_1}x \qquad (15)
\end{aligned}$$

$$C_1 = \exp(-\sqrt{\omega/2\alpha_1}x)\cos\sqrt{\omega/2\alpha_1}x+P_2[\exp(-2\sqrt{\omega/2\alpha_1}X_1-2\sqrt{\omega/2\alpha_2}X_2+\sqrt{\omega/2\alpha_1}x)+$$
$$+\exp(-2\sqrt{\omega/2\alpha_1}X_1-2\sqrt{\omega/2\alpha_2}X_2-\sqrt{\omega/2\alpha_1}x)]\cos(2\sqrt{\omega/2\alpha_1}X_1+2\sqrt{\omega/2\alpha_2}X_2-\sqrt{\omega/2\alpha_1}x)+$$
$$+P_3[\exp(-2\sqrt{\omega/2\alpha_1}X_1+\sqrt{\omega/2\alpha_1}x)+\exp(-2\sqrt{\omega/2\alpha_1}X_1-\sqrt{\omega/2\alpha_1}x)]\cos(2\sqrt{\omega/2\alpha_1}X_1-\sqrt{\omega/2\alpha_1}x)+$$
$$+2P_4\exp(-2\sqrt{\omega/2\alpha_2}X_2-\sqrt{\omega/2\alpha_1}x)\cos(2\sqrt{\omega/2\alpha_2}X_2)\cos\sqrt{\omega/2\alpha_1}x$$
$$+2P_2P_3\exp(-4\sqrt{\omega/2\alpha_1}X_1-2\sqrt{\omega/2\alpha_2}X_2+\sqrt{\omega/2\alpha_1}x)\cos(2\sqrt{\omega/2\alpha_2}X_2)\cos\sqrt{\omega/2\alpha_1}x$$
$$+P_2P_4[\exp(-2\sqrt{\omega/2\alpha_1}X_1-4\sqrt{\omega/2\alpha_2}X_2+\sqrt{\omega/2\alpha_1}x)+\exp(-2\sqrt{\omega/2\alpha_1}X_1-4\sqrt{\omega/2\alpha_2}X_2-\sqrt{\omega/2\alpha_1}x)]x$$
$$x\cos(2\sqrt{\omega/2\alpha_1}X_1-\sqrt{\omega/2\alpha_1}x)+P_3P_4[\exp(-2\sqrt{\omega/2\alpha_1}X_1-2\sqrt{\omega/2\alpha_2}X_2+\sqrt{\omega/2\alpha_1}x)+$$
$$+\exp(-2\sqrt{\omega/2\alpha_1}X_1-2\sqrt{\omega/2\alpha_2}X_2-\sqrt{\omega/2\alpha_1}x)]\cos(2\sqrt{\omega/2\alpha_1}X_1-2\sqrt{\omega/2\alpha_2}X_2-\sqrt{\omega/2\alpha_1}x)$$
$$+P_2^2\exp(-4\sqrt{\omega/2\alpha_1}X_1-4\sqrt{\omega/2\alpha_2}X_2+\sqrt{\omega/2\alpha_1}x)\cos\sqrt{\omega/2\alpha_1}x$$
$$+P_3^2\exp(-4\sqrt{\omega/2\alpha_1}X_1+\sqrt{\omega/2\alpha_1}x)\cos\sqrt{\omega/2\alpha_1}x+P_4^2\exp(-4\sqrt{\omega/2\alpha_2}X_2-\sqrt{\omega/2\alpha_1}x)\cos\sqrt{\omega/2\alpha_1}x \quad (16)$$

$$B_2 = (P_2+P_4)\exp[-\sqrt{\omega/2\alpha_1}X_1-\sqrt{\omega/2\alpha_2}(X_2+X_3-x)][\sin[\sqrt{\omega/2\alpha_1}X_1+\sqrt{\omega/2\alpha_2}(X_2+X_3-x)]$$
$$-P_2\exp(-2\sqrt{\omega/2\alpha_1}X_1-2\sqrt{\omega/2\alpha_2}X_2)\sin[\sqrt{\omega/2\alpha_1}X_1-\sqrt{\omega/2\alpha_2}(X_1-x)]$$
$$-P_3\exp(-2\sqrt{\omega/2\alpha_1}X_1)\sin[\sqrt{\omega/2\alpha_1}X_1-\sqrt{\omega/2\alpha_2}(X_2+X_3-x)]$$
$$+P_4\exp(-2\sqrt{\omega/2\alpha_2}X_2)\sin[\sqrt{\omega/2\alpha_1}X_1+\sqrt{\omega/2\alpha_2}(X_1-x)]]$$
$$+(1+P_3)\exp[-\sqrt{\omega/2\alpha_1}X_1+\sqrt{\omega/2\alpha_2}(X_1-x)][\sin[\sqrt{\omega/2\alpha_1}X_1-\sqrt{\omega/2\alpha_2}(X_1-x)]-$$
$$-P_2\exp(-2\sqrt{\omega/2\alpha_1}X_1-2\sqrt{\omega/2\alpha_2}X_2)\sin[\sqrt{\omega/2\alpha_1}X_1+\sqrt{\omega/2\alpha_2}(X_2+X_3-x)]$$
$$-P_3\exp(-2\sqrt{\omega/2\alpha_1}X_1)\sin[\sqrt{\omega/2\alpha_1}X_1+\sqrt{\omega/2\alpha_2}(X_1-x)]$$
$$+P_4\exp(-2\sqrt{\omega/2\alpha_2}X_2)\sin[\sqrt{\omega/2\alpha_1}X_1-\sqrt{\omega/2\alpha_2}(X_2+X_3-x)]] \quad (17)$$

$$C_2 = (P_2+P_4)\exp[-\sqrt{\omega/2\alpha_1}X_1-\sqrt{\omega/2\alpha_2}(X_2+X_3-x)][\cos[\sqrt{\omega/2\alpha_1}X_1+\sqrt{\omega/2\alpha_2}(X_2+X_3-x)]$$
$$+P_2\exp(-2\sqrt{\omega/2\alpha_1}X_1-2\sqrt{\omega/2\alpha_2}X_2)\cos[\sqrt{\omega/2\alpha_1}X_1-\sqrt{\omega/2\alpha_2}(X_1-X)]$$
$$+P_3\exp(-2\sqrt{\omega/2\alpha_1}X_1)\cos[\sqrt{\omega/2\alpha_1}X_1-\sqrt{\omega/2\alpha_2}(X_2+X_3-x)]$$
$$+P_4\exp(-2\sqrt{\omega/2\alpha_2}X_2)\cos[\sqrt{\omega/2\alpha_1}X_1+\sqrt{\omega/2\alpha_2}(X_1-x)]]$$
$$+(1+P_3)\exp[-\sqrt{\omega/2\alpha_1}X_1+\sqrt{\omega/2\alpha_2}(X_1-x)][\cos[\sqrt{\omega/2\alpha_1}X_1-\sqrt{\omega/2\alpha_2}(X_1-x)]$$
$$+P_2\exp(-2\sqrt{\omega/2\alpha_1}X_1-2\sqrt{\omega/2\alpha_2}X_2)\cos[\sqrt{\omega/2\alpha_1}X_1+\sqrt{\omega/2\alpha_2}(X_2+X_3-x)]$$
$$+P_3\exp(-2\sqrt{\omega/2\alpha_1}X_1)\cos[\sqrt{\omega/2\alpha_1}X_1+\sqrt{\omega/2\alpha_2}(X_1-x)]$$
$$+P_4\exp(-2\sqrt{\omega/2\alpha_2}X_2)\cos[\sqrt{\omega/2\alpha_1}X_1-\sqrt{\omega/2\alpha_2}(X_2X_3-x)]] \quad (18)$$

(18)

$$B_3 = P_1\exp[-\sqrt{\omega/2\alpha_1}X_1-\sqrt{\omega/2\alpha_2}X_2-\sqrt{\omega/2\alpha_3}(X_3-x)]\{\sin[\sqrt{\omega/2\alpha_1}X_1+\sqrt{\omega/2\alpha_2}X_2-\sqrt{\omega/2\alpha_3}(X_3-x)]$$
$$-P_2\exp(-2\sqrt{\omega/2\alpha_1}X_1-2\sqrt{\omega/2\alpha_2}X_2)\sin[\sqrt{\omega/2\alpha_1}X_1+\sqrt{\omega/2\alpha_2}X_2+\sqrt{\omega/2\alpha_3}(X_3-x)]$$
$$-P_3\exp(-2\sqrt{\omega/2\alpha_1}X_1)\sin[\sqrt{\omega/2\alpha_1}X_1-\sqrt{\omega/2\alpha_2}X_2+\sqrt{\omega/2\alpha_3}(X_3-x)]$$
$$+P_4\exp(-2\sqrt{\omega/2\alpha_2}X_2)\sin[\sqrt{\omega/2\alpha_1}X_1-\sqrt{\omega/2\alpha_2}X_2-\sqrt{\omega/2\alpha_3}(X_3-x)]\} \quad (19)$$

$$C_3 = P_1\exp[-\sqrt{\omega/2\alpha_1}X_1-\sqrt{\omega/2\alpha_2}X_2-\sqrt{\omega/2\alpha_3}(X_3-x)]\{\cos[\sqrt{\omega/2\alpha_1}X_1+\sqrt{\omega/2\alpha_2}X_2-\sqrt{\omega/2\alpha_3}(X_3-x)]$$
$$+P_2\exp(-2\sqrt{\omega/2\alpha_1}X_1-2\sqrt{\omega/2\alpha_2}X_2)\cos[\sqrt{\omega/2\alpha_1}X_1+\sqrt{\omega/2\alpha_2}X_2+\sqrt{\omega/2\alpha_3}(X_3-x)]$$
$$+P_3\exp(-2\sqrt{\omega/2\alpha_1}X_1)\cos[\sqrt{\omega/2\alpha_1}X_1-\sqrt{\omega/2\alpha_2}X_2+\sqrt{\omega/2\alpha_3}(X_3-x)]$$
$$+P_4\exp(-2\sqrt{\omega/2\alpha_2}X_2)\cos[\sqrt{\omega/2\alpha_1}X_1-\sqrt{\omega/2\alpha_2}X_2-\sqrt{\omega/2\alpha_3}(X_3-x)]\} \quad (20)$$

An alternative way of expressing the solutions in the middle layer and in the substratum leads to results which are simpler in appearance. In the first case, one may use Lachenbruch's (1959) solution for the two-layer problem, with amplitude and phase at the surface calculated from equations (17) and (18) at $x = X_1$. In the substratum one may use the simple solution for a uniform half space (Carslaw and Jaeger, 1959, p. 65), with surface amplitude and phase calculated from (19) and (20) at $x = X_3$. The apparent simplification achieved in this way proves to be of little value for practical calculation, however. A number of terms which are independent of x, such as those on the right side of (13), must be evaluated in order to obtain numerical results in the upper layer and at the interfaces. Once this is done it seems simpler to continue to use the three-layer theory rather than evaluating new expressions which appear in the two-layer theory, and which differ from those already evaluated. The extreme simplicity of the expression for temperature in a homogeneous medium, however, makes the alternative procedure more attractive than the use of equation (12) in the substratum.

The three-layer theory leads to expressions which are far too cumbersome for hand calculation. Numerical results are easily and rapidly obtained by a digital computer, however. Use of the exact theory insures that no unwanted initial transients affect the results. If finite difference methods are used, assurance of freedom from transients is secured only by repeatedly cycling the calculation, a procedure which is far more costly in machine time than is evaluating the exact theory.

B. Applications

In order to apply the theory developed above to the lunar surface, the parameters of the problem must either be fixed, or their ranges must be restricted by estimate or by lunar observations. There are eight independent parameters (two thermal constants for each layer plus the thickness of the upper two layers), since density and heat capacity always occur in the equations as the product $\underline{\rho}\ \underline{c}$ and can be considered a single parameter. Nevertheless a very large number of permutations of values remains, and it is important to fix as many parameters as possible.

We shall take $\underline{c}$ equal to 0.2 cal/gm °C in all models; this value is appropriate to all common silicate materials under lunar surface conditions. Fixing $\underline{c}$ does not of course reduce the number of parameters unless $\underline{\rho}$ is also fixed. Perhaps the best-known lunar parameter is the thermal inertia, β, of the surface layer, which is known from infrared temperature measurements during a lunation to be about 0.0023 cal/cm^2 °C sec$^{\frac{1}{2}}$ (see for example, Sinton, 1961, p. 411). From this result we take the product $\underline{K}\ \underline{\rho}\ \underline{c}$ for the lunar surface to be, nearly enough, 5×10^{-6} cal^2/cm^4 °C^{2}sec. The very low value of the thermal inertia is the principal evidence that the lunar surface is composed of granular material.

Analysis of radar echoes from the moon leads eventually to a determination of the product of density and dielectic constant. Since the latter quantity varies little among common silicates, the density may be inferred from these results. According to Evans' (1961) summary, material with the properties of loose sand would fit the radar data, i.e. a density between 1 and 2 gm/cm^3 would be expected. On the other hand, the radar reflections may originate from a level beneath the optically defined surface. Lower

surface densities would then be possible and would be the automatic consequences of several postulated models of lunar surface structure (Hibbs, 1963; Warren, 1963; Hapke, 1964). We shall consider models with ρ ranging from 0.1 to 2.0 gm/cm^3. Since c and β are regarded as fixed by other considerations, a choice of ρ also fixes K for the particular model of the surface layer.

We have no direct information about the properties of the subsurface layers. We shall assume that the substratum consists of unfractured basic rock; appropriate properties are shown in table 2. The intermediate layer is presumably made up of rubble, with properties between those of the surface layer and the substratum. Three possibilities have been considered in order to indicate the effects to be expected from such a layer. They do not exhaust the possible range of properties; models with the surface layer resting directly on a solid substratum or with an infinite thickness of surface material may be considered limiting cases. The thermal properties that have been considered in the following numerical calculations are collected in table 2.

It is useful at the outset to recognize two limiting types of amplitude - depth relations. In a homogeneous medium the amplitude of the temperature oscillation decreases with depth according to the relation $A = A_o \exp(-\sqrt{\omega/2\alpha}\, x)$. The exponential damping law is obeyed far from the lower contact of a thick surface layer of low thermal diffusivity. A different extreme is encountered if the density of the material becomes very small. The term in the equation of heat conduction containing the time derivative then becomes negligible, and the amplitude is found to decrease linearly with depth. The numerical results which follow contain examples of both types of behavior.

Table 2. Properties of layers.

	K cal/cm sec°C	ρ gm/cm^3	c cal/gm°C	α cm^2/sec	β cal/cm^2°C sec$^{\frac{1}{2}}$
I. Surface layer.					
1.	2.5×10^{-4}	0.1	0.2	1.25×10^{-2}	2.24×10^{-3}
2.	5×10^{-5}	0.5	0.2	5.0×10^{-4}	2.24×10^{-3}
3.	2.5×10^{-5}	1.0	0.2	1.25×10^{-4}	2.24×10^{-3}
4.	1.25×10^{-5}	2.0	0.2	3.12×10^{-5}	2.24×10^{-3}
II. Intermediate layer.					
A	1×10^{-3}	1.0	0.2	5.0×10^{-3}	1.41×10^{-2}
B	1×10^{-3}	2.0	0.2	2.5×10^{-3}	2.00×10^{-2}
C	2×10^{-3}	2.5	0.2	4.0×10^{-3}	3.16×10^{-2}
III. Substratum.					
	5×10^{-3}	3.0	0.2	8.33×10^{-3}	5.48×10^{-2}
IV. Blanket materials.					
SI-10	2.69×10^{-7}	0.032	0.2	4.20×10^{-5}	4.15×10^{-5}
SI-91	4.14×10^{-8}	0.120	0.2	1.72×10^{-6}	3.15×10^{-5}
Plastic	1.0×10^{-4}	1.3	0.2	3.85×10^{-4}	5.10×10^{-3}

In the calculations Ao was given the value 314°C. This is not the amplitude of the temperature fluctuation at the lunar surface, but rather is twice the amplitude of the fundamental mode in the Fourier analysis of lunar surface temperature given by Sinton (1961). This term is more interesting than the higher harmonics because it is about 5 times as large and because it penetrates the most deeply. Doubling the amplitude gives the total range of temperature directly.

Some typical results are shown in figs. 1 through 6. The curves of amplitude and phase vs. depth have characteristic shapes; the sharp drops in the curves as interfaces are approached are particularly noteworthy. Study of both amplitude and phase seems to give little more information than study of amplitude alone, although any program of temperature measurement would automatically yield both quantities.

The amplitudes decrease exponentially near the tops of layers about a meter or more in thickness. The law of decrease is the same as in a semi-infinite region, and the thermal diffusivity of the layer can be obtained from the damping observed. Where the exponential law is not obeyed, the properties of more than one layer are involved and it is doubtful whether they can ever be uniquely untangled. In the situations where a linear law applies (cf. figs. 1 and 2), the properties of the lower layers assume special importance relative to the upper layer in which the linear damping occurs.

In a case in which measurements of temperature cannot be made throughout the thickness of a layer, the proximity of an interface could be detected, if indeed one were near. No more than this qualitative result can be obtained unless the depth of the interface is also known (c.f. figs. 4, 5,

and 6). Temperatures must be measured at the interface in order to determine the properties of the underlying layer reliably, and little more than its thermal inertia can be deduced unless some penetration of the underlying layer is possible.

It is worthwhile remarking again that the above conclusions are correct only if linearization of the conduction equation is valid. This will certainly not be true close to the surface, and will only become valid at depths where the oscillations in temperature are severely damped. This depth is critically dependent on the surface material. In a homogeneous region of material 4 of table 2(I), the amplitude reaches 1 degree at a depth of 30 cm. In a homogeneous region of solid rock (substratum of Table 2) an amplitude of 1 degree occurs at a depth of 450 cm. In both cases the surface amplitude was taken to be 314 degrees, as before. The presence of layering would reduce those depths. In practice, the linear theory will probably be valid if the amplitudes are less than 10 degrees, but should be regarded with suspicion in cases of higher amplitudes.

.. STEADY PERIODIC TEMPERATURES NEAR A HOLE IN THE SURFACE LAYER

The poorly conducting lunar surface layer may locally be absent, and the substratum of higher conductivity may be exposed to high-amplitude fluctuations in temperature at the surface. Damping near such outcrops will be comparatively inefficient, and large amplitudes of the thermal wave may penetrate the substratum both laterally and vertically. We require an estimate of the extent of serious disturbance.

A simple geometrical model of an outcrop is obtained as follows. Imagine first a two-layer structure of the sort described in the last section, i.e. a uniform layer with one set of properties separated by a plane boundary from a substratum of different properties. We then remove a piece of the upper layer having the shape of a right circular cylinder, and fill the resulting hole with material of the substratum. The result is a cylindrical protuberance on the substratum extending to the original plane surface.

Analytical solutions to heat flow problems in heterogeneous regions of this degree of complexity are unknown, and recourse to numerical methods must be had. The following calculations were made from the simplest form of finite-difference approximation to the equation of heat conduction in cylindrical coordinates (see for example Carslaw and Jaeger, 1957, p. 468,470). The program written for the computer took account of different conductivities in the two layers, but did not allow for different densities and heat capacities. This simplification does not affect the qualitative conclusions drawn from the calculations. A second simplification was to assume that the surface temperature was

independent of position and varied with time in the manner shown by Sinton (1961, fig. 3). Actually the amplitude of the variation would be smaller in the hole, because of the better connection between the surface and the lunar interior there, and the extent of the perturbation of amplitudes is therefore slightly overestimated because of neglect of this effect.

Results of the calculations are shown in fig. 7 as contours of equal amplitudes. The conductivity of the surface layer is taken to be 1/10th that of the substratum. It is evident from figure that the effect of the hole is negligible at a distance from the equal to its diameter, and that serious perturbations do not extend further than about half this distance. The amplitudes decrease monotonically with depth everywhere, as is shown by the fact that no contour can be intersected more than once by any vertical line. Thus there is no tendency for high-amplitude fluctuations originating in the hole to "run under" the surface layer. It may be concluded from these results that the influence of an outcrop on amplitudes does not persist for a distance greater than its diameter.

4. STEADY-STATE PERTURBATIONS OF FLUX DUE TO IRREGULARITIES IN THE THICKNESS OF THE SURFACE LAYER

If the thickness of the poorly conducting surface layer is variable, heat tends to be funneled towards thin spots in the layer and away from thick spots, a phenomenon sometimes termed thermal refraction. Refraction causes the flux observed at the surface to be high where the insulating layer is thin and low where it is thick. Some studies of terrestrial heat flow have revealed irregularities which may be attributable to thermal refraction. Errors arising from this effect may be large in cases where the conductivity contrasts are large; a good terrestrial example would be near a salt dome in poorly consolidated, fine-grained sediments.

The contrast in conductivity near the lunar surface may exceed a factor of 10 (table 2), a contrast that is considerably larger than one would expect to encounter on earth. The proportional change in flux scales according to the ratio of the conductivity of the substratum to the conductivity of the surface layer, and hence large perturbations may be expected near the lunar surface. The question was investigated quantitatively by studying the steady-state temperature distribution around cylindrical protuberances on the interface between an upper poorly conducting layer and a better conducting substratum. The problem is analogous to the investigation of amplitudes near an outcrop discussed in the last section, but with constant surface temperature. The same machine program was used, steady-state conditions being achieved by allowing the calculation to iterate until the temperatures stopped changing.

In the application of a steady-state theory to the lunar surface, it must be assumed that the periodic transients either have been avoided

by measuring heat flow in a sufficiently deep hole or have been removed by observing temperatures over at least one cycle and calculating undisturbed steady-state means. The results of this section show that even if one of these ways of removing transient effects can be followed (neither will necessarily be easy to carry out), perturbations leading to erroneous measurements of lunar heat flow may still remain.

A number of typical results are shown in fig. 8. Cases (d) and (e), in which the substratum crops out at the surface, lead to the largest perturbations, but such localities are obviously atypical and could easily be avoided. The perturbations are greatly reduced if the irregularities in the interface are completely buried as in the other cases shown, but nevertheless they are appreciable. Local variations up to about 50% may be found in all of the cases examined. The results shown in fig. 8 were calculated for a ratio of conductivities of 10; reference to table 2 shows that this value is, if anything, too low. A conductivity ratio of 20 would lead to perturbations of a factor of 2 or more, depending on whether one considers enhancement or reduction of the undisturbed flux.

In order to be useful, a measurement of lunar heat flow must lead to an estimate of mean flux in a region with dimensions measured in kilometers which is accurate to better than 20%. If the error is much greater than this the numbers will have little significance for geophysical or cosmological theory. The mean value of 10 fairly closely spaced measurements would have the required accuracy, assuming that the individual values are disturbed by no more than 50% and that the disturbances are normally distributed with zero mean value. This latter requirement implies that the probability of finding a given positive disturbance must be the same as finding a

negative disturbance of the same amount. It is not at all clear that a system of randomly distributed, small, buried craters would have this property. Furthermore systematic error would invalidate this statistical method of achieving accuracy if, for example, all of the measurements were made within a large buried crater so that all were affected by a negative disturbance.

An alternative approach is to escape the near-surface perturbations by drilling deeply enough to make the measurement beneath them. It should be possible to do this, because porosity will be eliminated or greatly reduced by the weight of overburden, and very large contrasts in conductivity will no longer be possible. Considerable depths of penetration may be required, however, since disturbed temperatures extend to a distance beneath the bottom of the anomalous region roughly equal to its diameter.

5. THE BLANKET METHOD OF MEASURING LUNAR HEAT FLOW

A. Introduction.

If a sheet of material of known thermal conductivity is placed on the lunar surface and allowed to come into thermal equilibrium, the heat flow through the surface can be determined from measurements of the thermal gradient in the sheet. A device consisting of a suitable insulating material and temperature sensors for the determination of the gradient is known as a fluxmeter, or blanket. Such devices have found meteorological application in the study of heat exchange between the ground and the atmosphere, but they have never been successfully used in the measurement of terrestrial heat flow except in thermal regions where the heat flow is orders of magnitude higher than normal.

The extreme simplicity of the blanket method makes it appear attractive as a tool for determination of lunar heat flow. Associated difficulties seem to outweigh this advantage, however, as is discussed below.

B. Simple steady-state blanket theory.

Since one has complete control over the geometry of the blanket, it is possible to select a shape that is amenable to simple theoretical treatment. A circular disc with diameter greatly exceeding thickness proves to be a convenient choice. An approximate method of treating this problem has been suggested privately by A. H. Lachenbruch, and much of the following discussion is due to him.

Consider a half space with zero initial temperature. If, starting at $t=0$, the temperature of the surface is maintained at a constant value ΔT within a circle of radius R and zero outside the circle, then beneath

the center of the circle (Lachenbruch, 1957)

$$T = \Delta T[\operatorname{erfc} x/\sqrt{4\alpha t} - \{x/\sqrt{x^2+R^2}\}\operatorname{erfc}\sqrt{x^2+R^2}/\sqrt{4\alpha t}] \quad (21)$$

where x is depth. Beneath the center, as the depth approaches zero, the vertical gradient approaches

$$\nabla T = -\Delta T[1/R \operatorname{erfc} R/\sqrt{4\alpha t} + 1/\sqrt{\pi\alpha t}] \quad (22)$$

and the heat flow approaches

$$\Delta Q = \Delta T[K/R \operatorname{erfc} R/\sqrt{4\alpha t} + K/\sqrt{\pi t}] \quad (23)$$

(See table 1 for definitions of symbols.) In the steady state (23) reduces to

$$\Delta Q = K \Delta T/R \quad (24)$$

As an illustration of the application of these results, consider the case of a blanket placed on the plane lunar surface. The upper surface of the blanket is supposed to be at zero, as is the lunar surface outside the blanketed area. The assumption that the steady periodic transient has somehow been removed is implicit. If the lunar flux is everywhere Q, then ΔT in (24) becomes equal to $Q\bar{X}_b/K_b$, where $\bar{X}_b$ is the thickness of the blanket and the subscript b denotes blanket properties. From (24) we find a perturbation of flux

$$\Delta Q/Q = 1-Q_b/Q = \frac{\bar{X}_b K}{R K_b} \quad (25)$$

due to the blanket. This result is approximate first because the undisturbed flux Q was used to calculate ΔT, and secondly because ΔT is assumed constant when in fact it varies with radius in an unknown way. The first objection can be overcome by substituting Q_b for Q in the expression for ΔT, calculating the new disturbance, and iterating the process until it converges. For example, if $K/K_b = 10$ and $R/\bar{X}_b = 50$, we find $\Delta Q/Q = 0.2$ and $Q_b/Q = 0.8$. Substituting $\Delta T_b = 0.8\ \Delta T$ for ΔT leads to $Q_b/Q = 0.84$, and a second iteration gives $Q_b/Q = 0.842$. The process evidently converges rapidly. The second objection mentioned above is inherent in the method, since edge effects are neglected. The error is small if

R/X_b is large enough.

In order to get a quantitative idea of the meaning of "large enough" consider a second illustration of the method. A blanket is now supposed to be buried so that its upper surface coincides with the initial plane surface. The geometry is identical to that shown in figure 8(e). Again we assume uniform flux as a first approximation. The thermal gradient in the blanket is thin Q/K_b, and elsewhere it is Q/K; the corresponding temperatures at the level of the base of the blanket are QX_b/K_b and QX_b/K respectively. Equation (24) then gives

$$\Delta C/C = 1-C_b/C = \frac{\bar{X}_b}{R}[K/K_b-1] \tag{26}$$

in this case. Iteration again may be used to improve the result. This problem can also be solved by the finite-difference method used above in section 3, and a comparison of the results gives some idea of the range of applicability of the approximate method (figure 9). The finite-difference calculations agree well with equation (26) for $R/\bar{X}_b$ greater than about 20, but iteration does not improve the agreement. The iteration process becomes unstable for $R/\bar{X}_b$ equal to 10 or less. It appears that some compensation between the errors arising from neglected edge effects and those due to other approximations in the derivation of (26) takes place, and the use of (26) without iteration appears to give the more reliable results. Since the finite-difference calculations are probably not accurate to better than 5 per cent, the results given by the simple approach outlined here are satisfactory.

There is a second type of disturbance arising from the presence of a blanket on the lunar surface which may be treated exactly by the present method. If the albedo of the blanket does not match that of the lunar surface, the mean temperature of the top of the blanket will differ from the mean surface temperature. The disturbance of flux can be estimated directly from (23) and (24). For example, if a blanket 100 cm in radius

rests on material of conductivity 5×10^{-5} (material I(2) of table 2), then a difference in temperature of only $0.2^{\circ}C$ produces a steady-state disturbance in flux of 0.1×10^{-6} cal/cm^2 sec. Such a disturbance may already be intolerably large; it becomes worse if the surface material is a better conductor or if the radius of the blanket is reduced to a more manageable figure. It will be difficult to measure the mean temperature of the lunar surface to better than $1^{\circ}C$, so that a serious disturbance due to mismatching albedo may go completely undetected.

C. Time-dependent problems associated with the blanket method.

It is convenient to consider separately two causes of time-dependent temperatures. One is the steady periodic regime prevailing near the lunar surface, and the other is the transient disturbance arising from the emplacement of the blanket. The latter has two sources. The blanket may not be at the same initial temperature as the lunar surface, and after emplacement the establishment of the lunar thermal gradient within the blanket changes both its temperature and that of the lunar material. The first source of disturbance can be avoided by careful planning, but the second cannot.

Steady periodic temperatures in the blanket were investigated by the methods of section 2. The blanket, taken to be 5 cm thick, was assumed to rest on a thick layer having the properties of layer 2 of table 2(I), on 50 cm of such material which rested in turn on the substratum of table 2(III), or directly on the substratum. Three kinds of blanket materials were considered (table 2(IV). Two of them, SI-10 and SI-91, are "superinsulators" developed by Linde for the storage of cryogenic fluids. The thermal conductivity of these materials is extraordinarily low, as is shown in the table. A third blanket material was assumed to have properties corresponding roughly to those of ordinary plastics (e.g. bakelite or plexiglass).

Amplitudes and phases of the temperature variations at the bottom of the blanket are shown in table 3 for the various combinations of blanket materials and assumed lunar configurations. The amplitude-depth curve in the blanket has the same shape as the curves for the upper layer shown in figure 1a; that is, the amplitude at the center of the blanket exceeds the geometric mean of the surface amplitude (314°C) and the amplitude shown in the table. Clearly only the superinsulators are capable of reducing the fluctuation to manageable proportions (order of tens of degrees or less) in the lower half of the blanket. It is doubtful whether the mean temperature can be determined in the 'plastic' blanket to sufficient accuracy. The situation is made worse by the fact that the expected gradient is inversely proportional to the conductivity of the blanket. In the superinsulators the expected gradient is on the order of 1-10°C/cm, whereas in the "plastic" a gradient of 10^{-2}-10^{-3} °C/cm seems likely.

Hence we find that the use of superinsulators is indicated in order to eliminate the steady periodic fluctuations most effectively and to raise the mean thermal gradient to an easily measured value. But now we must consider the transient associated with blanket emplacement. We assume that the lateral dimensions of the blanket are great compared with its thickness, so that the problem can be treated as one of 1-dimensional heat flow. The blanket, occupying the region $-\underline{L} \leq \underline{x} \leq o$, is assumed to have initial temperature $\underline{To}$, and thermal properties indicated by the subscript $\underline{b}$. The lunar material (assumed uniform) has initial temperature $\underline{mx}$, where $x \geq o$ equals depth, and unsubscripted properties.

Writing $\bar{T}$ for the Laplace transform of T, as before, we find

$$\bar{T}_b = To/p + A \sinh q_b x + B \cosh q_b x \qquad (27)$$

and

$$\bar{T} = mx/p + C \exp(-qx) \qquad (28)$$

Table 3. Amplitude and phases at base of blanket 5 cm thick.

Blanket material	Substratum (table 2)	Amplitude °C	Phase
SI-10	I-2, III	4.5	-60
SI-10	I-2	4.5	-60
SI-10	III	0.2	-60
SI-91	I-2, III	0.1	-253
SI-91	I-2	0.1	-252
SI-91	III	0.004	-252
Plastic	I-2, III	274	-11
Plastic	I-2	274	-11
Plastic	III	60	-39

where A, B, C are constants independent of $\underline{x}$. Application of initial conditions $\underline{\bar{T}_b} = \underline{\bar{T}_o}$ and $\bar{T} = mx$, and the conditions of continuity of temperature and flux at $\underline{x} = o$ lead to

$$A = [KqT_o(\cosh q_b L - 1) - Km \cosh q_b L]/pD \tag{29}$$

$$B = [KqT_o \sinh q_b L + K_b q_b T_o - Km \sinh q_b L]/pD \tag{30}$$

$$C = [-K_b q_b T_o(\cosh q_b L - 1) - Km \sinh q_b L]/pD \tag{31}$$

where

$$D = -Kq \sinh q_b L - K_b q_b \cosh q_b L \tag{32}$$

Conversion of the hyperbolic functions in (29) through (32) to exponentials, and expansion of $\underline{D}$ by the binomial theorem then leads to the following expressions for the temperatures

$$T_b = To\left[1 - \frac{\beta}{\beta+\beta_b}\left[\sum_o^\infty (M)^n\left(\operatorname{erfc}\frac{2nL-x}{\sqrt{4\alpha_b t}} - \operatorname{erfc}\frac{(2n+2)L+x}{\sqrt{4\alpha_b t}}\right]\right.\right.$$
$$\left.\left. + M\sum_o^\infty (M)^n \operatorname{erfc}\frac{(2n+1)L-x}{\sqrt{4\alpha_b t}} - \sum_o^\infty (M)^n \operatorname{erfc}\frac{(2n+1)L+x}{\sqrt{4\alpha_b t}}\right\}\right.$$
$$\left. + \frac{2Km\sqrt{t}}{\beta+\beta_b}\left[\sum_o^\infty (M)^n\left(\operatorname{ierfc}\frac{2nL-x}{\sqrt{4\alpha_b t}} - \operatorname{ierfc}\frac{2n+2)L+x}{\sqrt{4\alpha_b t}}\right]\right.\right. \tag{33}$$

$$T = To\frac{\beta_b}{\beta+\beta_b}\sum_o^\infty (M)^n\left[2\operatorname{erfc}\left(\frac{(2n+1)L}{\sqrt{4\alpha_b t}} + \frac{x}{\sqrt{4\alpha t}}\right)\right.$$
$$\left. - \operatorname{erfc}\left(\frac{2nL}{\sqrt{4\alpha_b t}} + \frac{x}{\sqrt{4\alpha t}}\right) - \operatorname{erfc}\left(\frac{(2n+2)L}{\sqrt{4\alpha_b t}} + \frac{x}{\sqrt{4\alpha t}}\right)\right]$$
$$+ \frac{2Km\sqrt{t}}{\beta+\beta_b}\sum_o^\infty (M)^n\left[\operatorname{ierfc}\left(\frac{2nL}{\sqrt{4\alpha_b t}} + \frac{x}{\sqrt{4\alpha t}}\right)\right.$$
$$\left. - \operatorname{ierfc}\left(\frac{(2n+2)L}{\sqrt{4\alpha_b t}} + \frac{x}{\sqrt{4\alpha t}}\right)\right] + mx \tag{34}$$

Here $\underline{M} = (\beta-\beta_b)/(\beta+\beta_b)$ and the other symbols are defined in table 1.

Equations (33) and (34) are most convenient to use for small values of time, but they converge for all times. Numerical values of the flux in the blanket divided by the undisturbed lunar flux are shown in figure 10 for

blankets of material SI-10 and SI-91 on dust (table 2(I)2) and substratum (table 2 (III)). In the most favorable case the flux in the blanket is less than 15% of the equilibrium flux after 1 year. This result is virtually independent of the To term; it arises mainly from the m term. Hence no matter how carefully the initial temperature of the blanket is matched to the mean temperature of the lunar surface, a major disturbance is caused by emplacement of the blanket, and it persists for years if the blanket is made of superinsulating material. The higher the conductivity of the substratum, the longer is the time required to reach equilibrium. The "plastic" blanket, on the other hand, achieves equilibrium within a year.

Thus we see that the two classes of time-dependent temperatures pose difficulties that appear to require mutually incompatible sets of blanket properties for their solution. In the examples given one must face either a large periodic fluctuation throughout the blanket, or a prohibitively long time for equilibrium to be established. It does not appear that the use of a blanket material with intermediate properties would solve the problem. One would then be confronted with both a large periodic fluctuation and a long time constant. The thickness of the blanket affects its thermal behavior in much the same way as its thermal diffusivity, so that no escape can be found by changing this parameter.

A final consideration about the blanket type of flux meter concerns its contact with the lunar surface. In all of the foregoing calculations it has been assumed that there is no contact resistance between the blanket and the lunar surface, a situation that is difficult to achieve in practice. The effect of uniform contact resistance is to reduce the effectiveness with which the periodic fluctuation is damped out in the blanket and to increase the time required to equilibrate with the lunar surface. Nonuniform contact resistance, which is likely to be encountered due to irregularities on the lunar surface, will in addition

cause thermal refraction within the dimensions of the blanket. This will cause the flux in the blanket to differ from point to point, necessitating a large number of temperature sensors to give a proper mean gradient. Readout is not necessarily complicated by such a requirement, since a single readout of many resistance elements in series and/or parallel to give an appropriate mean value would in all probability be feasible.

6. CONCLUSIONS

A. One-dimensional steady periodic temperatures.

A limited amount of information about the thermal properties of a layer can be obtained from a study of amplitude or phase of the thermal wave as a function of depth, if the effect of other layers is small. The latter condition can be recognized by the exponential decrease in amplitude with depth. Study of both amplitude and phase gives little or no information in addition to that provided by study of amplitude alone. When the properties of more than one layer influence the temperatures to an important degree, it may be possible to determine the properties of those layers penetrated completely by a hole. Extrapolation beyond the deepest observation of temperature is not reliable unless the depth to the next interface is accurately known independently.

B. Propagation of the thermal wave near a hole in the surface layer.

A hole or thin spot in the surface layer will let high-amplitude fluctuations leak into the substratum, where they may propagate laterally to some distance. This effect does not appear to be serious, however. The amplitudes are essentially unaffected by the presence of the hole a few meters away.

C. Thermal refraction due to irregular thickness of the surface layer.

This steady-state phenomenon is far more serious than the periodic disturbance discussed under B. Conditions very probably exist near the lunar surface which cause differences in flux of 50% or more because of thermal refraction. Such anomalies can be avoided by measuring heat flow at depths below regions causing refraction. Errors due to this effect can

largely be removed by taking the means of several closely spaced observations. It seems best to try to take advantage of both techniques, and to measure temperatures in the deepest holes practicable at several points at a given lunar site.

D. The blanket method of measuring lunar heat flow.

The following difficulties are recognized as standing in the way of a measurement of lunar heat flow by a blanket-type fluxmeter.

1. The flux is disturbed by thermal refraction due to the presence of the blanket. This effect can be kept small by choice of proper geometry for the blanket, and the correction is calculable.
2. The flux is disturbed if the albedo of the blanket does not match that of the lunar surface and a difference in mean temperature between the blanket and the surface is thereby created. This disturbance is serious if the mismatch in temperature exceeds a few tenths of degrees.
3. The blanket must be made of poorly conducting material in order to damp out the steady periodic temperature fluctuation in a reasonable thickness, and also to have a readily measurable thermal gradient set up by the lunar flux. But a blanket satisfying these requirements takes years to come into equilibrium with the lunar flux. A blanket having a manageable time constant associated with its emplacement does not satisfy the requirements imposed by the steady periodic fluctuations and the small value of flux to be measured.
4. The flux through the blanket may vary from point to point because of variable contact resistance with the lunar surface. A large number of temperature sensors would be necessary to measure a meaningful average flux.

Difficulties (2) and (3) in particular seem insuperable and make the blanket method unattractive for the measurement of lunar heat flow.

7. ACKNOWLEDGMENTS

The simplified treatment of the blanket was suggested by Dr. A. H. Lachenbruch of the U. S. Geological Survey. Many of the results in section 5 are due to him. I have benefitted from discussions with him and with Dr. Marcus G. Langseth of the Lamont Geological Observatory.

8. REFERENCES CITED

Carslaw, H. S. and J. C. Jaeger, 1959, Conduction of heat in solids, London, Oxford Univ. Press, 510 pp.

Hapke, B., 1964, Photometric and other laboratory studies relating to the lunar surface, in The lunar surface layer, J. W. Salisbury and P. E. Glaser eds., New York Academic Press, 532 pp.

Hibbs, A. R., 1963, A hypothesis that the surface of the moon is covered with needle crystals, Icarus, 2, 181-186.

Lachenbruch, A. H., 1957, Three-dimensional heat conduction in permafrost beneath heated buildings, U. S. Geol. Survey Bull. 1052-B, p. 51-69.

_____, 1959, Periodic heat flow in a stratified medium with application to permafrost problems, U. S. Geol. Survey Bull. 1083-A, p. 1-36.

Sinton, W. M., 1961, Temperatures on the lunar surface, in Physics and astronomy of the moon, Z. Kopal ed., New York, Academic Press, 538 pp.

Warren, C. R., 1963, Surface material of the moon, Science, 140, 188-190.

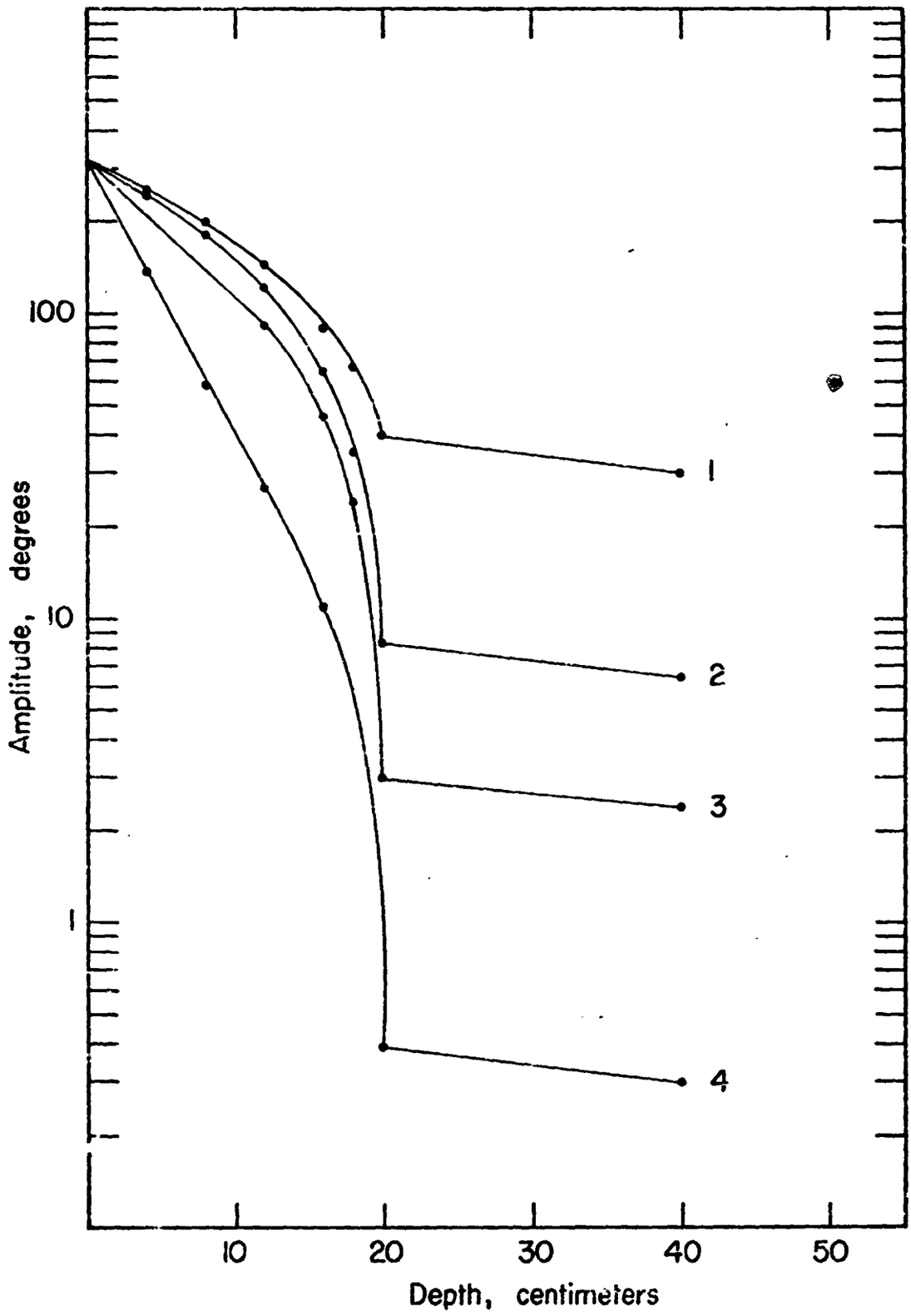

Figure 1a. Effect of properties of the surface material on amplitudes in a layer 20 cm. thick. Numbers beside the curves identify the rows in table 2 (I). Lower layer is substratum of table 2 (III).

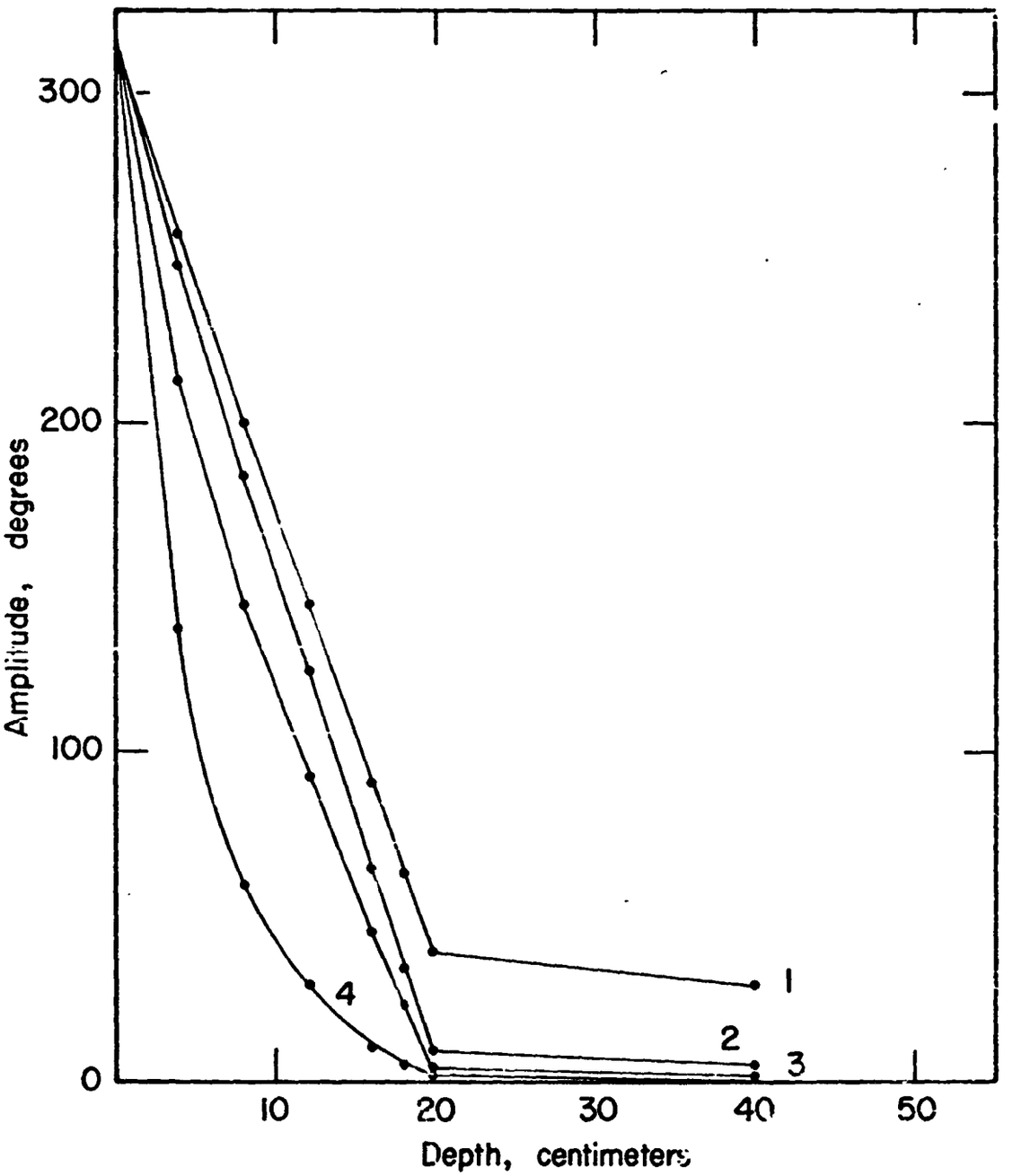

Figure 1b. Effect of properties of the surface material on amplitudes. Same as figure 1a except amplitude scale is linear.

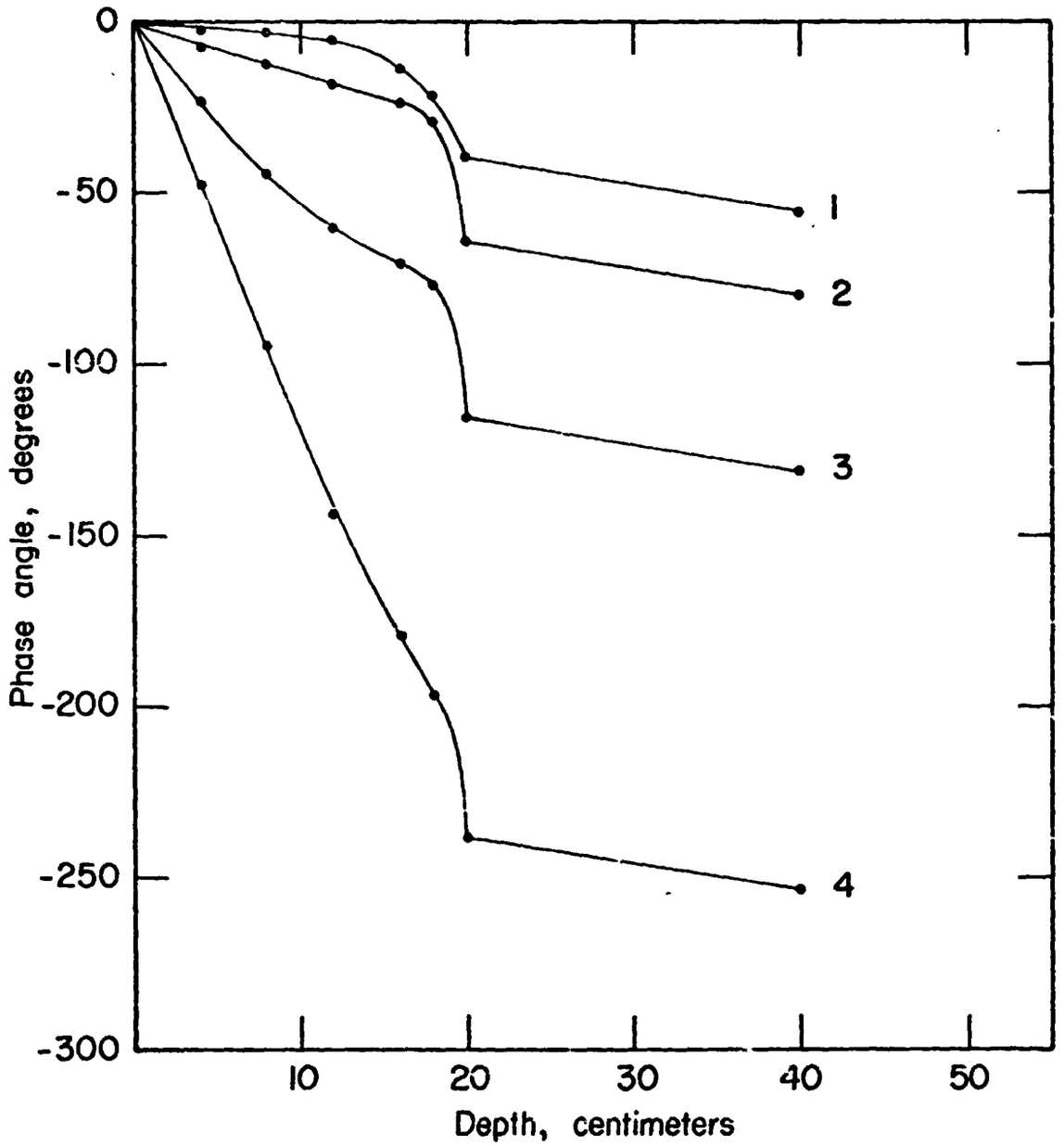

Figure 1c. Phase lags in surface layers of figure 1a.

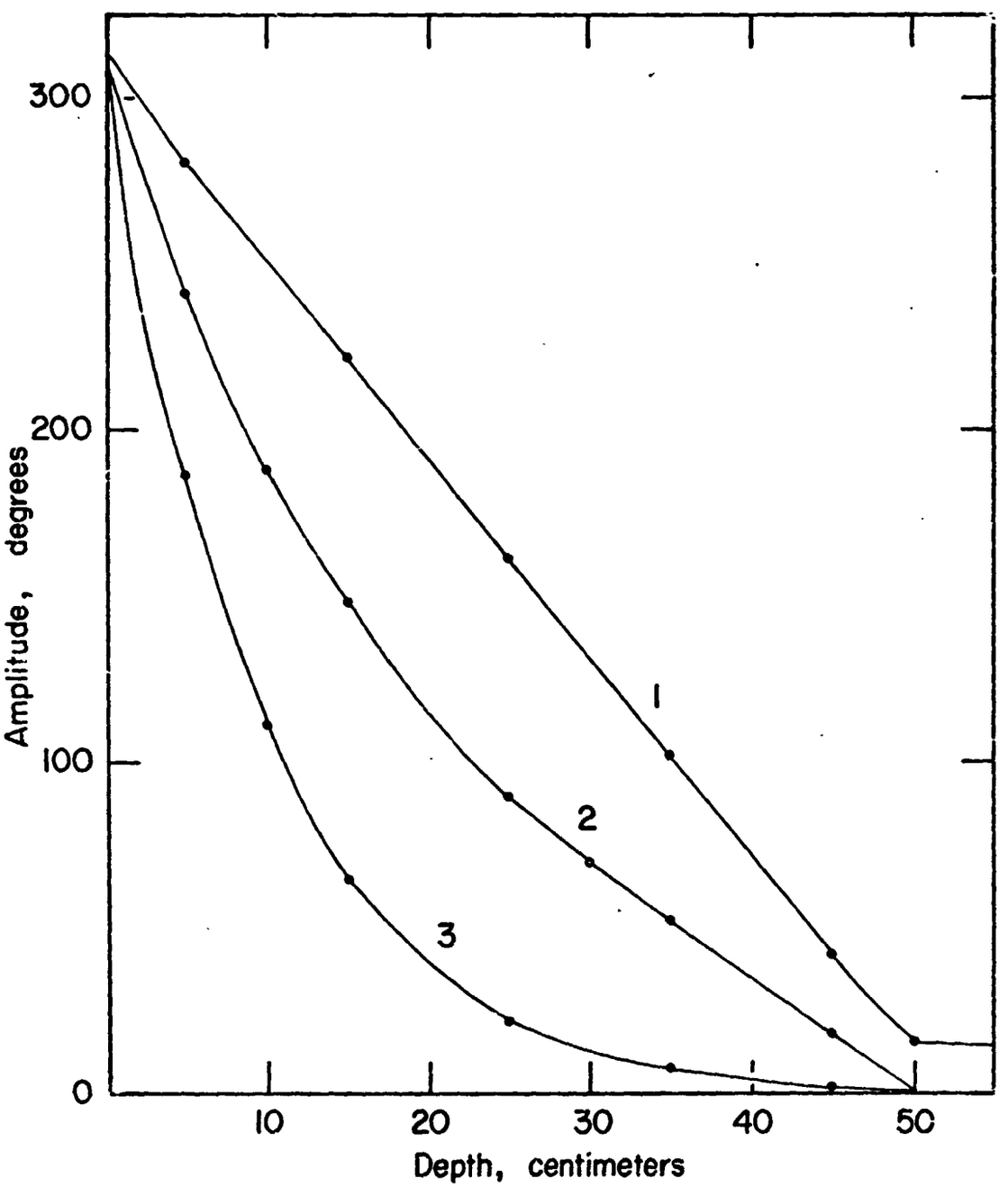

Figure 2. Amplitudes in a surface layer 50 cm. thick. Numbers beside the curves identify the rows in table 2 (I).

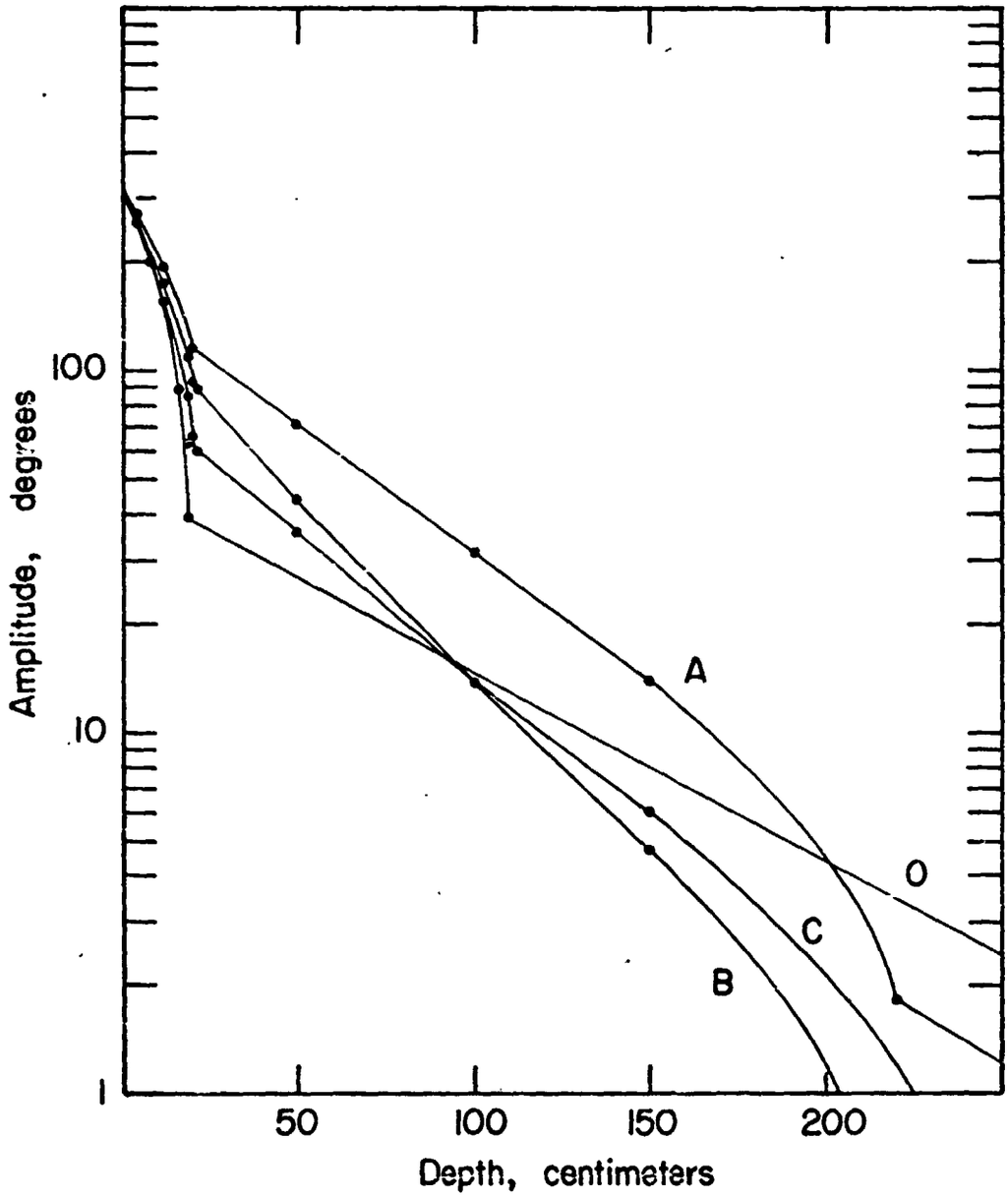

Figure 3a. Effect of properties of the intermediate layer on amplitudes. Upper layer 20 cm. thick of material I of table 2 (I). Curves A, B, C for 200 cm. thickness of materials A, B, C of table 2 (II). Curve O, no intermediate layer, surface material rests directly on substratum.

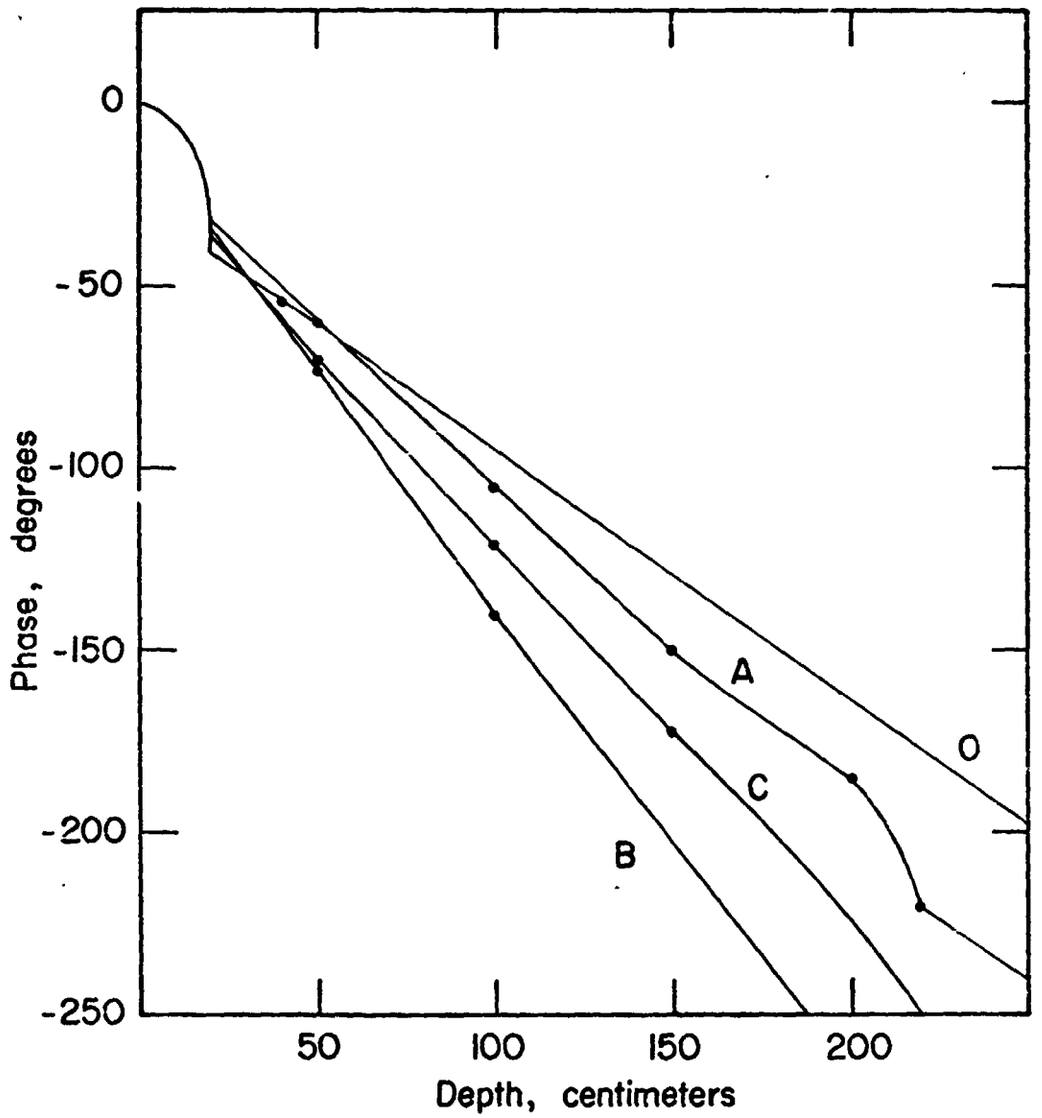

Figure 3 b. Phase lags in layers of figure 3 a.

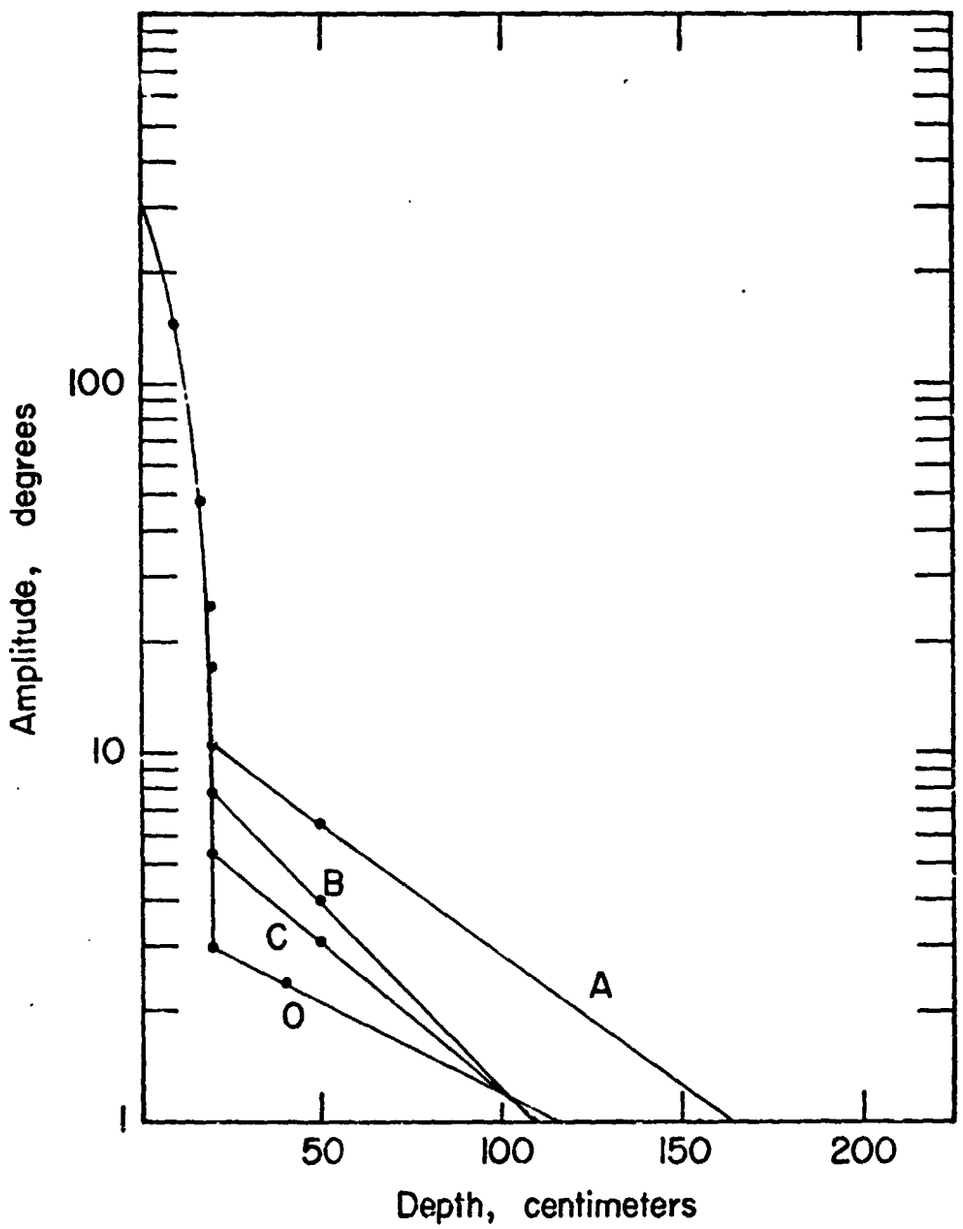

Figure 4 a. Effect of properties of the intermediate layer on amplitudes. Upper layer 20 cm. thick of material 3 of table 2 (I). Curves A, B, C for 200 cm of materials A, B, C of table 2 (II). Curve O, no intermediate layer, surface material rests directly on substratum.

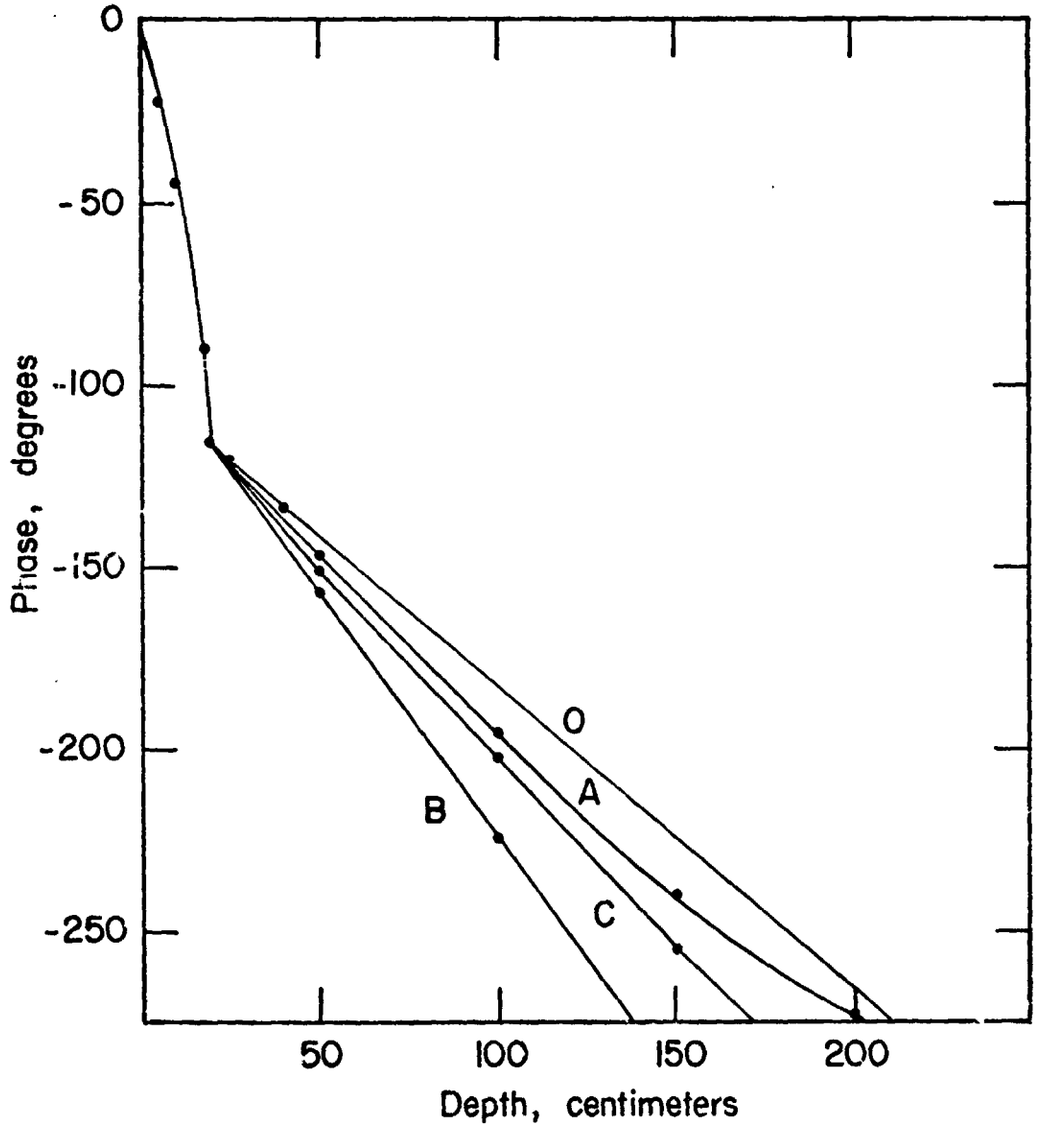

Figure 4 b. Phase lags in layers of figure 4 a.

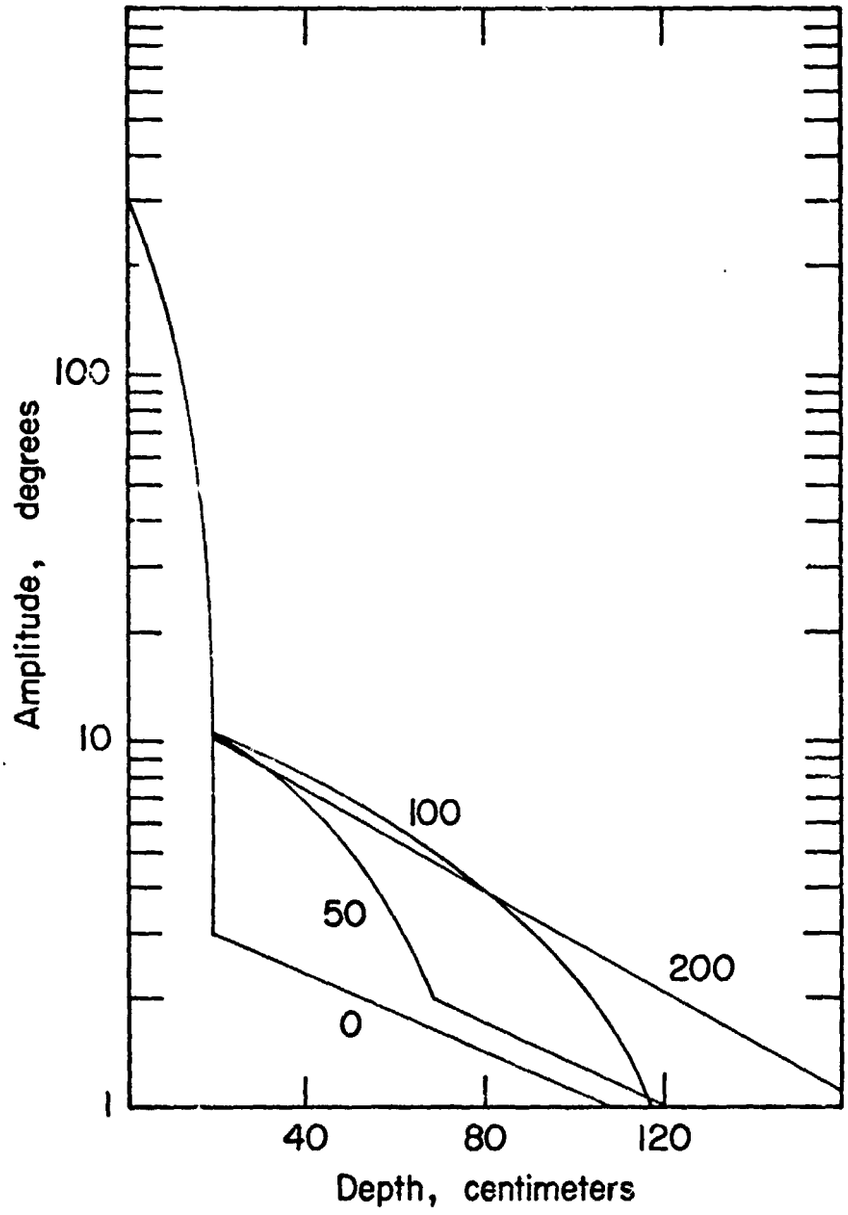

Figure 5. Effect of thickness of the intermediate layer on amplitudes. Upper layer 20 cm. thick of material 3 of table 2 (I), intermediate layer of material A of table 2 (II). Numbers beside curves give thickness of intermediate layer.

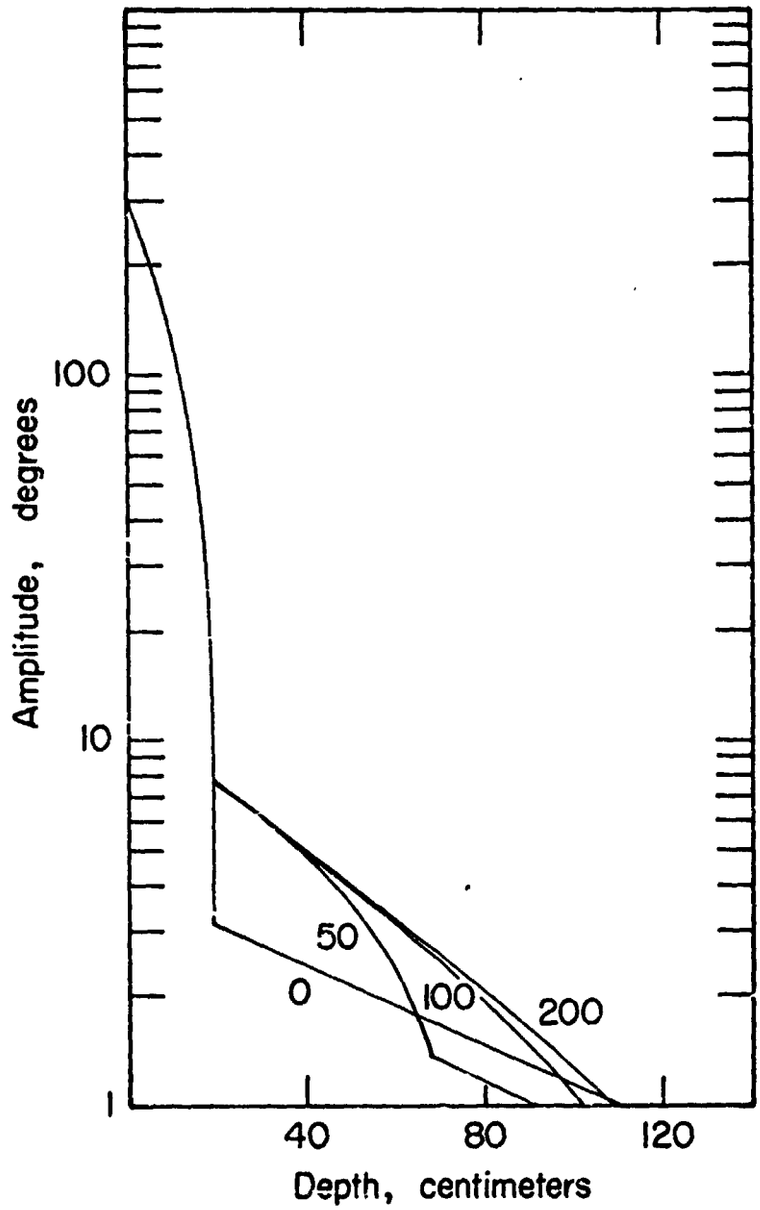

Figure 6. Effect of thickness of the intermediate layer on amplitudes. Upper layer 20 cm. thick of material 3 of table 2 (I), intermediate layer of material B of table 2 (II). Numbers beside curves give thickness of intermediate layer.

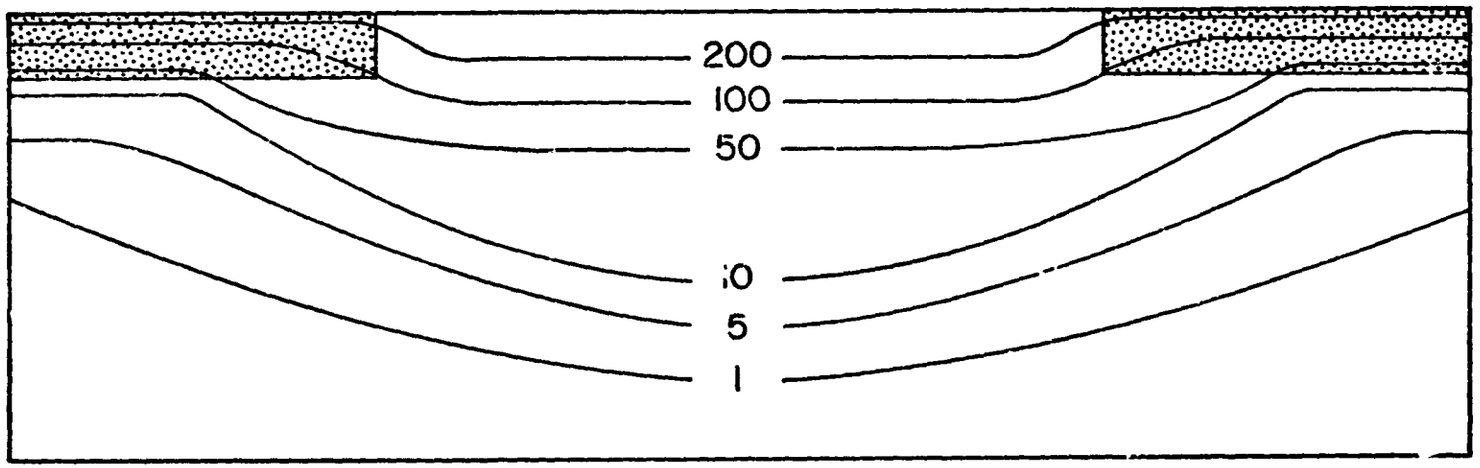

Figure 7. Amplitudes near a circular hole in the poorly conducting surface layer. Lines of constant amplitude are shown for a surface amplitude of 269° C, and a conductivity ratio of 10.

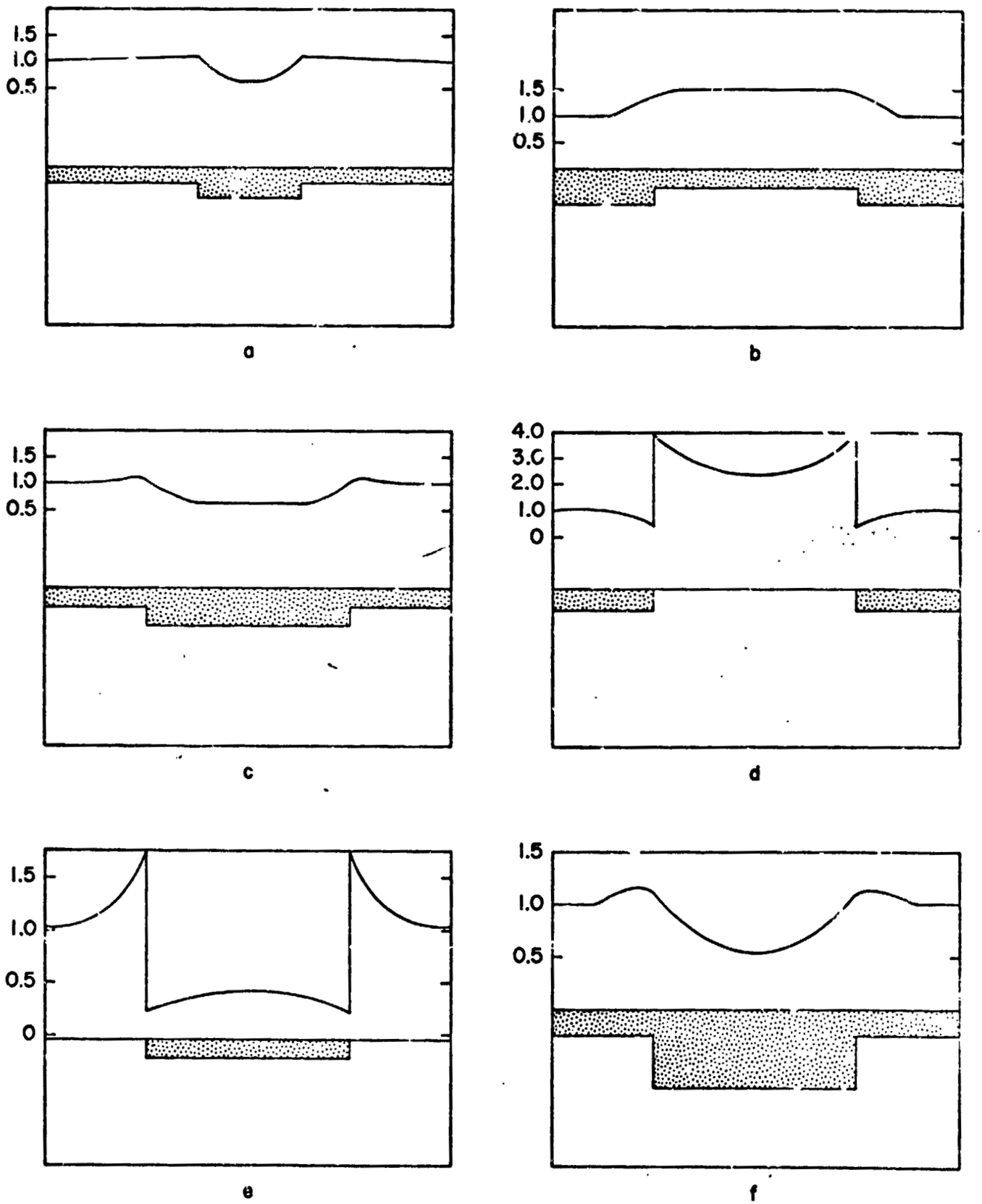

Figure 8. The effect of a number of configurations of the interface between the surface layer (stippled) and the substratum on heat flow. In all cases the protuberance has the shape of a right circular cylinder. The line at the top of each figure shows the ratio of flux at a given point to the flux at great distance from the irregularity for a conductivity contrast of 10. The configuration of layers is shown at the bottom of the figures.

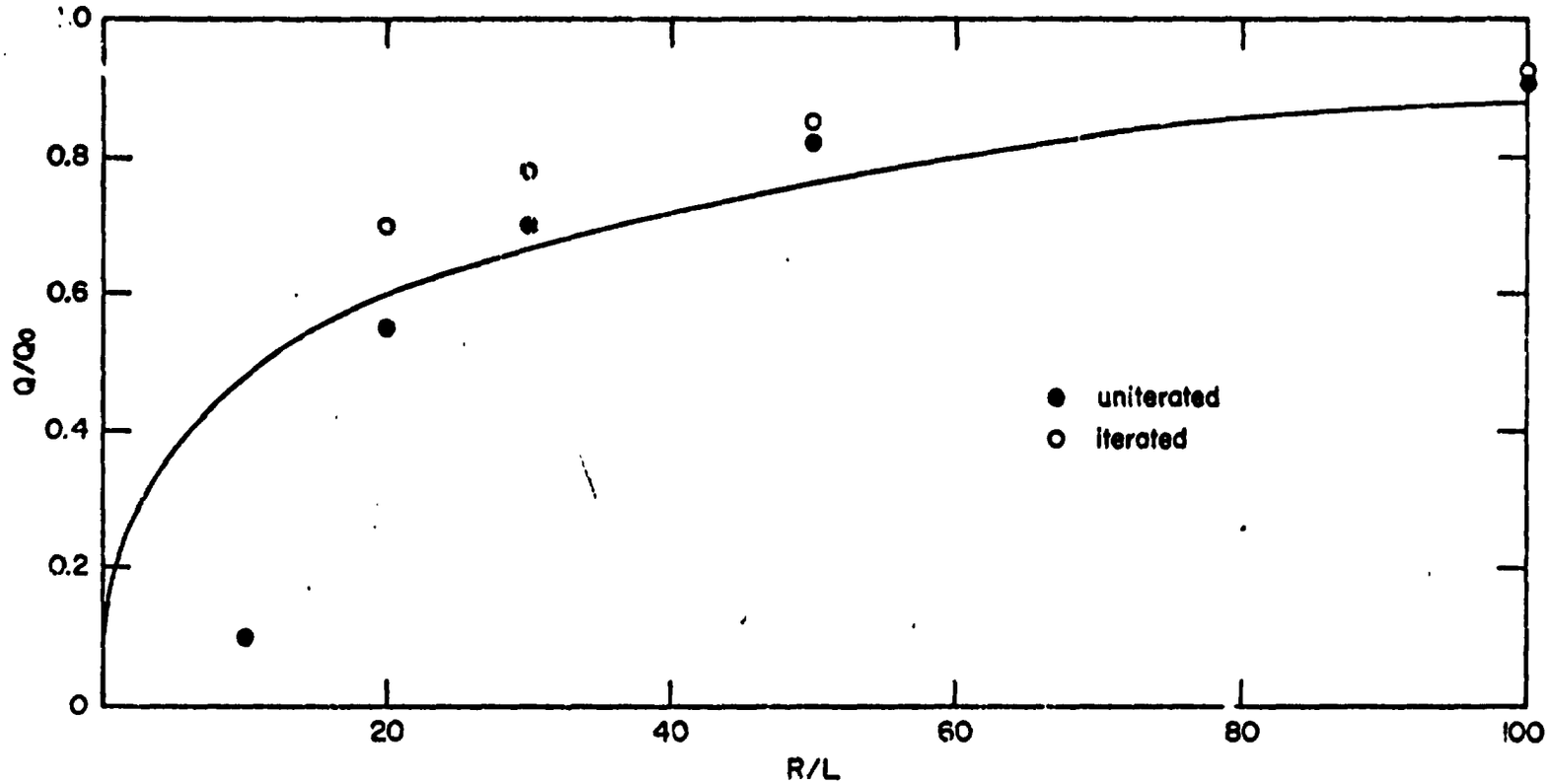

Figure 9. Comparison between the simple method of calculating the disturbance due to the blanket (equation 26) and the finite-difference calculation. The points were obtained from the equation with and without iterating the calculation and the line shows the finite-difference results.

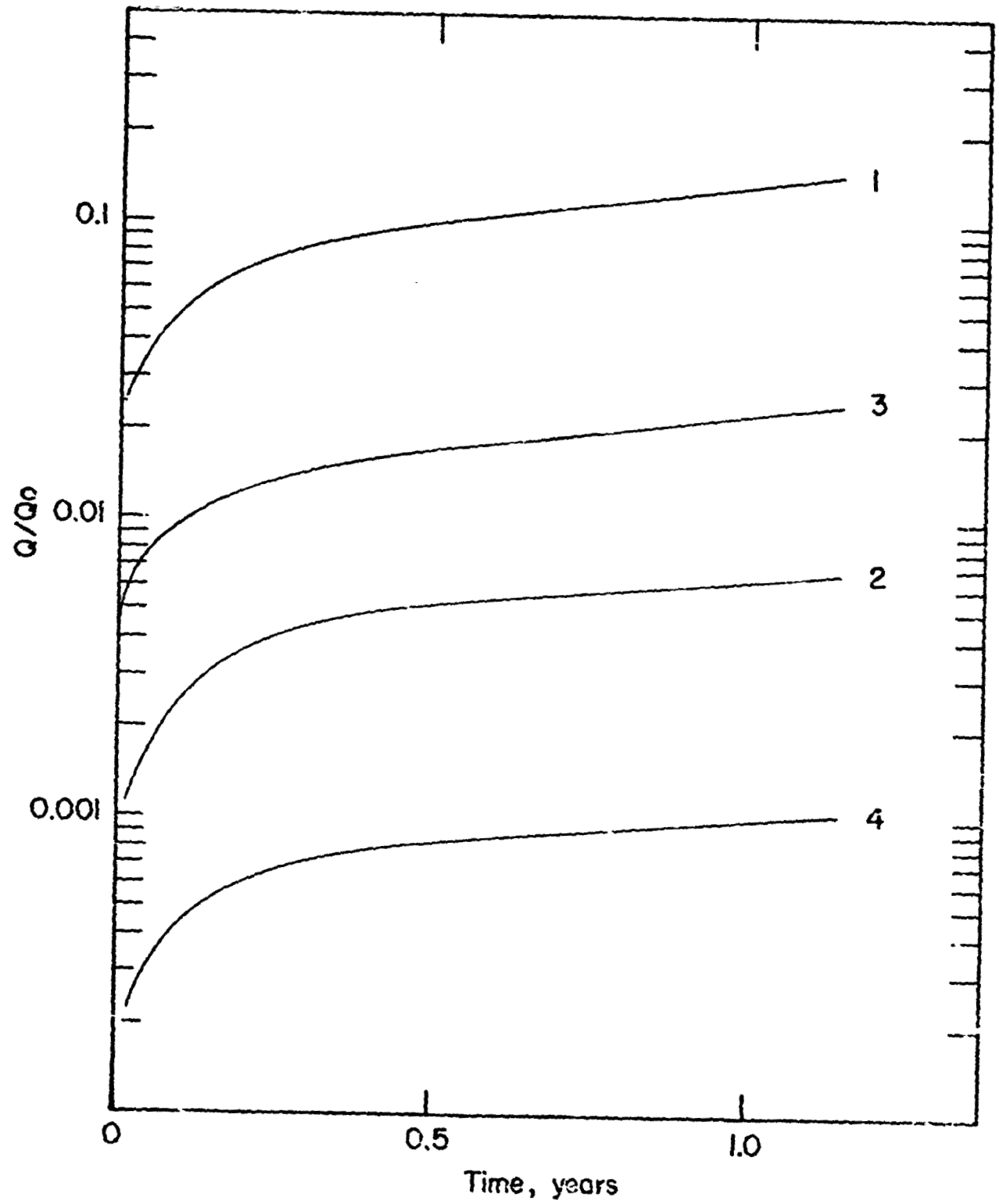

Figure 10. Ratio of transient to steady-state fluxes for times up to a year after blanket emplacement. Curves 1 and 2 for blanket of SI-10 material, curves 3 and 4 for SI-91 (table 2(IV)). Curves 1 and 3 for blanket resting on dust (table 2(I)2), and curves 2 and 4 for blanket resting on substratum (table 2(II)).

APPENDIX II

Numerical Simulation of the Conductivity Measurement

THE IN SITU MEASUREMENT OF LUNAR THERMAL CONDUCTIVITY

by Sydney P. Clark, Jr.

Interim Report

January 1967

Prepared under Grant No. NGR-07-004-039

Yale University

New Haven, Connecticut

NATIONAL AERONAUTICS AND SPACE ADMINISTRATION

Introduction

The measurement of heat flow at a lunar site requires knowledge of both the vertical thermal gradient and the local thermal conductivity. The former quantity can be measured more or less straight forwardly by a suitably instrumented probe emplaced in a drilled hole, but the latter presents special complications. In normal determinations of terrestrial heat flow, the conductivities of samples cored from the hole are measured in the laboratory. It is undesirable, and may even be impossible, to rely solely on this technique for lunar heat flow, since the sample may either be destroyed or may have its thermal properties seriously altered by the operations of collection and return to earth. Hence the determination of thermal conductivity *in situ* on the moon is clearly desirable and perhaps essential. This report deals with a preliminary study of a method of making this measurement which utilizes a cylindrical ring source. The results presented here form some of the fundamental criteria used in the design of a subsurface thermal probe for ALSEP by Arthur D. Little, Inc.

Theory

Consider a cylindrical hole of radius $\underline{R}$, infinite in length, containing a cylindrical probe, also of radius $\underline{R}$. Between $-\underline{Z}$ and $\underline{Z}$ the probe consists of a heater of thermal conductivity $\underline{k}_1$, density ρ_1, and heat capacity $\underline{c}_1$. For $|\underline{z}| > \underline{Z}$ the probe has thermal properties $\underline{k}_2$, ρ_2, and $\underline{c}_2$, and there is no thermal resistance at $\underline{z} = \pm \underline{Z}$. The lunar material surrounding the hole has thermal properties $\underline{k}_3$, ρ_3, and $\underline{c}_3$ and there is contact resistance at $\underline{r} = \underline{R}$ such that a temperature drop $\Delta\underline{T}$ occurs, given by $\Delta\underline{T} = \frac{\underline{k}_n \partial\underline{T}}{\underline{H} \partial\underline{r}}$ (the so-called radiation boundary condition). $\underline{k}_n$ would be k_1 at the outer surface of the heater, $\underline{k}_2$ at the outer surface of the probe, and $\underline{k}_3$ at the

inner surface of the hole. The temperature is initially zero everywhere, and heat is supplied uniformly over the surface of the heater at rate $\underline{Q}$ for time $o \leq \underline{t} \leq t_o$. We must find the temperature as a function of $\underline{r}$, $\underline{z}$, and $\underline{t}$.

The conditions set forth in the preceding paragraph completely specify a boundary value problem in heat conduction, but since they involve both radial and axial flow in a heterogeneous medium, they are intractable analytically. The problem was solved by finite differences in the following way. Consider intervals in space and time $\delta\underline{r}$, $\delta\underline{z}$, $\delta\underline{t}$, and intergers $\underline{i}$, $\underline{j}$, and $\underline{k}$ such that $\underline{z} = \underline{j}\delta\underline{z}$, $\underline{t} = \underline{k}\delta\underline{t}$, and $\underline{r} = \underline{i}\delta\underline{r}$ for $\underline{i} \leq I_1$ and $\underline{r} = (\underline{i} - 1)\delta r$ for $\underline{i} \geq \underline{I}_2 = \underline{I}_1 + 1$. The temperature may be regarded as a function of $\underline{i}$, $\underline{j}$, and $\underline{k}$. $\underline{I}_1\,\delta\underline{r} = \underline{I}_2\delta\underline{r} = \underline{R}$, the radius of the hole. However $\underline{T}(\underline{I}_1, \underline{j}, \underline{k}) \neq \underline{T}(\underline{I}_2, \underline{j}, \underline{k})$ because of the contact resistance, although the two points are only infinitesimally separated in space. On the other hand at $\underline{z} = \underline{Z} = \underline{J}\delta\underline{z}$, the temperature is continuous. Since the temperatures are symmetric about the axis of the cylinder and also about the plane $\underline{z} = o$, we need consider only positive values of $\underline{r}$ and $\underline{z}$.

The equations used in the finite-difference calculation depend on the points at which the temperature is to be obtained. Referring to the schematic space grid shown in Figure 1, let $\alpha_1 = \underline{k}_1/\rho_1 c_1$ be the thermal diffusivity in region 1, the heater, α_2 be the diffusivity in region 2, etc. Also, let $\underline{M}_n^{\underline{r}} = \alpha_n \delta\underline{t}/\delta\underline{r}^2$ and $M_n^{\underline{z}} = \alpha_n \delta\underline{t}/\delta\underline{z}^2$, where $n = 1, 2, 3$. Then we have on the axis

$$T(o, j, k + 1) = T(o, j, k)\,(1 - 4M_n^{\underline{r}} - 2M_n^{\underline{z}}) + T(1, j, k) \cdot 4M_n^{\underline{r}}$$

$$+ [T(o, j + 1, k) + T(o, j - 1, k)]M_n^{\underline{z}} \quad j \neq J,\ n = 1, 2, \qquad (1)$$

$$T(o, J, k+1) = T(o, J, k)\left[1 - \left(4\frac{\delta t}{\delta r^2} + 2\frac{\delta t}{\delta z^2}\right)\left(\frac{k_1 + k_2}{\rho_1 c_1 + \rho_2 c_2}\right)\right] + T(1, J, k) \cdot$$

$$\cdot 4\frac{\delta t}{\delta r^2}\frac{k_1 + k_2}{\rho_1 c_1 + \rho_2 c_2} + T(o, J+1, k) \cdot 2\frac{\delta t}{\delta z^2}\frac{k_2}{\rho_1 c_1 + \rho_2 c_2} +$$

$$+ T(o, J-1, k) \cdot 2\frac{\delta t}{\delta z^2}\frac{k_1}{\rho_1 c_1 + \rho_2 c_2} \qquad (2)$$

In the interiors of regions 1 and 2

$$T(i, j, k+1) = T(i, j, k)\,(1 - 2M_n^r - 2M_n^z) + [T(i, j+1, k) + T(i, j-1, k)]M_n^z$$

$$+ \left[\left(1 - \frac{1}{2i}\right) T(i-1, j, k) + \left(1 + \frac{1}{2i}\right) T(i+1, j, k)\right]M_n^r \qquad (3)$$

$$n = 1, 2,\ o < i < I_1,\ j \neq J.$$

and in region 3

$$T(i, j, k+1) = T(i, j, k)\,(1 - 2M_3^r - 2M_3^z) + [T(i, j+1, k) + T(i, j-1, k)]M_3^z$$

$$+ \left[\left(1 - \frac{1}{2i-2}\right)T(i-1, j, k) + \left(1 + \frac{1}{2i-2}\right)T(i+1, j, k)\right]M_3^r,$$

$$i > I_2 \qquad (4)$$

Along the outer skin of the heater and probe, we have, setting $f_n = \frac{2I_I - 1}{I_1 - 1/4} M_n^r$

$$g_n = \frac{2I_1 H \delta t}{(I_1 - 1/4)\rho_n c_n \delta r},$$

$$T(I_1, j, k+1) = T(I_1, j, k)\,(1 - 2M_n^z - f_n - g_n)$$

$$+ [T(I_1, j-1, k) + T(I_1, j+1, k)]M_n^z$$

$$+ T(I_1 - 1, j, k)f_n + T(I_1 + 1, j, k)g_n,\ n = 1, 2,\ j \neq J \qquad (5)$$

and

$$T(I_1, J, k+1) = T(I_1, J, k)\left(1 - \frac{2(K_1 + K_2)\delta t}{(\rho_1 c_1 + \rho_2 c_2)\delta z^2} - \frac{2I_1 - 1}{I_1 - 1/4}\,\frac{K_1 + K_2}{\rho_1 c_1 + \rho_2 c_2}\,\frac{\delta t}{\delta r^2}\right.$$

$$\left. - \frac{4I_1 h \delta t}{(I_1 - 1/4)(\rho_1 c_1 + \rho_2 c_2)\delta r}\right) + T(I_1, J-1, k)\,\frac{2H_1 \delta t}{(\rho_1 c_1 + \rho_2 c_2)\delta z^2}$$

$$+ T(I_1, J+1, k)\,\frac{2K_2 \delta t}{(\rho_1 c_1 + \rho_2 c_2)\delta z^2}$$

$$+ T(I_1 - 1, J, k)\,\frac{2I_1 - 1}{I_1 - 1/4}\,\frac{1 + 2}{\rho_1 c_1 + \rho_2 c_2}\,\frac{\delta t}{\delta r^2}$$

$$+ T(I_2, J, k)\,\frac{4I_1 H \delta t}{(I_1 - 1/4)(\rho_1 c_1 + \rho_2 c_2)\delta r} \qquad (6)$$

At times when the heater is on, terms accounting for its effect must be added to the right sides of (5) in region 1 and (6). We write

$$q = \frac{Q\delta t}{26.289\delta r^2 \delta z J(I_1 - 1/4)}, \qquad (7)$$

where the numerical factor includes the conversion from total power input, $\underline{Q}$, in watts to the units of c.g.s. and calories in which the thermal properties were expressed. Then a term $\underline{q}/\rho_1\underline{c}_1$ must be added in (5) and a term $\underline{q}/(\rho_1\underline{c}_1 + \rho_2\underline{c}_2)$ must be added in (6) to account for the heat input.

Along the wall of the hole in the lunar material we have, setting

$$\underline{f}' = \frac{2I_1 + 1}{I_1 + 1/4}\,M_3^r \quad \text{and} \quad g' = \frac{2I_1 H \delta t}{(I_1 + 1/4)(\rho_3 c_3 \delta r}\,,$$

$$T(I_2,\ j,\ k+1) = T(I_2,\ j,\ k)(1 - 2M_3^z - f' - g') + [T(I_2,\ j+1,\ k) +$$

$$+ T(I_2,\ j-1,\ k)]M_3^z + T(I_2+1,\ j,\ k)f + T(I_1,\ j,\ k)g \qquad (8)$$

Finally, along the junction between the heater and the rest of the probe

$$T(i,\ J,\ k+1) = T(i,\ J,\ k)\left[1 - \frac{2(K_1+K_2)\delta t}{(\rho_1 c_1 + \rho_2 c_2)\delta r^2} - \frac{2(K_1+K_2)\delta t}{(\rho_1 c_1 + \rho_2 c_2)\delta z^2}\right]$$

$$+ T(i,\ J+1,\ k)\frac{2K_2\delta t}{(\rho_1 c_1 + \rho_2 c_2)\delta z^2} + T(i,\ J-1,\ k)\frac{2K_1\delta t}{(\rho_1 c_1 + \rho_2 c_2)\delta z^2}$$

$$+ \left[T(i-1,\ J,\ k)\left(1 - \frac{1}{2i}\right) + T(i+1,\ J,\ k)\left(1 + \frac{1}{2i}\right)\right]$$

$$\frac{(K_1+K_2)\delta t}{(\rho_1 c_1 + \rho_2 c_2)\delta r^2},\quad 0 < i < I_1 \qquad (9)$$

Numerical stability proved to be a serious problem. In the interiors of the three regions, the stability criterion is

$$1 - 2M_n^z - 2M_n^r > 0,\quad n = 1,\ 2,\ 3. \qquad (10)$$

Depending on the relative thermal properties of probe, heater, and moon, a more stringent requirement may occur along the axis $\underline{i} = 0$, since here the criterion is

$$1 - 2M_n^z - 4M_n^r > 0,\quad n = 1,\ 2 \qquad (11)$$

But even with (10) and (11) satisfied, instability, which always originated at $\underline{i} = \underline{I}_1$ and $\underline{I}_2$, was sometimes encountered, particularly for relatively large values of $\underline{H}$. Imposing the additional constraints that

$$1 - 2M_n^z - f_n - g_n > 0,\quad n = 1,\ 2$$

and

$$1 - 2M_3^2 - f^2 - g^2 > 0,$$

did not remove the difficulty. This instability may result from the fact that the space step $\delta \underline{r}$ is effectively halved at $\underline{i} = \underline{I}_1$ and $\underline{I}_2$, but the matter remains unresolved. The time step, $\delta \underline{t}$, was simply reduced until the calculation became stable.

A second form of numerical difficulty, which may be termed semistability, was also encountered occasionally. Immediately after the heater was turned on or off, thus disturbing the system, the calculations oscillated, sometimes rather violently. The oscillations were damped, however, and the results gradually returned to a smooth trend with further cycles of iteration. This semistability could also be eliminated by reducing $\delta \underline{t}$, thus approximating more closely a smooth input of heat.

Models

A number of models of probes and of the lunar material have been subjected to numerical analysis. The results are extensive and only the more relevant ones have been selected for inclusion here. Thermal properties of 3 of the probes are shown in Table 1. The thermal conductivity of Probe 1 is too low to be practical from an engineering standpoint, but the lunar probe is expected to have properties in the range of Probes 5 and 6. Further calculations will be necessary when the final configuration of the lunar probe is established and its properties are measured.

Table 1. Thermal characteristics of probes.

No.	C	1	5	6
Heater				
k, cal/cm sec°C	0	3×10^{-7}	10^{-4}	10^{-3}
ρ, gm/cm^3	–	4×10^{-2}	0.5	0.5
c, cal/gm°C	–	0.2	0.2	0.2
Probe body				
k, cal/cm sec°C	0	3×10^{-7}	10^{-4}	10^{-3}
ρ, gm/cm^3	–	4×10^{-2}	0.5	0.5
c, cal/gm°C	–	0.2	0.2	0.2

Moon models are shown in Table 2. Three different thermal conductivities differing by factors of 10 were used, and for the lower conductivities, densities, and hence diffusivities, differing by a factor of 4 were considered. These models cover the range of values considered likely for material close to the lunar surface. The ability of a probe to discriminate between them is then a measure of its suitability.

Table 2. Thermal models of moon.

No.	k, cal/cm sec°C	ρ, gm/cm^3	c, cal/gm°C
1	10^{-5}	0.5	0.2
2	10^{-5}	2.0	0.2
6	10^{-3}	1.6	0.2
7	10^{-4}	0.5	0.2
8	10^{-4}	2.0	0.2

Another parameter entering the calculations is the contact resistance, measured by the quantity $\underline{H}$. For purely radiative contact $H = 5.5 \times 10^{-12} \underline{E}\underline{T}^3$, where E is the emissivity. With blackbody conditions $\underline{H} = 4.4 \times 10^{-5}$ at 200°K which is close to the mean lunar temperature. This is about the lowest value that $\underline{H}$ can attain, and it is an interesting case to consider because the probe may be designed to assure purely radiative coupling. $\underline{H}$ can then be calculated with confidence, whereas it otherwise remains an unknown parameter the value of which must somehow be extracted from the temperature-time curve. The effect of varying $\underline{H}$ was examined by making some runs with it set at 10 times the radiative value.

The lunar probes are to be about 1.9 cm in diameter. The quantity $\delta\underline{r}$ was taken to be 0.475 cm, which places the probe skin at $\underline{i} = 2$, and $\delta\underline{z}$ was taken equal to $\delta\underline{r}$. This is a rather coarse grid, but no refinement of it was made in these preliminary studies. The simulation of a 14-hour lunar experiment required over 30 minutes on a 7094 in unfavorable cases, and it is not worthwhile to choose smaller space steps (which requires reduction of the time step as well to maintain stability) until more than hypothetical values of the probe parameters are available.

The length of the heater was taken equal to its diameter, 1.9 cm. In rough design calculations it may be desirable to approximate the probe configuration using the exact solution for radial flow from a spherical heat source, and the "square" shape chosen for the heater gives the closest possible approximation to a sphere. Thus the results of this work may be compared directly with those obtained from the spherical approximation. It should be noted that in the latter approximation no account of different thermal properties between the body of the probe and the lunar material can be taken.

Numerical results

It is helpful at the outset to consider the solution for an infinite cylindrical source of heat in an infinite medium. In this case the temperatures depend on the thermal conductivity and thermal diffusivity of the medium, and on the contact resistance. One could hope that the dependence on diffusivity could be removed by heating until the temperatures became steady, but with this geometry there is no steady state. The temperature of the source continues to rise indefinitely. With a heater of finite length a steady state is reached; this was an initial reason to prefer the geometry adopted here to the "line source" geometry, because the possibility exists of eliminating the diffusivity as a factor upon which the temperature depends. Another attractive feature of the present configuration is its relatively low power requirement. A line source demands a certain amount of power per unit length to produce a given temperature rise. Hence a long source requires high power. In the present case, it was found that 2 milliwatts input power gave adequate temperature rises at the heater, and this value for the heat input was used in all the calculations.

The first calculations were aimed at investigating the possibility of achieving a steady state. Results are shown in Figure 2. In this figure and those following, the temperatures are those of the outer surface of the probe. In actual lunar probes the temperature sensors will be located on the axis, but the temperature difference between these 2 points is insignificant for present purposes. It is clear from the figure that for the lower values of $\underline{K}$ the steady state is not achieved after 14 hours, and several days of heating may be required to attain it if $\underline{K}$ is less than 10^{-4}. If $K = 10^{-3}$ a few hours suffice. The probe is evidently

capable of discriminating between various values of $\underline{K}$, particularly if the heater is operated at low power levels for a long time. The discrimination is best at low $\underline{K}$, and heating should last for the order of a day or more for optimum results.

Similar curves for the case of 1/10 as much contact resistance are shown in Figure 3. The discrimination is somewhat better than in Figure 2, and the curves have a different shape. The sharp initial rise in temperature is much reduced. In Figure 4 the results for a probe of higher conductivity are shown; the discrimination is not as good as in Figure 2. Clearly the thermal conductivity of the probe should be kept as low as possible.

These results show that it is likely that the temperature rise recorded during the lunar experiment will depend on the 3 quantities $\underline{K}$, α, and $\underline{H}$. Some process of curve fitting must be used to determine their values. This may be unsatisfactory since many combinations of parameters may give virtually identical results. It is therefore important to try to extract more information from the experiment, and an obvious way to do this is to record the temperatures at more than one point along the probe. The temperature rise at a point on the surface of the probe 8 cm from the center of the heater is shown in Figures 5 and 6. Figure 5 is for a probe of unrealistically low $\underline{K}$, but it shows the large differences in rise time that result from the different moon models. Intuitively one would expect the curves to be highly sensitive to α and this is born out by the difference between curves 1 and 2 of Figure 6. The rise times are about the same for the cases shown there, in which the conductivity of the probe is realistic. But if the moon is a better conductor than the probe discrimination still exists at short times, although it is not well-shown on a plot to the scale of Figure 6. Since this is just the

range of conductivity at which the temperatures at the center of the heater lose discrimination, complementary information can be obtained from the second sensor.

So far we have confined the discussion to times when the heater was turned on. But a number of short-term numerical experiments have been done in which the heater was turned on for only half the time. The durations of the tests were about ½ hour. The results were that the appearances of the cooling curves were virtually identical to the heating curves, but of course inverted and displaced in time. Thus there is no new information to be obtained from the cooling curves. On the other hand, following the cooling curve in effect constitutes repeating the heating experiment, but without the necessity of expending heater power. It is always desirable to repeat experiments if only to get better statistical control.

Operations on the moon

All lunar experiments must wait until drilling disturbances have died out near the hole. The thermal gradient will be determined next and then the heater will be turned on at low power (~ 2 milliwatts). The duration of the heating cycle will be determined by the conductivity encountered. The heater will then be turned off and the cooling curve followed until ambient conditions have essentially reestablished themselves. Then, especially if a high lunar thermal conductivity is indicated by this experiment, a second heating period will be initiated. The heater power will be higher (20 milliwatts or more) so that the second sensor, displaced along the probe from the heater, will record a readily measured temperature rise. By a process of curve fitting, which is not completely thought out as yet, the quantities $\underline{K}$, α, and $\underline{H}$ will be determined. The first 2 of these automatically yield a value of $\rho\underline{c}$, which

can be compared with the value measured on returned material to give a rough check on the internal consistency of the results. An alternative scheme would be to assure that $\underline{H}$ is known independently e.g. by making certain of radiative coupling alone; then only $\underline{K}$ and α need be obtained from the temperature curves and the accuracy of the measurements will be increased.

Conclusions

1. It appears feasible to measure lunar thermal conductivity using a cylindrical ring source of heat.
2. It is desirable to have 2 heating cycles, the first at a power level of a few milliwatts and the second at 10 or more times that power.
3. The duration of each heating will range from a few hours to a few days, depending on the lunar conductivity. The use of 2 sensors and 2 power levels could materially reduce the amount of heating time required.
4. There is something to be said for assuring radiative coupling to the moon so that the contact resistance can be calculated with confidence. Otherwise it represents a third unknown parameter to be determined from the temperature curves. Some discrimination of lunar conductivity is lost by this procedure, but nevertheless more accurate results will probably be obtained.
5. The best way of reducing the lunar data remains to be determined.

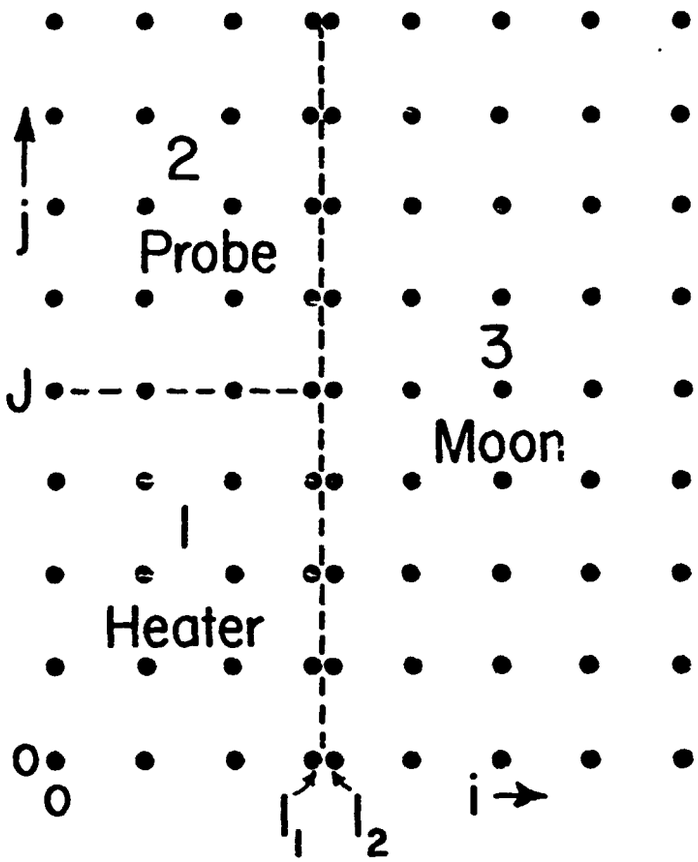

The grid used in the finite-difference approximation.

Fig. 1

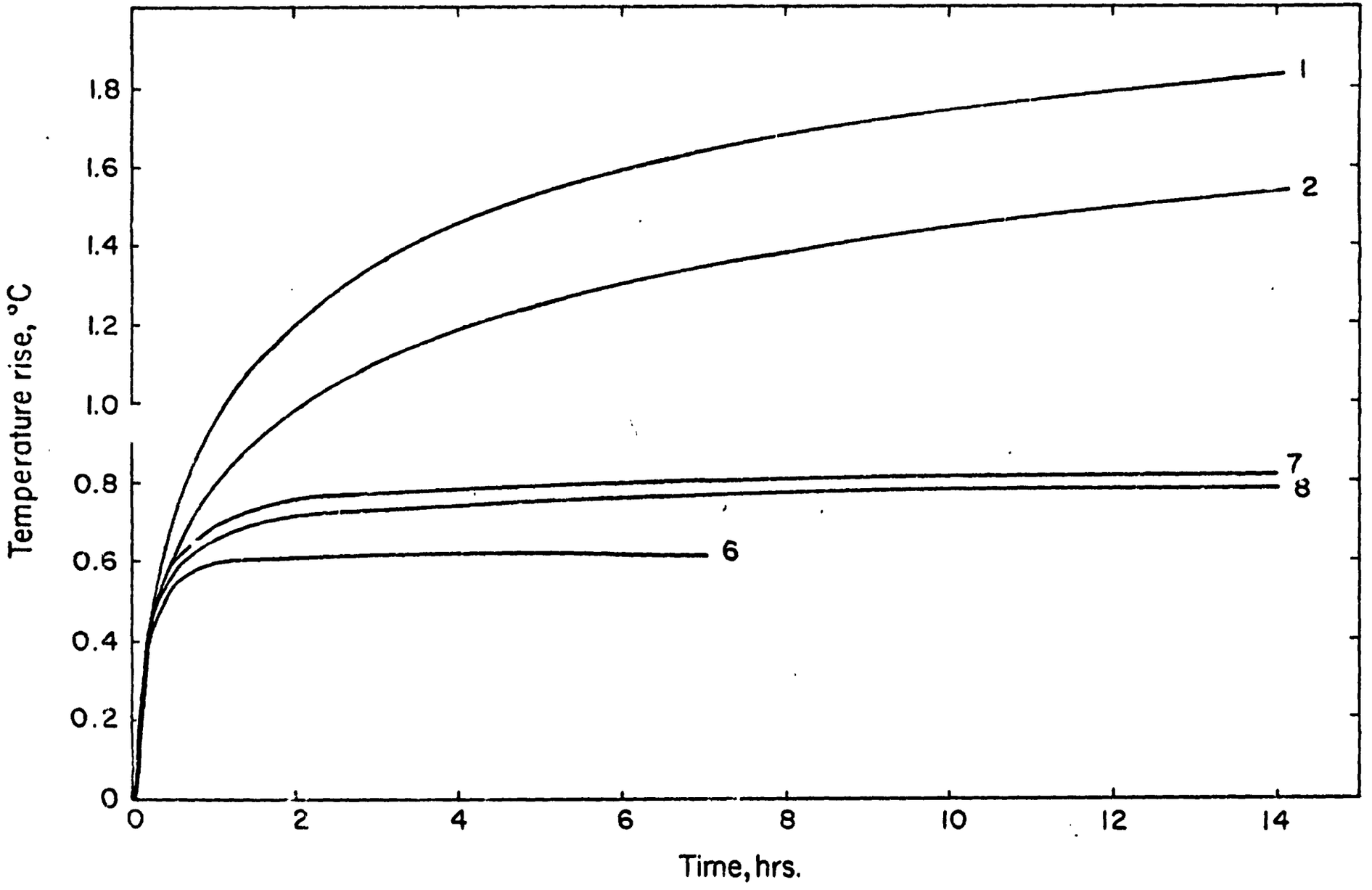

Temperature rise at the center of the heater. Probe 5, radiative coupling. Numbers beside the curves refer to moon models (Table 2).

Fig. 2

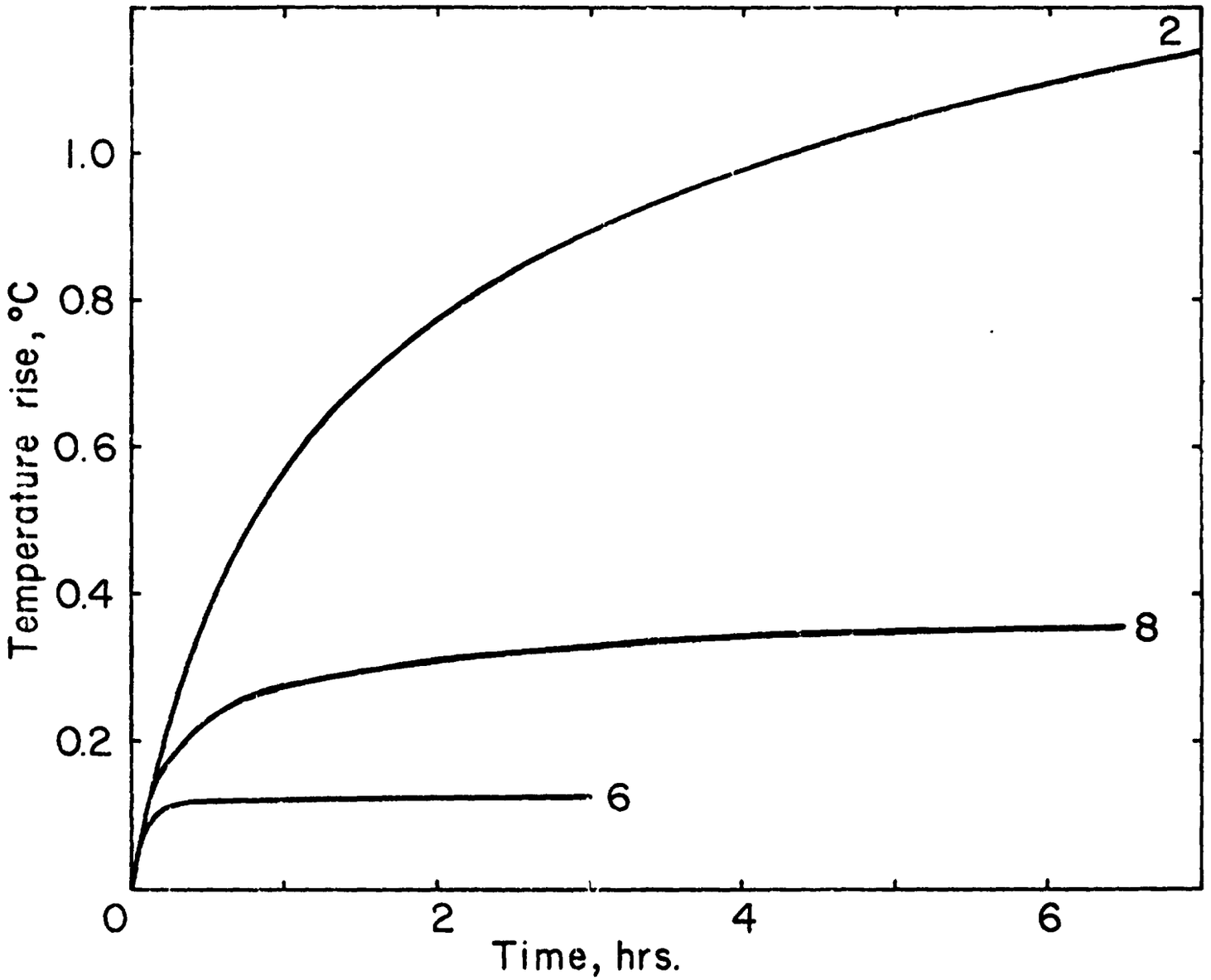

Temperature rise at the center of the heater. Probe 5, 10 times radiative coupling. Numbers beside the curves refer to moon models (Table 2).

Fig. 3

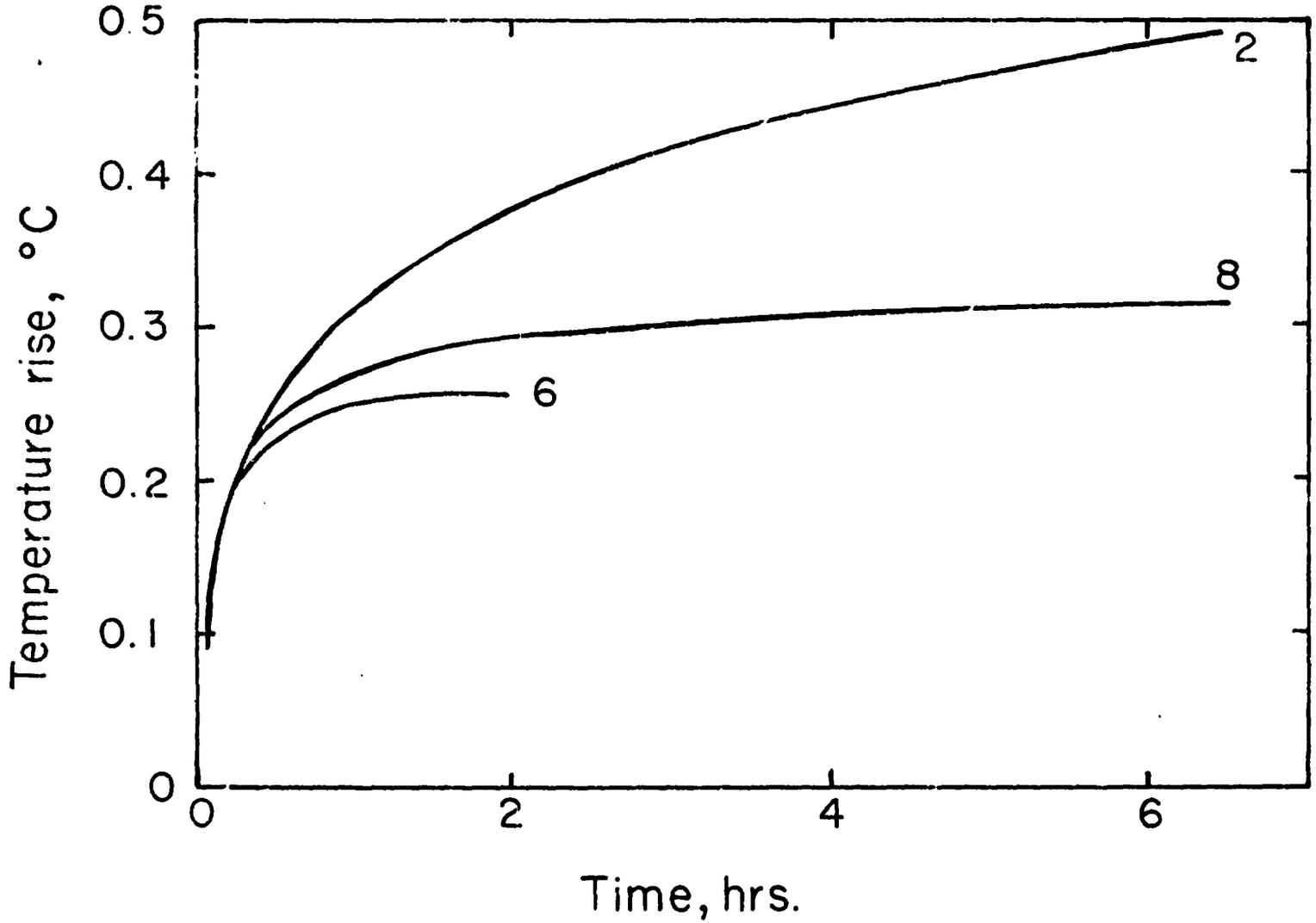

Temperature rise at the center of the heater. Probe 6, radiative coupling. Numbers beside the curves refer to moon models (Table 2).

Fig. 4

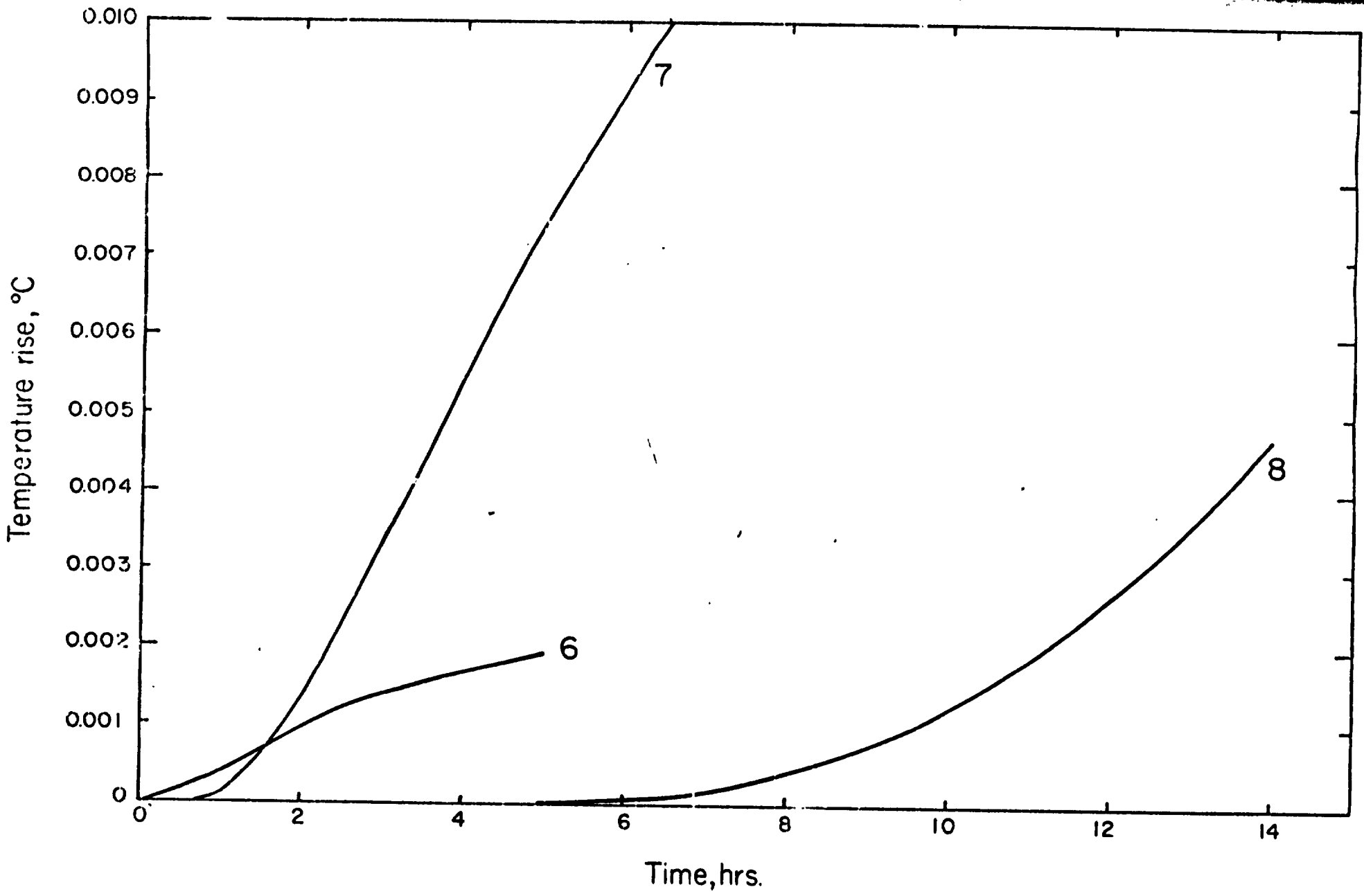

Temperature rise 8 cm from the center of the heater. Probe I, radiative coupling. Numbers beside the curves refer to moon models (Table 2).

Fig. 5

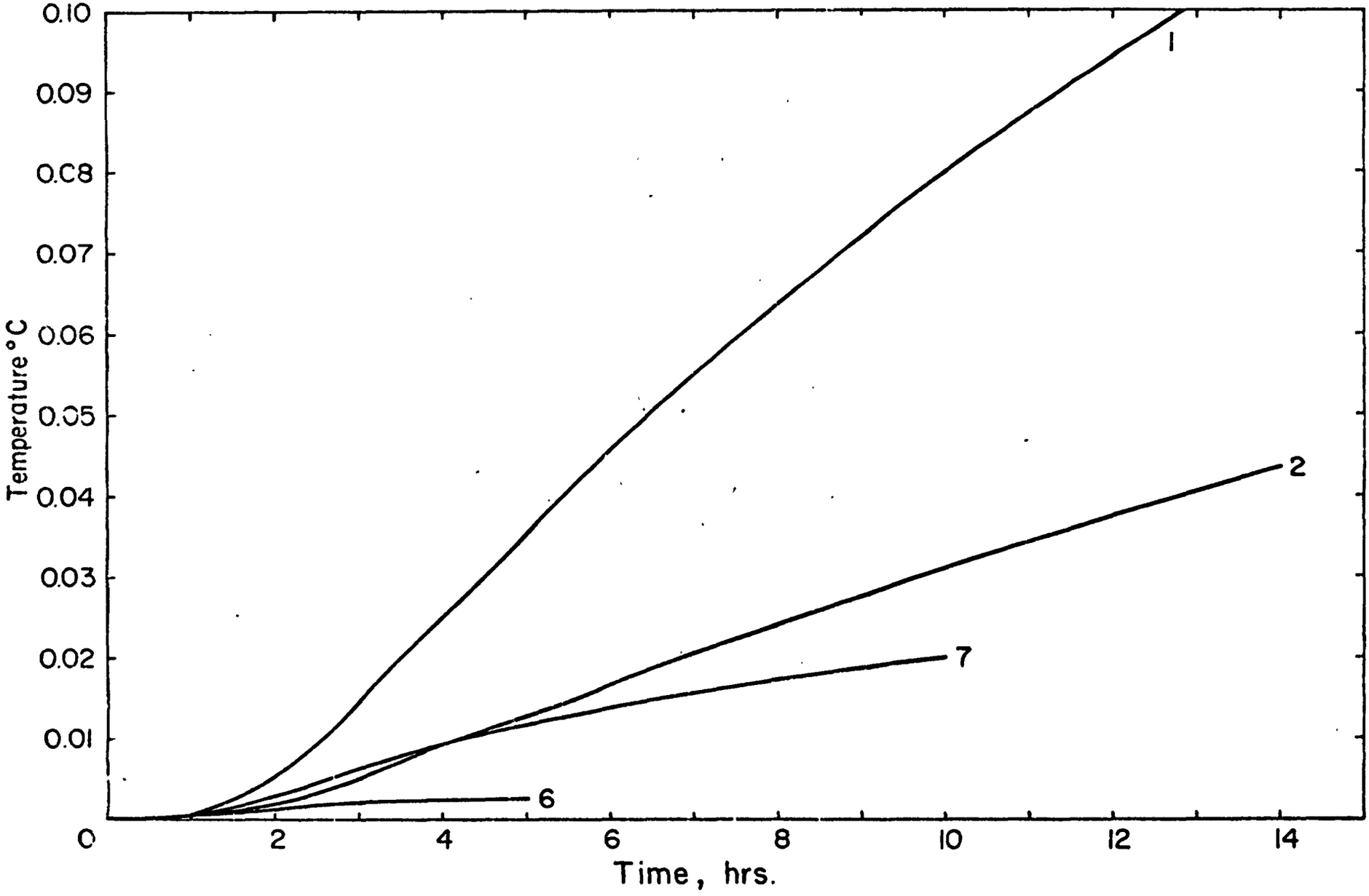

Temperature rise 8cm from the center of the heater. Probe 5, radiative coupling. Numbers beside the curves refer to moon models (Table 2)

Fig. 6

APPENDIX III

Results of the Apollo 15 and 17 Missions from the Preliminary Science Reports

Apollo 15 Preliminary Science Report

11. Heat-Flow Experiment

Marcus G. Langseth, Jr.,[a†] *Sydney P. Clark, Jr.,*[b] *John L. Chute, Jr.,*[a]
Stephen J. Keihm,[a] *and Alfred E. Wechsler*[c]

The purpose of the heat-flow experiment is to determine the rate of heat flow from the lunar interior by temperature and thermal-property measurements in the lunar subsurface. Heat loss is directly related to the internal temperature and the rate of internal heat production; therefore, measurements of these quantities enable limits to be set on long-lived radioisotopic abundances (the chief source of interior heating), the internal temperature, and the thermal evolution of the Moon.

Preliminary analysis of the data from one heat-flow probe indicates that the heat flow from depth below the Hadley Rille site is 3.3×10^{-6} W/cm^2 (±15 percent). This value is approximately one-half the average heat flow of the Earth. Further analysis of data over several lunations is required to demonstrate that this value is representative of the heat flow at the Hadley Rille site. Subsurface temperature at a depth of 1 m below the surface is approximately 252.4 K at one probe site and 250.7 K at the other site. These temperatures are approximately 35 K above the mean surface temperature and indicate that the thermal conductivity in the surficial layer of the Moon is highly temperature dependent. Between 1 and 1.5 m, the rate of temperature increase as a function of depth is 1.75 K/m (±2 percent) at the probe 1 site. In situ measurements indicate that the thermal conductivity of the regolith increases with depth. Thermal-conductivity values between 1.4×10^{-4} and 2.5×10^{-4} W/cm-K were determined; these values are a factor of 7 to 10 greater than the values of the surface conductivity. Lunar-surface brightness temperatures during the first lunar night have been deduced from temperatures of thermocouples above and on the lunar surface. The cooldown history after sunset suggests that a substantial increase in conductivity occurs at a depth on the order of several centimeters. Temperature measurements were also recorded during the total eclipse on August 6, 1971.

[a]Lamont-Doherty Geological Observatory.
[b]Yale University
[c]Arthur D. Little, Inc.
[†]Principal investigator.

EXPERIMENT CONCEPT AND DESIGN

Heat Budget in the Surface Layer of the Moon

The temperature and the heat flux at the surface of the Moon are determined mainly by the solar energy impinging on the surface during one-half of the 29.5-day lunation cycle. During the lunar day, the surface temperature rises to approximately 380 K, which results in heat flow into the subsurface. After lunar sunset, the surface temperature drops to nearly 100 K, and heat flows out of the subsurface and is lost by radiation into space. These very large temperature excursions, in part, are a result of the extremely low thermal conductivity and volumetric heat capacity of the fine rock powders that mantle most of the lunar surface (ref. 11-1) and, in part, are a result of the very tenuous atmosphere of the Moon. The low thermal conductivity of the bulk of the regolith (ref. 11-2) strongly inhibits the flow of energy into and out of the subsurface. At a depth of approximately 50 cm, the large surface variation of 280 K is attenuated to a nearly undetectable amplitude.

At low lunar latitudes, the surface temperature, averaged over one lunation, is approximately 220 K. This mean surface temperature is determined by the balance of solar energy flowing into and energy radiated out of the surface during a complete lunation. The mean temperature in the subsurface (at decimeter depths) may be higher than the mean

surface temperature by a few tens of degrees. As will be shown in more detail later in this section, the mean subsurface temperature at the Hadley Rille site is considerably higher than the mean surface temperature. This increase in mean temperature is a result of the important role of heat transfer by radiation in the fine powders on the surface. The efficiency of radiative heat transfer between particles varies in proportion to the cube of the absolute temperature (ref. 11-3); consequently, during the lunar day, heat flows more readily into the Moon than it flows out during the night. The subsurface heat balance, over one lunation, requires that a substantial steady-state heat loss be maintained in the upper several centimeters of lunar material to eliminate the excess heat that penetrates during the day (ref. 11-4). This outward heat flow causes a steep downward increase in mean temperature that extends to a depth of a few decimeters, the depth to which diurnal waves penetrate.

At depths greater than those to which diurnal waves penetrate, the thermal regime is dominated by heat flow from the lunar interior. This flow results from high interior temperatures and, in the subsurface, is directly proportional to the increase of temperature with depth (the vertical temperature gradient) and to the thermal conductivity. These quantities are related by the equation

$$F_z = -k \frac{dT}{dz} \qquad (11\text{-}1)$$

where F_z is the vertical component of the heat flow, k is the thermal conductivity, T is the temperature, and z is the depth. The average heat flow of the Earth has been determined to be 6.2×10^{-6} W/cm^2 by numerous measurements (ref. 11-5). Estimates of the lunar heat flow, based on microwave emission from the Moon, have ranged from 1.0×10^{-6} W/cm^2 (ref. 11-6) to 3.3×10^{-6} W/cm^2 (ref. 11-7), or one-sixth to one-half the Earth heat flow. Thermal-history calculations, based on chronolitic- and terrestrial-isotope abundances for the Moon (ref. 11-8), result in heat-flow estimates of 1×10^{-6} to 2.5×10^{-6} W/cm^2 for this period in the lunar history. Because of the extremely low conductivity of the regolith, even these very low heat flows would result in gradients ranging from a few tenths of a degree per meter to a few degrees per meter.

Instrument Design

The essential measurements for determining heat flow are made by two slender temperature-sensing probes that are placed in predrilled holes in the subsurface, spaced approximately 10 m apart. Two probes enable two independent measurements of the heat flow to be made in order to gain some knowledge of the lateral variation of heat flow at the Hadley Rille site. Each probe consists of two nearly identical 50-cm-long sections (fig. 11-1). Each section of each heat-flow probe has two accurate (±0.001 K) differential thermometers that measure temperature differences between points separated by approximately 47 and 28 cm. With these thermometers, a measurement (with an accuracy of ±0.05 K) of absolute temperature at four points on each probe section also can be made.

Additional temperature measurements are provided by four thermocouple junctions in the cables that connect each probe to the electronics unit. The thermocouple junctions are located at distances of approximately 0, 0.65, 1.15, and 1.65 m from the topmost gradient sensors (fig. 11-1). The reference junction for these thermocouples is thermally joined to a platinum-resistance reference thermometer, which is mounted on the radiator plate of the electronics unit. The temperature measurements obtained from the heat flow experiment are summarized in table 11-I.

The differential thermometers consist of four platinum resistance elements wired in a bridge configuration (fig. 11-2). The bridge is excited by successive 2.6-msec, 8-V pulses, first of one polarity and then of the other. The output voltage, the excitation voltage, and the bridge current are measured and used to determine the absolute temperature and the temperature difference. The ratio of bridge output voltage to excitation voltage and the bridge resistance are calibrated for 42 different pairs of temperature and temperature-difference values. The accuracy of these calibrations is better than the accuracies specified in table 11-I. The thermocouples are calibrated at four temperature points, and the reference bridge is calibrated at five temperature points.

Conductivity measurements are made by means of heaters that surround each of the eight gradient-bridge sensors. The experiment is designed to measure conductivity in two ranges: a lower range of $1 \times$

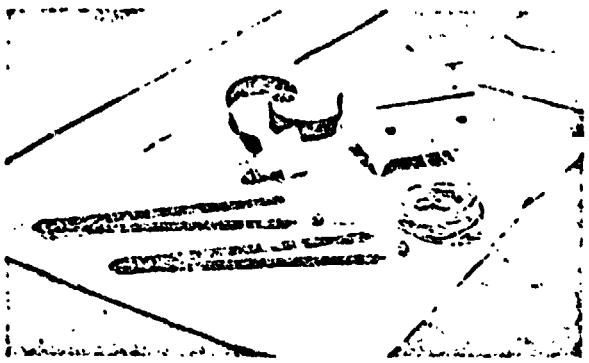

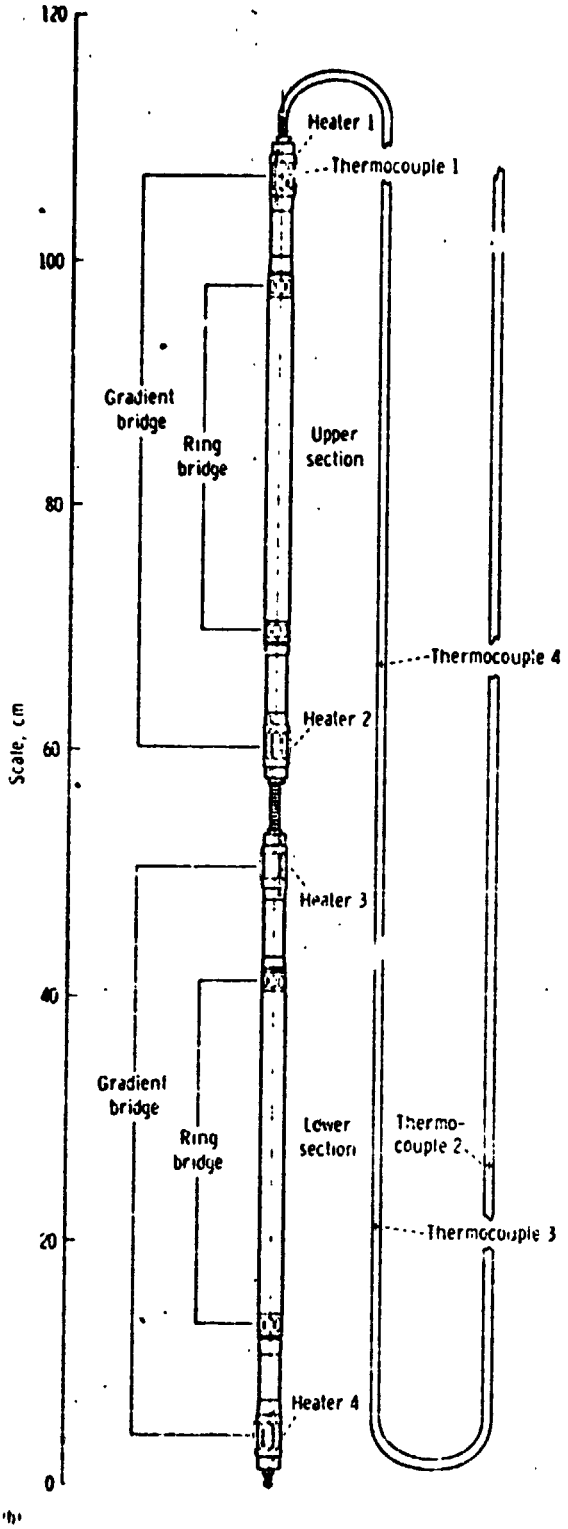

FIGURE 11-1 –Heat-flow experiment and dual-purpose heat-flow probe. (a) Heat-flow-experiment equipment. (b) Schematic of heat-flow probe.

10^{-5} to 5×10^{-4} W/cm-K and a higher range of 2×10^{-4} to 4×10^{-3} W/cm-K. To enable measurements in the lower range to be made, a heater is energized at 0.002 W, and the temperature rise of the underlying gradient sensor is recorded as a function of time for a period of 36 hr. The temperature rise and the rate of temperature rise can be interpreted in terms of the conductivity of the surrounding lunar material. Measurements in the higher range of conductivities are made by energizing the same heater at 0.5 W and monitoring the temperature rise at the ring sensor 10 cm away for a period of approximately 8 hr.

Operation of the Experiment

During normal operation of the experiment (mode 1 operation), temperatures of all gradient bridges, thermocouples, and the reference bridge (as well as temperature differences of all gradient bridges) are sampled every 7.2 min. When a heater is turned on at 0.002 W to enable measurements to be made in the lower conductivity range, the experiment is said to be operating in mode 2. The mode 3 operation is designed for the measurement of conductivity in the higher range. In this mode, temperature and temperature difference at a selected ring bridge are read every 54 sec. These modes of operation and heater turnon are controlled by commands transmitted from Earth.

The detection circuitry for measuring bridge voltages and thermocouple outputs is contained in a housing separate from the Apollo lunar surface experiments package (ALSEP) central station (fig. 11-1(a)) and is designed to compensate for amplifier offset and gain change. This compensation is achieved

TABLE 11-I.–*Summary of the Heat-Flow-Experiment Temperature Measurements*

Thermometer	Number	Location	Temperature difference, K		Absolute temperature, K	
			Range	Accuracy	Range	Accuracy
Gradient bridge[a]	1 per section	Sensors separated by 47 cm	±2 ±20	±0.001 ±0.01	190 to 270	±0.05
Ring bridge	1 per section	Sensors separated by 28 cm	±2	±0.002	190 to 270	±0.05
Thermocouple	4 per probe	Spaced 65 cm apart in the first 2.5 m of the cable above the probe	--	--	70 to 400	±0.07
Thermocouple reference bridge	1 per experiment	Mounted on the radiation plate of the electronics box	--	--	253 to 363	±0.01

[a]Gradient-bridge measurements of temperature difference are made at 2 sensitivities, with a ratio of 10 to 1.

by making all bridge measurements with bipolar excitation and by measuring the ratio of the output voltage to the excitation voltage (fig. 11-2).

EMPLACEMENT OF THE EXPERIMENT AT THE HADLEY RILLE SITE

Drilling of the holes to emplace the heat-flow probes was more difficult than had been expected. The resistant nature of the subsurface at the Hadley Rille site prevented penetration to the planned depth of 3 m. Instead, at the probe 1 site, the borestem penetrated 1.62 m (fig. 11-3); and, at the probe 2 site, the borestem penetrated approximately 1.60 m. The configuration of the probe in each hole is shown in figure 11-3. An obstruction, which was probably a break in the stem at a depth of approximately 1 m, prevented probe 2 from passing to the bottom of the borestem. Because of the very large temperature differences over the upper section, which extends above the surface, no valid temperature measurements were obtained by the ring and gradient bridges on the probe 2 upper section during most of the lunation cycle.

The shallow emplacement of the probes resulted in five of the cable thermocouples lying on, or just above, the lunar surface. These cable thermocouples come into radiative balance with the lunar surface and space, and the measured temperatures can be interpreted in terms of lunar-surface brightness temperatures. A sixth thermocouple is in the borestem projecting above the lunar surface at the probe 1 site.

When this section was written, surface-temperature and subsurface-temperature data had been recorded for nearly one and a half lunation cycles. During the first lunar noon (August 6), a full eclipse of the Sun by the Earth occurred. The thermocouples recorded surface-temperature data at 54-sec intervals during this eclipse. Six in situ conductivity measurements for the low range of values also have been conducted. Only three of these measurements are reported herein.

SUBSURFACE TEMPERATURES

The surface-temperature measurements during the lunar night and during the August 6 eclipse indicate that the surface layer surrounding the probes has an extremely low thermal conductivity. The subsurface measurements reveal that the conductivity must increase substantially with depth, and values of approximately 1.5×10^{-3} W/cm-K are found at a depth of 1 m. With these values of conductivity, it is unlikely that any measurable time variation of temperature as a result of the diurnal cycle existed at depths below 50 cm before the borestem and the heat probe were emplaced. However, after emplacement, the relatively high thermal conductance of the borestem and the radiative transfer along the inside of the stem allowed surface-temperature variations to penetrate to greater depths. After several lunations, a new periodic steady-state condition will be established

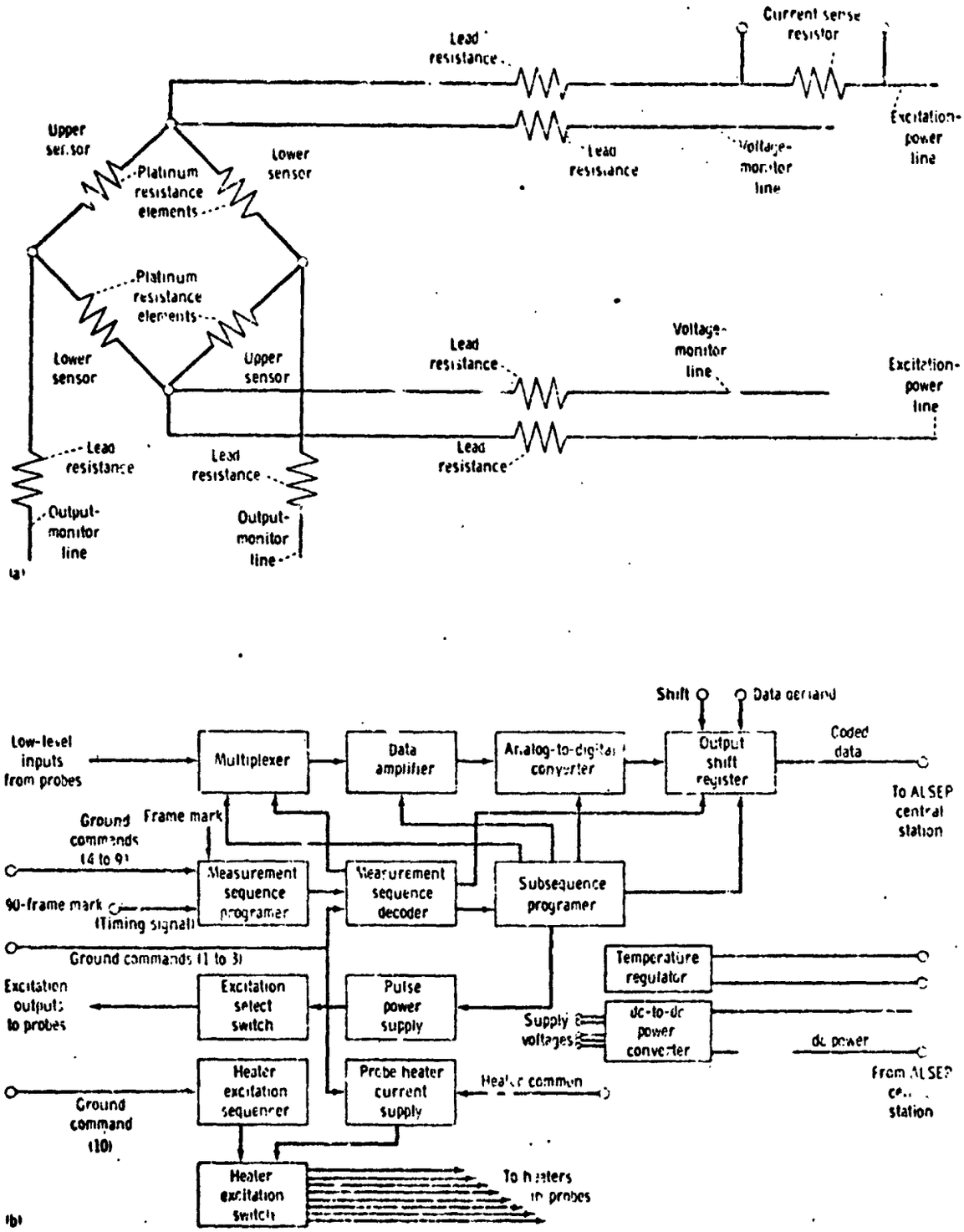

FIGURE 11-2.–Heat-flow experiment. (a) Circuit diagram of the differential thermometer. (b) Block diagram of the experiment electronics.

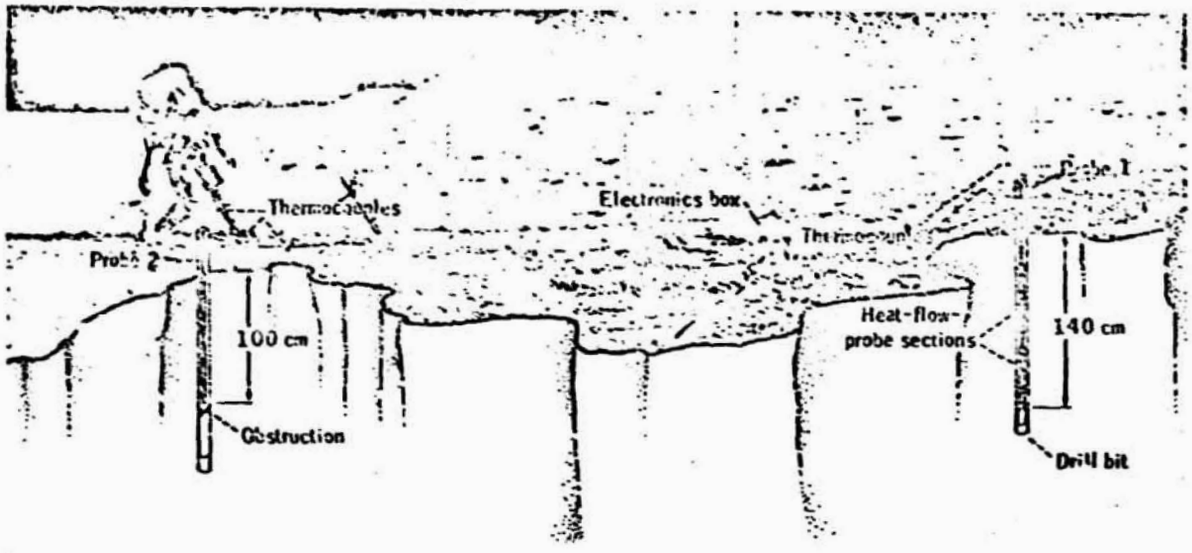

FIGURE 11-3.–Panorama of the heat-flow-experiment emplacement site (composite of photographs AS15-87-11847 and AS15-87-11848) and a cutaway drawing of the heat-probe and thermocouple locations.

around the borestem; initially, however, the borestem and probes will equilibrate toward temperatures that existed in the subsurface before emplacement. By applying the theory of the cooling of a cylinder, which is discussed in the appendix of this section, it is possible to deduce the undisturbed temperature profile at depths where diurnal variations are negligible and to obtain some estimate of the thermal properties of the regolith from the first few hundred hours of equilibration.

The temperature histories of all subsurface thermometers and the evolution of the profiles of temperature as a function of depth for probes 1 and 2 are shown in figures 11-4 and 11-5, respectively. All sensors initially cooled very rapidly, and those sensors at depths greater than 0.7 m continued to cool monotonically with time and were still cooling after 300 hr. The thermometers at depths less than 0.7 m responded to the high temperatures of the borestem projecting above the surface. The temperature in the top of the probe 1 borestem, which is projecting above the surface, was 348 K at lunar noon. As shown in figure 11-5, an obstruction prevented heat-flow probe 2 from passing to the bottom of the hole; consequently, the platinum-resistance thermometers in the top section are not on scale. The cooldown duration of probe 2 is longer than that of probe 1, probably because of the lower conductivity material surrounding the borestem and the higher initial heat input that resulted from extended drilling.

Extrapolation to Equilibrium Values

To extrapolate the sensor temperatures to equilibrium values, the first-order approximation of the long-term solution of the cooling-cylinder problem

$$\frac{T - T_\infty}{T_0 - T_\infty} = \left(\frac{4\pi kt}{S_1 + S_2}\right)^{-1} \qquad (11\text{-}2)$$

is used, where T is the absolute temperature of the probe in K, T_∞ is the true equilibrium temperature of the probe, and T_0 is the probe initial temperature; and where S_1 and S_2 are the thermal heat capacities per unit length of the inner and outer cylinders, respectively, in W-sec/cm-K, and t is time in seconds. A more complete discussion of the derivation of equation (11-2) and definitions of the variables can be found in the appendix of this section.

If an initial estimate of the equilibrium temperature T'_∞ is made, it can be shown that the error in the estimate δ is given by

$$\delta = \frac{v_1' - v_2' \frac{t_2}{t_1}}{\frac{t_2}{t_1} - 1} \qquad (11\text{-}3)$$

where $v_1 = T_1 - T_\infty'$, $v_2' = T_2 - T_\infty'$ and T_1 and T_2 are two temperatures selected from the long-term cooling history at times t_1 and t_2, respectively. Then the true equilibrium temperature is simply $T_\infty' + \delta$. The equilibrium temperature determined in this way is independent of the initial-temperature estimate. The equilibrium temperatures for all sensors not affected by the diurnal variation are shown in table 11-II. The values also are plotted as functions of depth in figures 11-4 and 11-5. The accuracy of these equilibrium temperatures is ±0.05 K.

At the probe 1 site, the subsurface temperature, which increases regularly with depth, is approximately 252.0 K at a depth of 80 cm. The increase along the lower 60 cm of probe 1 is approximately 1 K. For probe 2, the temperature at a depth of 80 cm is approximately 250.5 K. The two probe 2 sensors that are unaffected by the diurnal variations indicate an increase in temperature with depth at a rate comparable to the rate detected by the probe 1 sensors. This gradient in temperature is a result of the outward flow of heat from the Moon.

Equilibrium Temperature Differences Along the Heat-Flow Probes

The gradient and ring bridges enable measurement of temperature differences between points 47 cm and 28 cm apart on the probe with an accuracy of ±0.001 K, which is far greater than the accuracy of the absolute-temperature measurements. An analysis similar to that used for the equilibration of the individual sensors can be used to extrapolate the temperature differences to equilibrium values. By using the first term of equation (11-13) in the appendix, the equilibrium temperature difference ΔT_∞ between two points on the probes is given by the expression

$$\Delta T_\infty = \frac{\Delta T_1 - \Delta T_2 \frac{t_2}{t_1}}{1 - \frac{t_2}{t_1}} \qquad (11\text{-}4)$$

where ΔT_1 and ΔT_2 are temperature differences measured at times t_1 and t_2, respectively. Equation 11-4 is valid only for very long times ($t > 300$ hr); consequently, only those differential thermometers that have not been affected by the diurnal variations in the first few hundred hours of observation can be used in this analysis.

The only differential thermometers that have not been affected by the diurnal variations are those on the bottom section of probe 1. The calculated equilibrium-temperature difference across the gradient bridge on the bottom section of probe 1 is 0.779 K and, across the ring bridge, 0.483 K. These results can be interpreted in terms of the temperature difference between adjacent points on the borestem wall by taking into account the effect of radiative

TABLE 11-II.—*Lunar Conductivities Determined From Heat-Probe and Cooldown Histories*

Sensor	Depth, cm	Equilibrium temperature, K	Minimum-conductivity case		Maximum-conductivity case	
			Initial temperature, K	Deduced conductivity, W/cm-K	Initial temperature, K	Deduced conductivity, W/cm-K
TG11B	83	251.96	315	0.8×10^{-4}	349	1.5×10^{-4}
TR22A	87	250.53	[a]323	1.1	--	--
TG12A	91	252.28	317	1.2	349	1.7
TG22B	96	250.70	[a]323	1.2	--	--
TR12A	100	252.40	317	1.2	349	1.7
TR12B	129	252.87	313	1.9	349	2.9
TG12B	138	253.00	313	2.1	349	3.3

[a]The borestem at the probe 2 site was drilled down approximately 1 m during the first extravehicular activity (EVA). During EVA-2, 22 hr later, the borestem was drilled an additional 1 m to a depth of approximately 1.5 m. The initial temperature was estimated by calculating the cooldown from the preemplacement temperature for 22 hr between the EVA periods and adding the additional heat of drilling during EVA-2. This procedure resulted in an estimate of initial temperature (323 K) very close to the value determined by extrapolation of temperature data in the 1st hour after insertion.

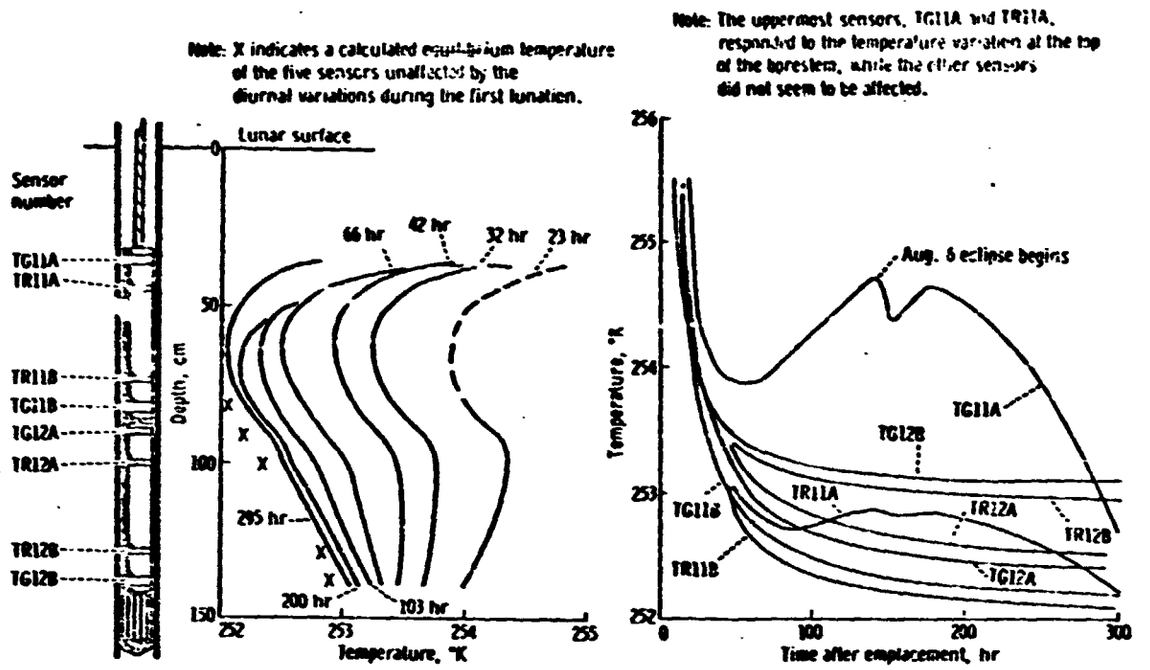

FIGURE 11-4.–Temperature histories of the sensors on heat probe 1 during the first 300 hr after emplacement. The subsurface geometry of the probe and temperature as a function of depth are shown on the left. Temperature as a function of time is shown on the right.

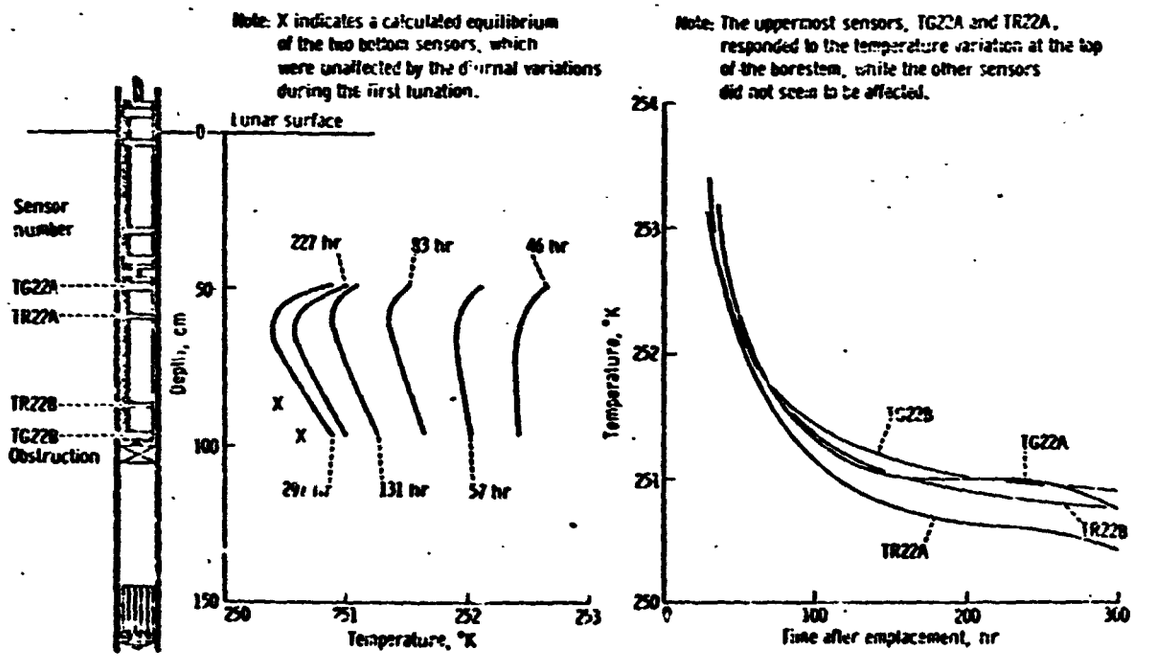

FIGURE 11-5.–Temperature histories of the sensors on heat probe 2 during the first 300 hr after emplacement. The subsurface geometry of the probe and temperature as a function of depth are shown on the left. Temperature as a function of time is shown on the right.

TABLE 11-III. *Summary of Equilibrium-Temperature-Difference Measurements and Subsurface-Temperature Gradients*

Differential thermometer	Equilibrium temperature difference, K		Lunar temperature gradient, K/m
	Probe	Borestem	
Gradient bridge	0.779	0.819	1.74
Ring bridge	.483	.502	1.77

coupling between the walls and the probe and the finite axial conductance of the probe. The temperature difference over the probe is always slightly less than the temperature difference between the adjacent points on the borestem. The ratio of the two, which is called the shorting ratio, was determined experimentally in the laboratory for each section of the probes. The temperature differences at points in the borestem adjacent to the differential thermometers after the shorting ratio has been applied are listed in table 11-III.

The relatively high axial conductance of the borestem results in some axial shunting of the steady-state heat flow; therefore, to determine the undisturbed gradient (i.e., the gradient at large radial distances from the borestem), some correction must be made. The shunting effect can be estimated by modeling the borestem as a prolate spheroid surrounded by a medium with a lower conductivity. By using an effective axial conductivity of 2.3×10^{-3} W/cm-K for the borestem and a lunar conductivity of 1.7×10^{-4} W/cm-K, the model indicates that a plus-1-percent correction should be applied to the borestem temperature gradients. This correction has been applied to the temperature gradients listed in table 11-III.

Diurnal Temperature Variations

Variations in temperature synchronous with the solar phase were observed at depths as great as 70 cm during the first one and a half lunations after emplacement. The temperature variations measured by probes 1 and 2 are shown in figures 11-6 and 11-7, respectively. The peak-to-peak amplitude of the variation at the top of probe 1 is approximately 6 K, a 43-to-1 attenuation of the 260 K temperature excursion measured in the part of the borestem that projects above the lunar surface. The ring sensor TR11A, which is located 9 cm below the top of the probe, measured variations with a 2 K amplitude. The sensors on the lower section of probe 2 that detected variations are somewhat deeper (49 and 58 cm) and recorded correspondingly smaller amplitudes. There are two interesting features of the observed variations. The phase shift of the peaks is extremely small, in view of the large attenuation factors, and a considerable portion of the high-frequency component of the solar radiation penetrates to these depths, as indicated by the rapid rates of temperature change at dawn and sunset. These features suggest that much of the heat transfer to the probe occurs by direct radiative exchange with the upper part of the borestem. The thin, aluminized Mylar disk that is located on top of each probe as a radiation shield apparently does not prevent significant radiative exchange between the top of the probe and the lunar surface.

The heat exchange during a lunation cycle is very complex, because the borestem conducts heat from and toward the lunar surface more efficiently than the regolith material. Thus, the low nighttime temperatures penetrate downward along the borestem, which enlarges the low-temperature area viewed by the top of the probe and, hence, increases the heat loss from the probe to the surface. A similar, but opposite, effect occurs during the day. This phenomenon may, in part, explain the asymmetry of the plots of temperature as a function of time.

Diurnal temperature variations that propagate along the borestem have an important effect on the mean temperature in the borestem. Because the conductivity of the borestem is not as temperature dependent as the adjacent lunar material, heat will be lost more readily along the borestem at night. Consequently, the heat balance over a full lunation will require that the borestem, to depths that diurnal variations penetrate, have a lower mean temperature at a given depth than the regolith. Thus, a net cooling of the borestem in the upper meter can be anticipated, which is an effect that is already apparent in the substantial decrease in peak temperature during the second lunation. Comparisons with the cooling curves of deeper sensors show that this difference cannot be explained by cooling from initial temperatures alone. This cooling effect results in a gradient in mean temperature in the upper meter of the borestem that is unrelated to the heat flow from the interior.

It is essential to note that the mean temperatures and temperature differences in those sections of the

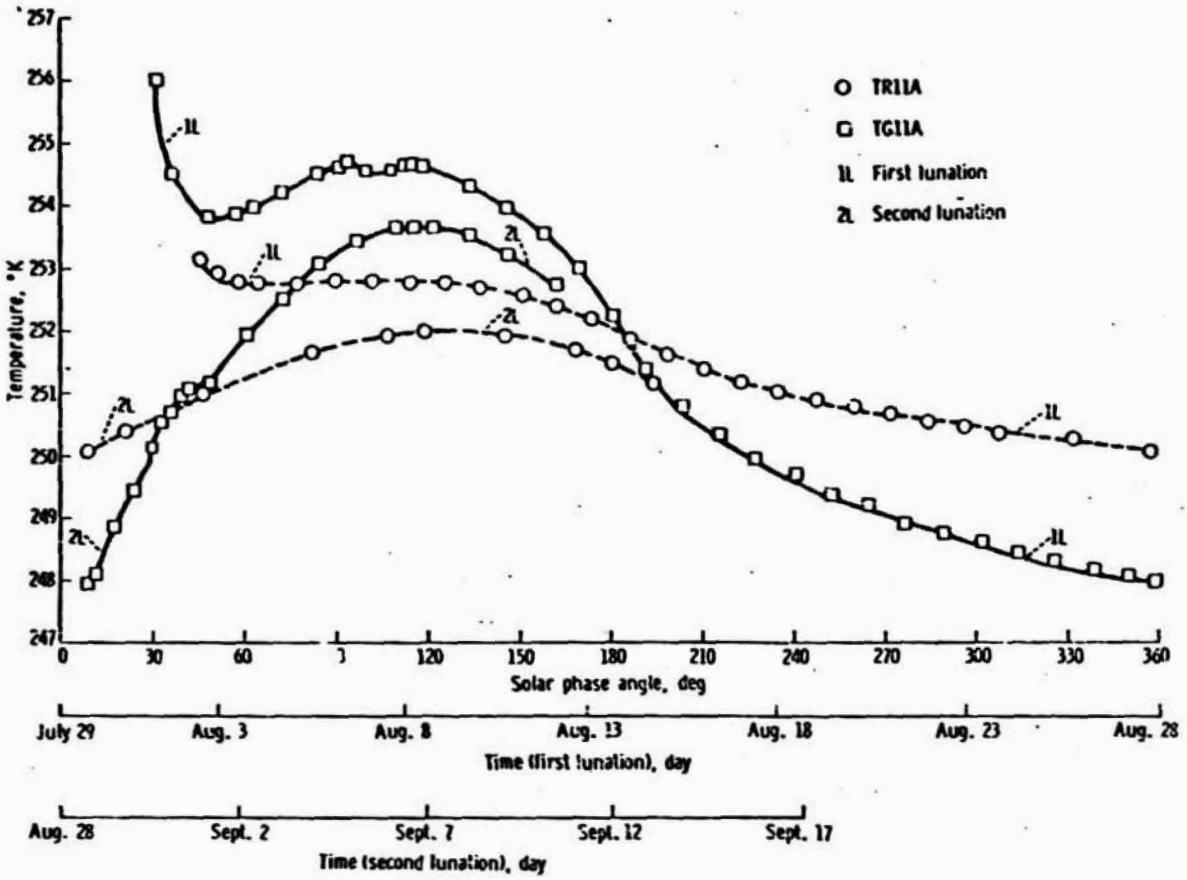

FIGURE 11-6.–Temperature as a function of solar phase angle for probe 1 sensors TR11A and TG11A (the sensors that detect diurnal variations) for the first one and a half lunations after emplacement.

borestem that see diurnal variations cannot be used to determine gradients related to the heat flow from the lunar interior until the effect of temperature-dependent conduction in the borestem and the surrounding lunar material is analyzed and the effect quantitatively determined. Such an analysis is beyond the scope of this preliminary report, but the analysis will be made on future subsurface-temperature data after the upper part of the borestem has equilibrated nearer to the mean periodic steady-state temperature. This analysis will add two independent measurements of heat flow to the result already reported here.

Implications of the Large Mean-Temperature Gradients in the Upper 50 cm at the Hadley Rille Site

By using a finite-difference model to generate daytime lunar-surface temperatures (which depend almost exclusively on the solar flux) and by using the reduced thermocouple temperatures to obtain lunation nighttime surface temperatures, a mean lunar-surface temperature of 217 K (±3 K) was obtained. This result indicates an increase in mean temperature (35 K higher than the mean surface temperature) at depths beyond which the diurnal variation penetrates. This phenomenon can be explained in terms of a strong temperature dependence of the thermal conductivity, which previously has been investigated by Linsky (ref. 11-4) and others. Because of the near lack of an atmosphere on the Moon, radiative transfer of heat between and through particles of the lunar fines can contribute significantly to the effective thermal conductivity. This temperature-dependent conductivity has been found to obey a relation of the form (ref. 11-3)

$$k(T) = k_c + k_r T^3 \qquad (11\text{-}5)$$

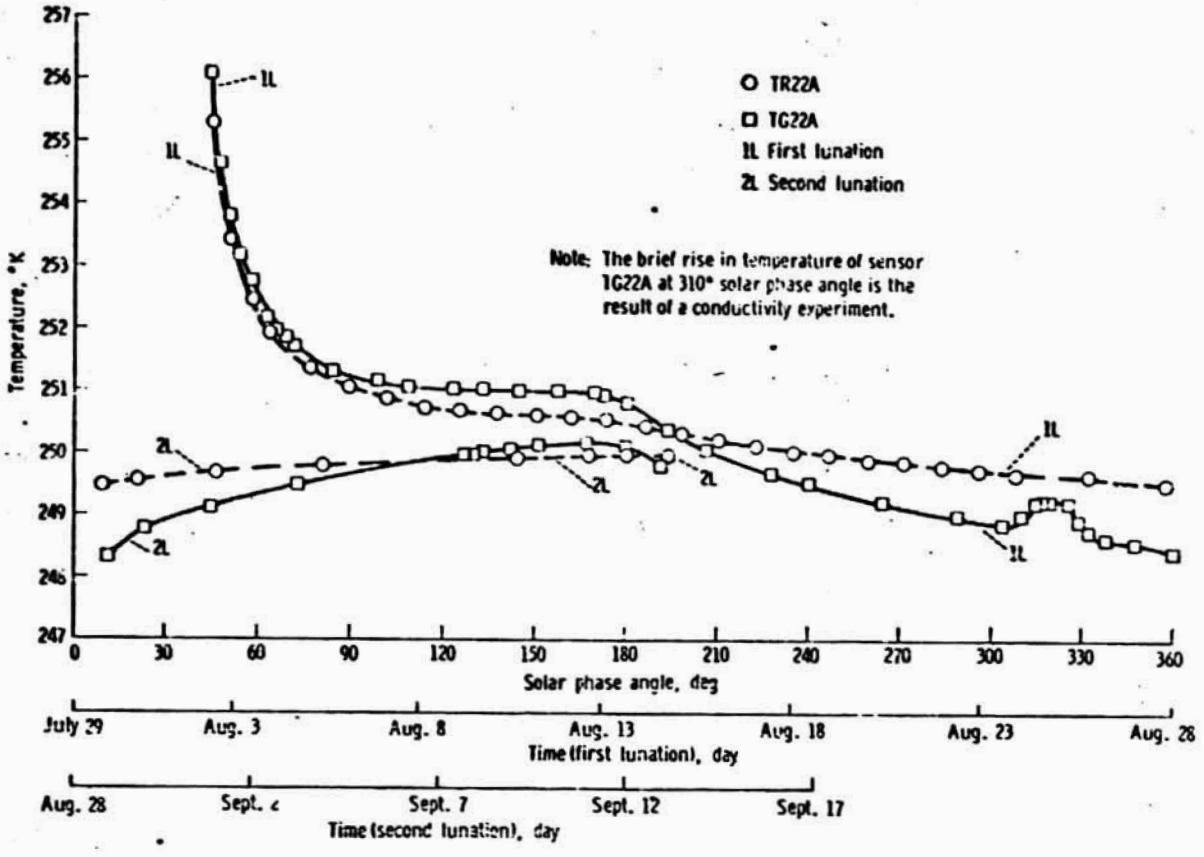

FIGURE 11-7.–Temperature as a function of solar phase angle for probe 2 sensors TR22A and TG22A (the sensors that detect diurnal variations) for the first one and a half lunations after emplacement.

where k_c is the contribution from conduction and $k_r T^3$ represents the radiative exchange between and through particles. Linsky (ref. 11-4) has used computer models of the lunar surface to evaluate this effect in the absence of a steady-state heat flow. By interpolating from these models, the relative contributions of the conductive and radiative terms can be estimated. For a difference of 35 K in mean temperature between the surface and depths at which no significant time variations of temperature exist, the ratio of radiative to conductive terms is approximately 2 at a temperature of 350 K. The relatively small steady-state gradient (1.75 K/m) produced by the measured steady-state heat flow will have only a slight effect on this ratio. Conductivity measurements have been performed for a wide range of temperatures on returned lunar samples from the Apollo 11 and 12 missions (ref. 11-9). The results also indicate the significant temperature dependence of conductivity. For Apollo 11 and 12 samples, the data cited in reference 11-9 indicated that the ratios are 0.5 and 1.5, respectively. The conductivity of the more highly temperature-dependent lunar fines from the Apollo 12 site seem to be more comparable to the upper regolith conductivity at the Hadley Rille site. Further refinement of surface-thermocouple data, combined with a more accurate determination of conductivity as a function of depth and direct measurements of the conductivity of returned Apollo 15 samples, will result in the first directly measured profile of regolith conductivity to a depth of 1.5 m.

CONDUCTIVITY OF THE REGOLITH

Preliminary Deductions from the Heat-Flow-Probe Histories

The rate of equilibration of the probes depends on the thermal diffusivity κ of the surrounding lunar material, the ratio α of heat capacity per unit volume

of the lunar material to the heat capacity per unit volume of the heat probe, and the contact conductances H_1 and H_2, where

$\alpha = 2\pi b^2 \rho c/(S_1 + S_2)$

c = heat capacity per unit mass of the surrounding lunar material, W-sec/cm-K

ρ = density of the surrounding lunar material g/cm^3

H_1, H_2 = contact conductances of the inner- and outer-cylinder boundaries, respectively, W/cm^2-K

A more complete discussion can be found in the appendix of this section. By using an estimate of the volumetric heat capacity of the lunar material ρc, a value for α can be determined, because the thermal properties of the probe and the borestem are known. From an analysis of the cooling history of the probes, an estimate of the diffusivity, and, thus, the conductivity, can be made. Measurements of the heat capacity of samples that represent a wide range of lunar rock types result in very uniform values (ref. 11-10). The density of the regolith material is quite variable; preliminary measurements of samples taken by core tubes at the Hadley Rille site result in values that range from 1.35 to 1.91 g/cm^3. At the depth of the probes, the densities are probably near the high end of this range and not so variable. For the analysis described in this section, a density of 1.8 g/cm^3 and a heat capacity of 0.66 W-sec/g-K have been assumed.

It is not possible to determine a value of κ from the ratios of temperatures at various times during the cooldown, because, as the long-term solution indicates, the temperature ratios depend solely on the ratio of the times. Bullard (ref. 11-11) has pointed out this property of cooling cylinders in his discussion of sea-floor heat-flow measurements. To estimate a value for κ, the initial temperature must be known. Estimates of the initial temperature can be made by extrapolating data recorded soon after the probes were inserted to the time the borestem was emplaced. This estimate is considered to be a minimum value, because cooling during the first several minutes is faster as a result of enhanced radiative transfer at high temperatures. Alternately, the assumption can be made that the initial temperature is the temperature of the borestem before emplacement, plus some estimated temperature rise as a result of the heat produced during drilling. Temperatures recorded before emplacement by probe 2, which was stored temporarily in the drill rack between EVA-1 and EVA-2, were used as estimates of the borestem temperature before emplacement. The temperature rise that resulted from drilling is estimated to be 15 K/min, based on estimated torque levels. The initial-temperature estimates based on these assumptions are considered to be maximum estimates.

The cooling histories of all subsurface sensors that are not affected by diurnal variations were analyzed to determine the conductivity of the surrounding lunar material for the two limiting estimates of initial temperature. By using the equilibrium temperature T_∞ for each sensor, the ratio $(T - T_\infty)/(T_0 - T_\infty)$ was determined for the first few hundred hours of equilibration. A typical plot of this ratio as a function of time is shown in figure 11-8. The procedure for determining conductivity is to make an initial estimate of the parameters h and A, where

$h = k/bH_2$

$A = S_2 \gamma \kappa / b^2 (S_1 + S_2)$

$\gamma = S_1/2\pi a H_1$

a = radius of the inner cylinder (heat-flow probe) in centimeters

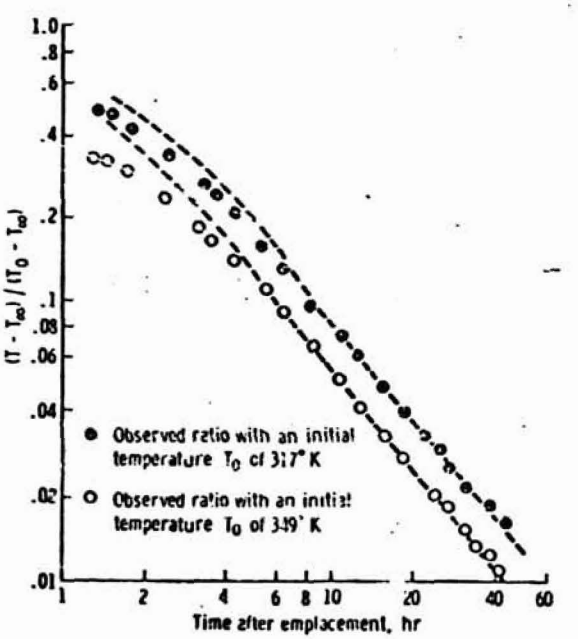

FIGURE 11-8.–Ratio of temperatures measured by sensor TG12A during the initial equilibration of heat probe 1 with the lunar subsurface compared with the theoretical cooldown curves computed from equation (11-12) (dashed lines).

Then, by equating observed temperature ratios for several times in the cooling history with the ratios computed from equation (11-12) in the appendix, a value for the dimensionless parameter τ can be found that corresponds to each time. Once a value for τ is known, k can be determined from the relation $\tau = kt/\rho cb^2$. The conductivity value determined for a large value of τ will be the most accurate, because, at long times, $f(A,h,\alpha,\tau)$ is nearly independent of h and A, where $f(A,h,\alpha,\tau)$ designates the right-hand side of equation (11-12) in the appendix. By using this initial long-time estimate and comparisons of observed and computed ratios at early times, a best value of k and H_2 can be determined with two or three repetitions of the procedure.

Theoretical curves fitted to the data obtained from sensor TG12A by this procedure and ratios for both limiting initial-temperature estimates are shown in figure 11-8. The parameters h and A have been chosen to fit data for times greater than 6 to 8 hr. The theoretical curve at earlier times lies well above the observed data; however, it is not possible to find a value for H_2 to fit data obtained at times earlier than 6 hr without degrading the fit at later times. To obtain the most accurate value of k, the curve must be fit to the data for large values of τ.

In table 11-II, the maximum and minimum conductivity values determined by the procedure are shown arranged in order of increasing depth. The conductivities that were determined for minimum and maximum initial-temperature estimates differ, on the average, by 50 percent. The more accurate conductivity measurements, which were made by using the heaters that surround the gradient sensors, resulted in values that lie within the ranges listed in table 11-III. The deduced conductivity values are considerably higher than the value obtained from measurements on returned lunar fines. The value for the returned lunar fines is approximately 2.2×10^{-5} W/cm-K at 250 K (ref. 11-12). The higher conductivity values that were obtained may be representative of fragmental regolith material in a more dense and compressed state than the surface fines.

In Situ Measurements

Six in situ conductivity measurements in mode 2, which is the low-conductivity mode, were conducted at the end of the first lunar night and during the first half of the second lunar day. The two heaters on the upper section of probe 2 were not turned on because the gradient bridges were off scale. The mode 2 measurements indicated the subsurface conductivity to be in the lower range of measurement and, in addition, showed that a substantial contact resistance exists between the borestem and the lunar material. A decision was made, therefore, not to run the mode 3 (high-conductivity mode) measurements at this time because of the possibility that the gradient sensors might reach temperatures potentially dangerous to the sensor calibration. Mode 3 measurements are planned at some future time after the effects of heater turnon are examined by using the conductivities determined from the mode 2 results.

Three of the conductivity measurements have been analyzed. Two of these measurements were obtained by the use of heaters on the lower section of probe 1, the section across which the best temperature gradient was determined. The third measurement was obtained by the use of the upper heater on the lower section of probe 2.

The interpretation of the response of the temperature-gradient sensor to heater turnon, in terms of the lunar conductivity, is accomplished by using a detailed finite-difference model (ref. 11-13). A simple analytical model of the gradient-sensor long-term ($t >$ 20 hr) performance deduced from the experimental data and the finite-difference models will be briefly discussed in the following paragraphs.

The temperature increase as a function of time at a given heater-sensor location upon heater turnon depends on the quantity of heat generated and the rate at which the generated heat can diffuse outward from the heater source. This rate will depend on the thermal properties of the material that surrounds the source. The heat will propagate axially along the probe and radially from the probe to the drill casing, across the contact-resistance layer outside the casing, and into the lunar medium. Both radiative transfer and conductive transfer are involved in the dissipation of heat. Shortly after heater turnon, the rate of temperature increase at the gradient sensor will depend primarily on the thermal properties of the probe and the borestem in the immediate vicinity of the heater and on the resistive gaps between the probe and the borestem and between the borestem and the lunar material. As the near-sensor probe parts and the borestem temperature increases, a temperature drop is established across the resistive gaps. When this temperature difference builds to a relatively large

value, heat will flow out from the borestem, across the contact-resistance gap, and into the medium; and the rate of temperature increase at the sensor will level off. At long times (times greater than 1000 min in this experiment), the temperature increase $\Delta v(t)$, measured at the sensor, closely fits a relation of the form

$$\Delta v(t) = C_1 \ln(t) + C_2 \qquad (11\text{-}6)$$

where C_1 and C_2 are constants that depend on the contact conductances H_1 and H_2 and the properties of the lunar material. The finite-difference thermal model of the probe in the lunar material shows the same long-term characteristics. This relationship has the same form as the long-term solution to the problem of a uniformly heated infinite cylinder (ref. 11-14). As in the case of the long-term solution for a cylinder, it has been determined from the finite-difference models that, at long times after heater turnon, the constant C_1 is almost solely a function of the conductivity of the surrounding material and the heat input. Thus, the slope $[\Delta v(t_2) - \Delta v(t_1)]/\ln(t_2/t_1)$, for times greater than 1000 min, is a sensitive measure of the conductivity of the surrounding material for a constant heat input. Plots of temperature increase as a function of time for the three conductivity measurements are shown in figure 11-9 and compared with best-fitted theoretical models.

The magnitude of temperature increase at any time greater than 0.5 hr after heater turnon is very sensitive to the magnitude of the contact conductance H_2. The value of the contact conductance, however, has no detectable effect on the slope of the curve of Δv as a function of $\ln(t)$ at long times; therefore, the determination of a value for k can be made independently of H_2 by matching slopes at times greater than 1000 min. By using this value of k, a value for H_2 was determined by varying H_2 in the finite-difference models until the experimental curves of Δv as a function of t were bracketed within a small tolerance. Examples of models that bracket the experimental curves of the three in situ experiments are shown in figure 11-9.

A rather accurate determination of the conductivity of the lunar subsurface material that surrounds each heater location can be made. For example, at heater location 1123 (the location of sensor TG22A), the long-time slope data could be bracketed by models of $k = 1.3 \times 10^{-4}$ and $k = 1.4 \times 10^{-4}$ W/cm-K. A linear interpolation between these models resulted in a value $k = 1.37(\pm 0.02) \times 10^{-4}$ W/cm-K. However, the assumption cannot be made that the models represent the physical situation this accurately; a value $k = 1.4(\pm 0.1) \times 10^{-4}$ W/cm-K would be more realistic. Further examination of the effects of the errors introduced by the assumptions about the model parameters (probe properties, heat-transfer linkages, etc.) must be made so the actual precision of the k values can be determined. From previous limited parametric studies, a range of ±10 percent should represent a maximum bound in the error of the k-value determinations.

The best determinations of conductivity values are listed in table 11-IV. As shown in the table, the conductivity determinations from the heater experiments fall within the range of the k predictions of the initial probe cooldown analyses and indicate a significant increase of conductivity with depth.

The contact-conductance values determined from the in situ measurements vary. The contact conductance probably corresponds to a thin zone around the borestem that is filled with lunar fines. If the assumption is made that these fines have a conductivity of 2×10^{-5} W/cm-K, which is similar to the conductivity of the surface fines, the widths of the disturbed zones would be 2.7, 2.0, and 1.3 mm for the locations of sensors TG22A, TG12A, and TG12B, respectively. The larger value of H_2 at the location of sensor TG12B might result from greater compaction of the fines, rather than a thinner zone. The thicker disrupted zone around probe 2 may have resulted from the longer period of drilling.

STEADY-STATE HEAT FLOW FROM THE LUNAR INTERIOR BELOW THE HADLEY RILLE SITE

The conductivity of the regolith is shown by the measurements returned from the experiment to be significantly variable with depth over the lower section of probe 1. To compute the heat flow from temperature differences over a finite depth interval, the thermal resistance must be known. The thermal resistance can be calculated from the equation

$$R_{x_1 - x_2} = \int_{x_1}^{x_2} \frac{dx}{k(x)} \qquad (11\text{-}7)$$

where x_1 and x_2 are the end points of the interval.

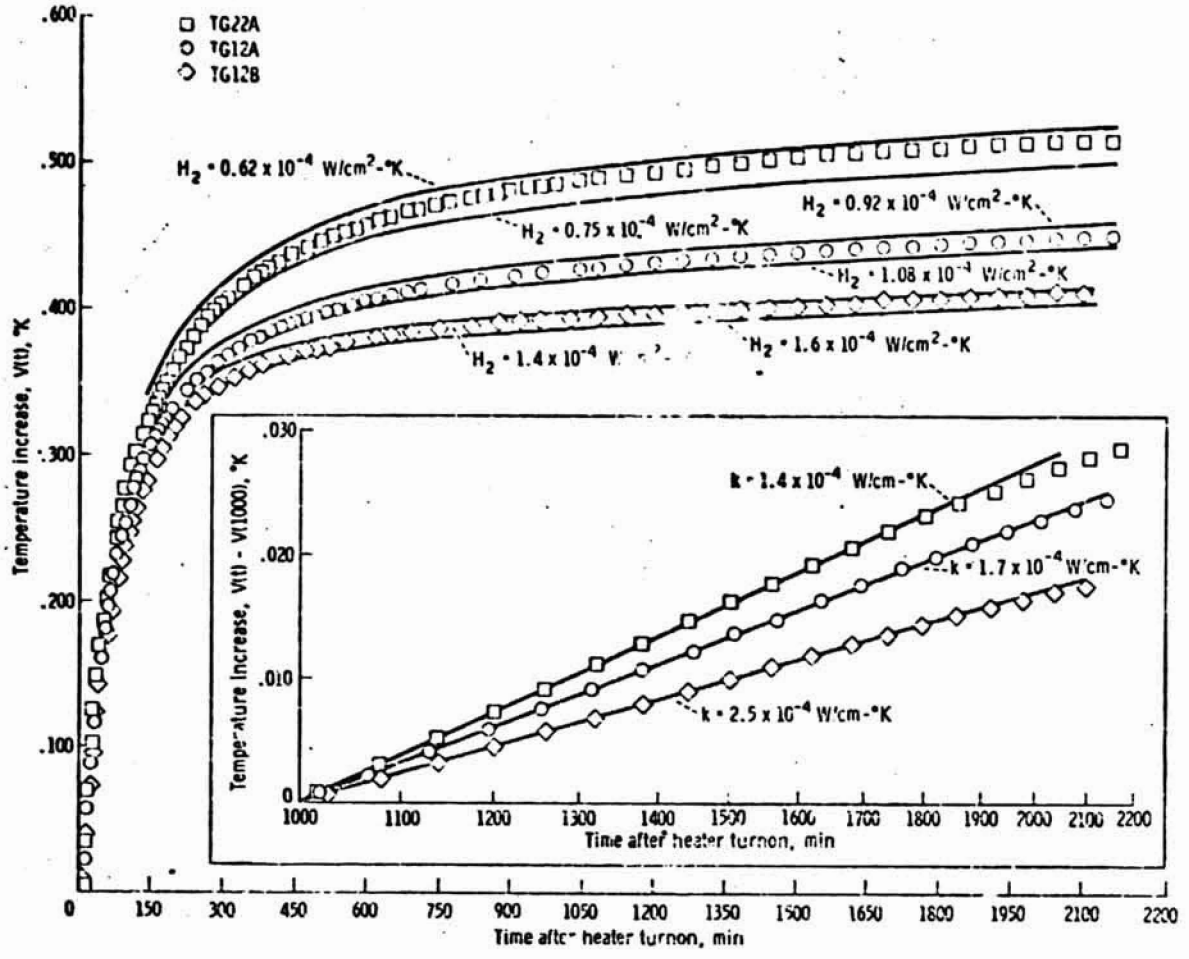

FIGURE 11-9.–Temperature increase as a function of time after heater turnon for heaters located at sensors TG22A, TG12A, and TG12B. Two computed models that closely bracket the data are shown for each of the three heater locations. Temperature increase as a function of time after 1000 min is shown in the inset on an expanded scale. The solid lines in the inset are best fitting computer models.

TABLE 11-IV.–*Conductivity Determinations From in Situ Experiments*

Heater sensor	*Depth, cm*	*Thermal conductivity, k, W/cm-K*	*Contact conductance of the borestem, H_2, W/cm^2-K*
TG22A	49	1.40 (±0.14) x 10^{-4}	0.7 x 10^{-4}
TG12A	91	1.70 (±0.17)	1.0
TG12B	138	2.50 (±0.25)	1.5

Thus, for the flux to be determined, k-value variation in the interval between the gradient sensors, which are located at depths of 91 and 138 cm, must be known. Accurate measurements of k were made only at the end points; however, a constraint can be applied on the variation with depth from the ratio of the temperature differences measured by the ring bridge and the gradient bridge. If the heat flow is uniform with depth, the constraint required by the ratio of temperature differences is

$$\frac{\int_{100}^{129} \frac{dx}{k(x)}}{\int_{91}^{138} \frac{dx}{k(x)}} = \frac{\Delta T_{ring}}{\Delta T_{gradient}} = 0.613 \quad (11\text{-}8)$$

Three possible conductivity profiles are shown in

figure 11-10. Profile B is based on the trend of conductivities from the cooldown curves and obeys the constraint of equation (11-8). Profile A also obeys the constraint of equation (11-8) but includes a uniform conductivity of 1.7 W/cm-K to a depth of 136 cm and, then, a thin layer with a conductivity of 2.5×10^{-4} W/cm-K in which the bottom sensor is embedded. Profile A would result in a lower limit for the heat flow; profile C indicates a uniform increase in conductivity over the probe section. Profile C does not obey the constraint of equation (11-8), but defines an upper limit for the heat-flow value. The trend of conductivity up to a depth of 50 cm that is indicated by the probe 2 measurement makes cases with higher conductivity than shown in profile C unreasonable. Based on these three profiles shown in figure 11-10, the temperature difference over the lower section of probe 1 results in the heat-flow values listed in table 11-V. The uncertainty of the conductivity measurements (±10 percent) should be considered as error bounds on each of the heat-flow values listed in table 11-V.

Analysis of data obtained during a full year will enable the previous determinations to be refined considerably. In addition, a comparison of the value obtained from the bottom section of probe 1 with the values obtained from the upper section of probe 1 and the lower section of probe 2 can be made once an analysis of the effects of the diurnal variations has been completed.

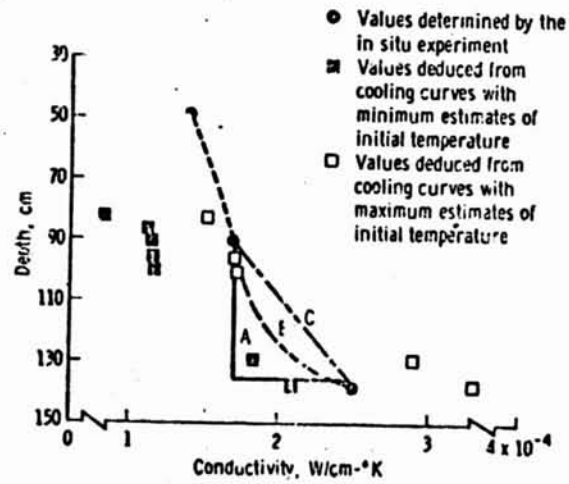

FIGURE 11-10.–Conductivity as a function of depth, with three possible conductivity profiles (A, B, and C) (table 11-V).

TABLE 11-V.– *Heat-Flow Data Obtained From the Lower Section of Probe 1*

Profile	Heat flow, W/cm²	Comment
A	2.99×10^{-6}	Lower limit
B	3.31	Best value
C	3.59	Upper limit

SURFACE TEMPERATURES DEDUCED FROM THE CABLE THERMOCOUPLES

Of the eight thermocouples designed to measure the temperature profile in the upper 1.5 m of the heat-flow borehole, six presently measure temperatures that may be used to deduce the variation of lunar-surface brightness temperature throughout the lunation period. Of particular interest is the determination of temperature during total eclipses and lunar nights, which are measurements difficult to obtain by Earth-based telescopic observation. The thermocouples in the cable of the heat-flow experiment, lying on or just above the lunar surface, provide a means by which these measurements can be obtained at a sampling rate previously unattainable (one measurement set each 54 sec).

During the lunar night, the thermocouples come into radiative balance with the lunar surface and space. To determine the relationship between the cable temperature and the lunar-surface brightness temperature, the heat balance for a small cylindrical cable element of radius a and length dl can be considered. The heat balance for such an element arbitrarily oriented above the lunar surface during the lunar night can be represented by

$$F_{C\text{-}M}\, 2\pi a\, dl\, \epsilon_{CM}\, \sigma\, T_M^4 - 2\pi a\, dl\, \epsilon_C\, \sigma\, T_C^4 - V\rho c\, \frac{\partial T_C}{\partial t} = 0 \qquad (11\text{-}9)$$

where the first term is the energy received by the cable element from the Moon per unit time, the second term is the energy lost from the cable element per unit time, and the third term is the energy required to change the temperature of the cable element per unit time; and where

$F_{C\text{-}M}$ = view factor of the cable element to the lunar surface

σ = Stefan-Boltzmann constant (5.67×10^{-8} W-sec/m²-K⁴)

ϵ_M = lunar-surface emittance

ϵ_C = cable-element emittance
α_{CIR} = cable-element infrared absorptance
V = cable-element volume
ρc = volumetric heat capacity of the cable element
T_M = lunar-surface brightness temperature
T_C = cable-element temperature

For $\epsilon_M = 1$ and a flat lunar surface, equation (11-9) reduces to

$$T_M^4 = \frac{1}{\alpha_{CIR}} \left(\frac{a\rho c}{o} \frac{\partial T_C}{\partial t} + 2\epsilon_C T_C^4 \right) \quad (11\text{-}10)$$

The term $\frac{a\rho c}{o} \frac{\partial T_C}{\partial t}$, which accounts for the thermal time constant of the cylinder, is retained only for eclipse calculations, because the constant is on the order of minutes.

The orientations of the thermocouples that are outside the borestems are unknown. The time at which a given thermocouple reaches the maximum temperature and the value of that maximum are strong functions of the orientation of the cable section in which the thermocouple is embedded. This effect, which is shown in figure 11-11, is a result primarily of the variation in the incidence angle of the solar radiation; therefore, lunar-surface brightness temperatures deduced during the lunar day are subject to error that results from the orientation uncertainties.

For the calculation of the lunar-surface brightness temperatures, the assumption was made that the view factors from the cable to space and from the cable to the surface are identical. The irregular horizon formed by the Apennine Mountains increases the effective view factor to the lunar surface, and the view factor to space is reduced correspondingly. Some of the thermocouples may be close enough to the surface so that local topographic irregularities affect the horizon seen by the cable. For a 10-percent increase in the effective view area to the topographic surfaces, the calculated surface brightness temperatures would be reduced by 2.25 percent during the lunar night.

A more serious error in lunar-night calculations results from the uncertainty in the values of the cable absorptance and emittance. For the temperatures given in figure 11-12, the emittance-to-absorptance ratio was assumed to be unity. A 20-percent increase in this ratio would result in an increase of 4.5 percent in the calculated value of the surface brightness temperature. A value of 0.97 was chosen for both the cable infrared emittance and absorptance, where the assumption was made that the sections of cable in which the thermocouples are embedded are covered by a significant amount of lunar-surface material. Photographs show that most of the cable areas are coated with lunar material.

The surface-brightness-temperature history for the first lunar night, as deduced from thermocouple temperatures, is shown in figure 11-12. A very rapid cooling of the surface is indicated for the first 80 hr after sunset; subsequently, the rate of cooling slows significantly. A cooling curve (ref. 11-15) based on astronomical observations at two different latitudes is shown for comparison. Two theoretical curves based on finite-difference calculations of thermal models of the lunar surface and subsurface are also shown. Curve A, which is derived from a model with a linear conductivity increase starting at a depth of 8 cm (inset, fig. 11-12), duplicates the rate of cooling for times greater than 80 hr, whereas curve B, which is based on a temperature-dependent-conductivity model (ref. 11-12), duplicates the earlier part of the observed curve. For both models, the heat capacity was defined by the following equation (from ref. 11-16)

$$c(T) = -0.034T^{1/2} + 0.008T - 0.0002T^{3/2} \quad (11\text{-}11)$$

The assumed densities are 1.2 g/cm^3 for curve A and 1.0 g/cm^3 for curve B. The flattening of the observed curve could, in part, be a result of a significant increase in density in the upper several centimeters.

The temperature dependence of conductivity that is indicated by the cooling curves is in agreement with the large increase in mean temperature described previously. The substantial increase in conductivity and density with depth that is suggested by the flattening of the cooling curves is in agreement with earlier conclusions that were based on astronomical observations (e.g., ref. 11-16). The mechanical properties of the soil measured near the Apollo 15 ALSEP site revealed that the shear strength increased rapidly with depth in the upper 20 cm (sec. 7). This increase in shear strength probably is related to a near-surface density gradient.

Surface brightness temperatures during the umbral stage of the August 6 eclipse were deduced from the

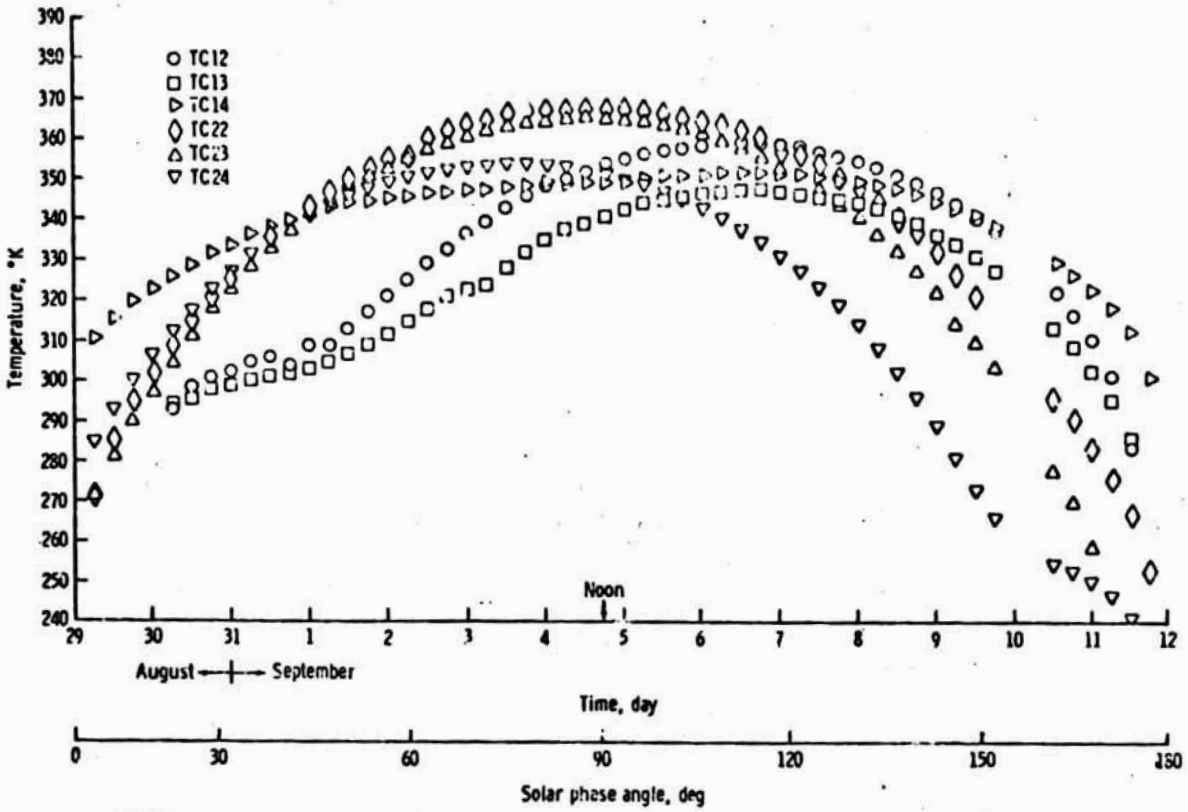

FIGURE 11-11.–Thermocouple temperatures as functions of time for the second lunar day. Thermocouples TC12 and TC13 measure the probe 1 cable temperatures; TC22, TC23, and TC24 measure the probe 2 cable temperatures; and TC14 measures the probe 1 borestem temperature.

thermocouple temperatures. For these calculations, the thermal time constant of the cable must be considered. The thermal mass of the cable per unit length in which the thermocouple is embedded was estimated by summing the properties of the 35 conductors. Uncertainties result from the fact that noise in the thermocouple measurements makes an accurate determination of the slope difficult. A sample of thermocouple data for the later part of the umbra was reduced by determining the rate of change of the cooling curve by graphical techniques. These very preliminary results indicate that the umbral temperatures reached at the lunar surface correspond well with the temperatures predicted by the theoretical curve based on the relationship between conductivity and temperature for lunar fines (ref. 11-12).

In summary, the surface-temperature data for lunar night and the umbral part of the August 6 eclipse support the conclusion that the upper few centimeters of the lunar-surface material have thermal conductivity-versus-temperature relationship similar to that found for samples of lunar fines measured in the laboratory. The lunar nighttime observations reveal a substantial conductivity gradient with depth that probably results from increasing material density with depth.

DISCUSSION OF HEAT-FLOW-EXPERIMENT RESULTS

Local Topographic Effects

The heat-flow determinations at the Hadley Rille site are susceptible to a number of disturbances. Corrections for some of these disturbances (such as the thermal perturbations caused by visible topographic features) can readily be made with sufficient accuracy, but other disturbances may result from refraction associated with sloping interfaces between

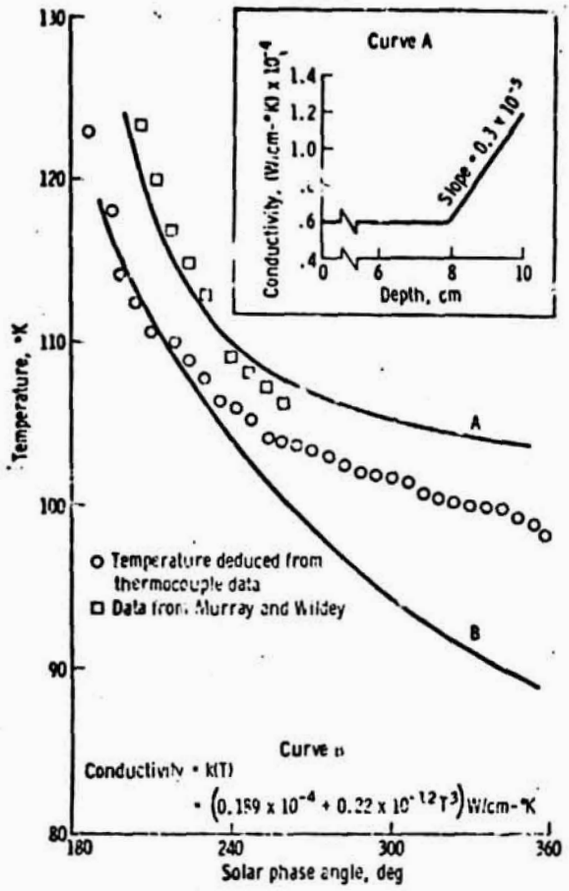

FIGURE 11-12.--Surface cooling as a function of time for the first lunar night, as deduced from thermocouple measurements. Two theoretical curves are given as references. Curve A is the expected curve for a conductivity increase with depth, starting at a depth of 8 cm; curve B is the theoretical curve for a temperature-dependent conductivity. The data from reference 11-16 are included for comparison. Conductivity as a function of depth for the curve A data is shown in the inset.

materials of differing thermal conductivity. Such interfaces, if present at all, are hidden in the lunar interior, and only a qualitative discussion of the effects can be given.

Probe 1, from which data were used for the preliminary determination of heat flow, is located in a small crater that has been almost filled and nearly obliterated by later bombardment. The topography associated with this old crater is so subdued that no correction for the topography is required. However, the possibility remains that the event that produced this crater also locally altered both the thickness and the physical properties of the regolith. The truth of this hypothesis cannot be verified because no observational evidence is available; however, after the data from probe 2 have been analyzed, a comparison of the two heat-flow values may provide more information.

The two most conspicuous and important topographic features near the heat-flow-experiment site are Hadley Rille and the Apennine Front. The topographic effect of the rille was calculated by fitting the rille profile with a two-dimensional Lees-type valley (refs. 11-17 and 11-18). This procedure results in a correction of 4.5 percent, and further allowance for the Elbow, where the rille abruptly changes direction, reduces the correction to 3.5 percent.

A second effect of the topography around the Hadley Rille site is that the surface in the area is shaded during part of the day; consequently, the average surface temperature is lower than flat portions of the lunar surface. This local cold-spot effect has been estimated quantitatively in two ways. The radiation balance for a point halfway down the rille wall (including factors for incoming solar radiation and radiation from the opposite wall), at appropriate times of the lunar day, was calculated and used to derive the mean temperature in the rille. Alternatively, the temperature at the vertex of the rille, which was assumed to have a symmetrical V-shape, was calculated from the solar input alone; for this geometry, the vertex sees neither wall. The temperature was assumed to vary linearly from the vertex to the top of the rille. The radiation-balance method resulted in a correction of 5 to 10 percent, and the vertex method resulted in a correction of 10 to 20 percent. The former value is considered to be the more reliable, mainly because the profile of the rille does not particularly resemble a V-shape. A correction of 10 percent is considered to be reasonably close to the upper limit of the effect that results from the cold rille wall.

The thermal effect of the Apennine Front was estimated in a preliminary way from the two-dimensional-slope method of Lachenbruch (ref. 11-19). By assuming two-dimensional symmetry, the curves given by Lachenbruch indicate that the correction, which is negative in this case, is 10 percent at a maximum. Actually, the heat-flow-experiment site is in an embayment in the Apennine Front, which invalidates the two-dimensional approximation and reduces the

correction. A correction of 5 percent would be more realistic.

In summary, the topographic effect of Hadley Rille is approximately canceled by the effect of the Apennine Front, which leaves only the cold-spot effect of the rille as a remaining correction resulting from the visible topography. This latter correction is the largest correction, in any case, and seems most likely to approximate 10 percent of the measured heat flow.

Implications of the Results

In this section, the view was adopted that the heat flow observed at the Hadley Rille site is representative of the moonwide value, in spite of the possibilities of local and regional disturbances and large-scale variations in the lunar heat flow. Thus, the measurement is considered at face value, with full realization that future measurements may produce major changes in the conclusions. Because of the preliminary nature of the results, simple models were used for this report. Only the linear equation of heat conduction was considered, for which the thermal diffusivity was constant.

The value that is considered to be an upper limit to the heat flow resulting from the initial heat is calculated by assuming that, at the end of a convective stage in the early history of the Moon, temperatures throughout the Moon lay along the solidus for lunar basalt (ref. 11-20). After 3×10^9 yr, the heat flow resulting from these very high initial temperatures is in the range of 0.2×10^{-6} to 0.4×10^{-6} W/cm^2. If, as suggested by the greater ages of all known lunar rocks, partial melting throughout the Moon took place earlier, still lower values of heat flow would be associated with the initial heat. It is likely that the assumed initial temperatures are too high; however, by revising the assumed temperatures downward, the flux from the initial heat is further reduced. The initial heat contributes little to the present lunar heat flow, and the contribution can be neglected for present purposes.

The major portion of the heat flow from the Moon probably results from radioactive heat generation in the interior. It is possible to construct an infinite number of models based on nonuniform distributions of radioactivity; however, in this report, the discussion was confined to consideration of the Moon as a sphere with uniform and constant internal heat generation. The ratio of the surface heat flow q (expressed in 10^{-6} W/cm^2) and the heat production Q (expressed in 10^{-13} W/cm^3) is shown for several times in the following list.

Time, yr	q/Q, cm
3×10^9	3.22×10^7
4	3.58
5	3.89
Infinite	5.78

With a lunar heat flow of 3.3×10^{-6} W/cm^2, the value of Q must be in the range of 0.57×10^{-13} to 1.0×10^{-13} W/cm^3. This number is far lower than the heat production of lunar basalt, which has a value of approximately 3.5×10^{-13} W/cm^3. However, the basaltic rocks are presumably differentiates that are far more radioactive than the parent material. On the other hand, ordinary chondrite and type I carbonaceous chondrites generate heat at rates of approximately 0.17×10^{-13} and 0.22×10^{-13} W/cm^3, respectively. The respective average rates of heat generation over the last 4.5×10^9 yr are 0.61×10^{-13} and 0.67×10^{-13} W/cm^3. Even these last figures are barely sufficient to provide the necessary flux. The conclusion is that, if the observed lunar heat flow originates from radioactivity, then the Moon must be more radioactive than the classes of meteorites that have formed the basis of Earth and Moon models in the past.

APPENDIX

Equilibration of an Infinitely Long Cylinder in a Homogeneous Medium by Conduction

In this appendix, the theory of the cooling of a cylinder by conduction is reviewed and applied to the heat-flow probe. Cylindrically shaped probes are commonly used in making geothermal measurements, and, as a consequence, the theory of heat flow in cylindrical coordinates has been thoroughly investigated (refs. 11-11, 11-14, and 11-21). The investigation of the effect of a finite contact resistance between a cylinder and the surrounding medium (ref. 11-14) is particularly applicable to problems of the cooling of the lunar probes. In this appendix, the solution (ref. 11-14) has been extended to a somewhat more complex model that includes a solid cylinder inside a thin-walled concentric cylinder which, in turn, is surrounded by an infinite medium with a conductivity k. The cylinders are assumed to be perfect conductors; that is, each cylinder is isothermal, which is very nearly true in the case of the heat-flow probe. Contact resistances exist at the two cylindrical boundaries. In this model, the inner cylinder is an idealization of the heat-flow probe, which is radiatively coupled to the borestem (the concentric cylinder). The borestem, in turn, loses heat by conduction to the surrounding regolith, of conductivity k, through a thin zone of lunar material that has been disturbed by drilling and, hence, has a different conductivity. The initial temperature of the surrounding infinite medium is zero; and, initially, the two inner cylinders have a temperature v_0.

By defining the dimensionless parameter τ as $\kappa t/b^2$ (where κ is the thermal diffusivity of the surrounding infinite medium, t is time in seconds, and b is the radius of the outermost cylinder), the ratio of the inner-cylinder temperature $v(\tau)$ to the inner-cylinder initial temperature v_0 is given by

$$\frac{v(\tau)}{v_0} = \int_0^\infty \frac{(1 - Au^2)\exp(-u^2\tau)\,du}{u\left(\left[u(1 - Au^2)J_0(u) - [hu^2(1 - Au^2) - \alpha(1 - Bu^2)]J_1(u)\right]^2 + \left[u(1 - Au^2)Y_0(u) - [hu^2(1 - Au^2) - \alpha(1 - Bu^2)]Y_1(u)\right]^2\right)} \qquad (11\text{-}12)$$

where

$\alpha = 2\pi b^2 \rho c/(S_1 + S_2)$
$h = k/bH_2$
$A = S_2\gamma\kappa/b^2(S_1 + S_2)$
$B = \gamma\kappa/b^2$
$\gamma = S_1/2\pi a H_1$

a = radius of the inner cylinder (heat-flow probe) in centimeters

b = outer radius of the concentric outer cylinder (borestem) in centimeters

S_1, S_2 = thermal heat capacities per unit length of the inner and outer cylinders, respectively, W-sec/cm-K

H_1, H_2 = contact conductances at the inner- and outer-cylinder boundaries, respectively, W/cm^2-K

ρ = density of the surrounding material, g/cm^3

c = heat capacity per unit mass of the surrounding material, W-sec/g-K

k = thermal conductivity of the surrounding material, W/cm-K

κ = thermal diffusivity ($k/\rho c$) of the surrounding material, cm^2/sec

Also, $J_0(u)$, $J_1(u)$, $Y_0(u)$, and $Y_1(u)$ are the zero- and first-order Bessel functions of the first and second kinds.

By following the method described in reference 11-11, the expression on the right-hand side of equation (11-12) can be redesignated $f(A,h,\alpha,\tau)$; therefore, equation (11-12) can be written as $v(\tau)/v_0 = f(A,h,\alpha,\tau)$. A more complete derivation of equation (11-12) and the resulting tabulated values will be published at a later date. Two typical plots of $f(A,h,\alpha,\tau)$ are shown in figure 11-8. The values of k

and H_2 that were used for computing the theoretical curves are given in table 11-II. Other parameters are α = 3.33, H_1 = 3.25 × 10^{-4} W/cm^2 · K, γ = 445 sec, and a and b are 0.95 and 1.259 cm, respectively.

By using asymptotic values of the Bessel functions for large values of τ (after a method outlined in ref. 11-21), a solution that is valid for long times can be derived as follows.

$$\frac{\theta(\tau)}{\theta_0} = \frac{1}{2\alpha\tau} - \frac{1}{4\alpha^2\tau^2}\left\{4\gamma h\left[\frac{2S_1 \cdot S_2}{(S_1 - S_2)^2}\right] + 4h - 2 - 4\gamma - 2\ln\left(\frac{4\tau}{S}\right)\right\} \qquad (11\text{-}13)$$

where ln (S) = 0.5772 (Euler's constant). The long-term solution exhibits some interesting features of the function $f(A,h,\alpha,\tau)$. At long times ($\tau > 20$), the function becomes nearly equal to $(2\alpha\tau)^{-1}$, or $(4k\pi t/S_1 + S_2)^{-1}$, which is independent of ρc. A log-log plot of $f(A,h,\alpha,\tau)$ is shown in figure 11-8; for long times, the function describes a straight line with a slope of very nearly −1. This property of the function enables the temperature histories to be extrapolated to equilibrium values by the procedure described in the text of this section and a value for k to be determined independently of ρc from long-time portions of the equilibration curves. In addition, as shown by equation (11-13), the contact conductances H_1 and H_2, which are contained in the constants γ and h, become less important with time (because they are multiplied by t^{-2}).

REFERENCES

11-1. Wesselink, A.J.: Heat Conductivity and Nature of the Lunar Surface Material. Bull. of the Astron. Inst. Neth., vol. 10, 1948, pp. 351-363.

11-2. Birkebak, Richard C.; Cremers, Clifford J.; and Dawson, J.P.: Thermal Radiation Properties and Thermal Conductivity of Lunar Materials. Science, vol. 167, no. 3918, Jan. 30, 1970, pp. 724-726.

11-3. Watson, K.L.: Thermal Conductivity Measurements of Selected Silicate Powders in Vacuum from 150-350 K, II. An Interpretation of the Moon's Eclipse and Lunation Cooling Curve as Observed Through the Earth's Atmosphere from 8-14 Microns. Thesis, Calif. Inst. Technol., 1964.

11-4 Linsky, Jeffrey L.: Models of the Lunar Surface Including Temperature Dependent Thermal Properties. Icarus, vol. 5, 1966, pp. 600-634.

11-5. Lee, William H.K.; and Uyeda, Seiya: Review of Heat Flow Data. Terrestrial Heat Flow, ch. 6, William H.K. Lee, ed., Am. Geophys. Union of Natl. Acad. of Sci.-Natl Res. Council (Washington), 1965, pp. 87-190.

11-6. Baldwin, J.E.: Thermal Radiation from the Moon and the Heat Flow Through the Lunar Surface. Royal Astronomical Society Monthly Notice 122, 1961, pp. 513-522.

11-7. Troitskiy, V.S.; and Tikhonova, T.V.: Thermal Radiation from the Moon and the Physical Properties of Its Upper Mantle. NASA TT F-13455, 1971.

11-8. Tricker, Peter E.; Reynolds, Ray T.; and Summers, Audrey L.: On the Thermal History of the Moon. J. Geophys. Res., vol. 72, no. 10, May 15, 1967, pp. 2649-2663.

11-9. Cremers, C.J.; and Birkebak, R.C.: Thermal Conductivity of Fines from Apollo 12. Proceedings of the Second Lunar Science Conference, vol. 3, A.A. Levinson, ed., MIT Press (Cambridge, Mass.), 1971, pp. 211-216.

11-10. Robie, Richard A.; Hemingway, Bruce S.; and Wilson, William H.: Specific Heats of Lunar Surface Materials from 90 to 350 Degrees Kelvin. Science, vol. 167, no. 3918, Jan. 30, 1970, pp. 749-750.

11-11. Bullard, E.C.: The Flow of Heat Through the Floor of the Atlantic Ocean. Proc. Royal Soc. London, A, vol. 222, 1954, pp. 408-429.

11-12. Cremers, C.J.; Birkebak, R.C.; and White, J.E.: Lunar Surface Temperatures at Tranquility Base. AIAA paper 71-79, AIAA Ninth Aerospace Sciences Meeting (New York, N.Y.), Jan. 25-27, 1971.

11-13. Langseth, M.D., Jr.; Drake, E.I.; and Nathanson, D.: Development of an In Situ Thermal Conductivity Measurement for the Lunar Heat Flow Experiment. Lunar Thermal Characteristics, John Luce, ed., AIAA Lunar Progress Series, 1971.

11-14. Jaeger, J.C.: Conduction of Heat in an Infinite Region Bounded Internally by a Circular Cylinder of a Perfect Conductor. Australian J. Phys., vol. 9, 1956, pp. 167-179.

11-15. Murray, Bruce C.; and Wildey, Robert L.: Surface Temperature Variations During the Lunar Nighttime. Astrophys. J., vol. 139, no. 2, Feb. 15, 1964, pp. 734-750.

11-16. Winter, D.F.; and Saari, J.M.: A Particulate Thermophysical Model of the Lunar Soil. Astrophys. J., vol. 156, no. 3, June 1969, pp. 1135-1151.

11-17. Birch, Francis: Flow of Heat in the Front Range, Colorado. Bull. Geol. Soc. Am., vol. 61, no. 6, June 1950, pp. 567-630.

11-18. Jaeger, J.C.; and Sass, J.H.: Lees's Topographic Correction in Heat Flow and the Geothermal Flux in Tasmania. Geofis. Pura Appl., vol. 54, 1962, pp. 53-63.

11-19. Lachenbruch, A.H.: Rapid Estimation of the Topographic Disturbance to Superficial Thermal Gradients. Rev. Geophys., vol. 6, no. 3, Aug. 1968, pp. 365-400.

11-20. Ringwood, A.E.; and Essene, E.: Petrogenesis of Apollo 11 Basalts, Internal Composition and Origin of the Moon. Proceedings of the Apollo 11 Lunar Science Conference, vol. 1, A.A. Levinson, ed., Pergamon Press (New York, 1970, pp. 769-799.

11-21. Blackwell, J.H.: A Transient-Flow Method for Determination of Thermal Constants of Insulating Materials in Bulk. J. Appl. Phys., vol. 25, 1955, pp. 137-144.

ACKNOWLEDGMENTS

The authors wish to express their sincere appreciation to the many individuals whose enthusiasm and efforts have made possible the successful undertaking of this experiment. In particular, we wish to thank the personnel of the five corporations that developed, fabricated, and tested the essential instrumentation: Bendix Corporation of Ann Arbor, Michigan; Arthur D. Little, Inc., of Cambridge, Massachusetts; The Data Systems Division of Gulton Industries, Inc., of Albuquerque, New Mexico; Martin-Marietta Corporation of Denver, Colorado; and Rosemount Engineering Company of Minneapolis, Minnesota. The advice, encouragement, and active support of M. Ewing and the efforts of H. Gibbon, K. Peters, and R. Perry, all of the Lamont-Doherty Geological Observatory, were essential to the success of the program. The support of G. Simmons of the NASA Manned Spacecraft Center throughout the development of the experiment also is appreciated.

Revised
May 10, 1973

APOLLO 17 PRELIMINARY SCIENCE REPORT

HEAT FLOW EXPERIMENT

Marcus G. Langseth, Jr.

Stephen J. Keihm

John L. Chute, Jr.

Lamont-Doherty Geological Observatory of Columbia University

Palisades, New York 10964

HEAT FLOW EXPERIMENT

Introduction and Background

The objective of the Heat Flow Experiment (HFE) is to make a direct measurement of the vertical component of heat flow from the lunar interior through the surface. A second important objective is to determine the thermal properties of the upper 3 m of the lunar regolith.

The age of the Moon is placed at 4.6 AE. For a planetary body as small as the Moon, much of its initial heat energy has been lost to space since formation. Even if the Moon were initially at molten temperatures, the present flux at the surface would be small. The major contribution to the surface heat flow comes from heat generated by the disintegration of long-lived radio isotopes of ^{235}U, ^{238}U, ^{40}K and ^{232}Th. Thus the present surface heat flux reflects the abundance of these isotopes to a depth of about 300 km, or 43% of the volume of the Moon. It is now certain that extensive differentiation occurred during the early history of the Moon which would concentrate these isotopes in its outer shells. In this case the present surface heat flow would very nearly indicate the total abundance of these isotopes.

Over 5000 heat flow determinations have been made on Earth and they show the average global flux is 6.3×10^{-6} W/cm^2 (ref. 1). (Throughout this report we will use W-sec as the unit of heat energy. Other commonly used units are the calorie which equals 4.18 W-sec, and the erg which equals 10^{-7} W-sec. The average Earth heat flow is 1.5×10^{-6} cal/cm^2-sec and 63 ergs/cm^2-sec.) Urey (ref. 2) pointed out that the total rate of heat flow from the Earth is essentially equal to the total rate of heat production in the Earth if it were constituted of materials with chondritic abundants of U, K and Th. However, Gast (ref. 3) showed that

Earth rocks were strongly depleted in potassium relative to solar and chondritic abundances, which led Wasserburg et al. (ref. 4) to propose that to explain the Earth's heat flow, a higher abundance of uranium, nearly 3 times that of chondrites, is needed. He estimated a uranium abundance of about 30 ppb for the Earth.

Large variations of heat flow are observed over the surface of the Earth. These variations are principally related to the present tectonism of the Earth's lithosphere (ref. 5). The largest variations are observed at extensional and compressional boundaries of vast lithospheric plates that are moving relative to each other. Seismic observations (ref.6) and the preservation of ancient surface features on the Moon demonstrate that no comparable tectonic movements have occurred on the Moon for the past 3 AE. The Moon is tectonically dead compared to the Earth and therefore any variations in surface heat flow over the surface should reflect either deep-seated changes in abundances of radio isotopes or convective patterns in the Moon. The static nature of the Moon's outer crust makes it an attractive planet for heat flow measurements, since determinations at a single location might be quite representative of a very large region of the Moon if local surficial effects such as refraction by conductive inhomogeneities and topography are properly accounted for.

Numerous attempts have been made to determine the surface heat flow from the Moon by detecting thermal radiation from the Moon in the microwave band. Due to the partial transparency of lunar surface material, energy with wavelengths greater than 1 mm received at earth-based antennas originates in the subsurface and contains information on subsurface temperatures. By making estimates of thermal and electrical properties the heat flow can be determined from the change of brightness temperature with wavelength. The earliest heat-flow determination was that of Baldwin (ref. 7) who estimated

an upper limit of 1 x 10^{-6} W/cm^2. Russian investigators estimated the heat flow to be very nearly equal to that of the Earth based on a very careful set of radio telescope observations in the wave length band 3-50 cm (ref.8). These same measurements were later revised to give heat flows in the range 3 to 4 x 10^{-6} W/cm^2 using different thermal properties and a layered model (ref. 9).

On Apollo 15 the first direct measurement of heat flow through the lunar surface was made at Hadley Rille (26°06'N and 3°39'E). Now a second measurement has been made on Apollo 17 at the Taurus Littrow site (20°09'N and 30°45'E). At Taurus Littrow two probes to determine heat flow were emplanted about 11 m apart. Analysis of data taken during the first 45 days after emplacement indicates that the heat flow from one probe location is 2.8 x 10^{-6} W/cm^2 (0.67 μcal/cm^2-sec) and 2.5 x 10^{-6} W/cm^2 (0.60 μcal/cm^2-sec) at the second probe location. For comparison the value measured at Hadley Rille is 3.1 x 10^{-6} W/cm^2. The Hadley Rille measurement and the Taurus Littrow probe #1 measurement have an estimated error of ±20%. The probe #2 measurement at Taurus Littrow has a slightly larger uncertainty because the heat flow appears to be locally disturbed

Experiment Concept and Design

The concept upon which the Heat Flow Experiment is based is to measure directly the vertical flow of heat through the regolith. The measurement should be made far enough below the surface so that the time varying heat flow resulting from the very large diurnal variations of surface temperature is small compared to the flow from the interior. At Taurus Littrow this depth is about 100 cm. Below this depth the increase in temperature with depth principally results from the hotter lunar interior. The outward flow of heat, F_z, is directly proportional to the rate of temperature increase with depth, dT/dz:

$$F_z = -k_m \frac{dT}{dz} \qquad \text{(Eq.1)}$$

The constant k_m is the thermal conductivity. The negative sign simply indicates that heat flows in a direction opposite to the increase of temperature.

The experiment is designed to accurately measure the vertical temperature gradient in the lunar soil to a depth of 2.3 m. Surface temperature measurements are also made which can be used to deduce the thermal properties of the upper 10 to 15 cm of the regolith. In situ measurements of thermal conductivity of the regolith at depths where the gradient is measured are also carried out. Two measurementsof heat flow at locations separated by about 10 m are made to detect possible lateral variations.

Instrument Design: The essential parts of the heat flow instrument are two identical temperature sensing probes. (A drawing of a probe is shown in figure 1.) Each probe consists of two sections about 50 cm long. In each probe section there are two platinum resistance bridges. Each bridge consists of four 500-ohm filamentary platinum elements interconnected by evanohm wire. (A diagram of the bridge is also shown in figure 1.) Opposing arms of a bridge are wound together in a single sensor housing, and two sensor housings, comprising a complete bridge, are mounted at opposite ends of a probe section.

Voltage measurements on a bridge can be interpreted in terms of average bridge temperature, T_a, and temperature difference, ΔT, between sensors, by means of accurate calibrations. The temperature at each sensor can be

determined simply by $T_a \pm 1/2\ \Delta T$. The accuracies of the heat flow experiment temperature measurements are given in Table 1.

The cable thermocouples consist of a string of 4 chromel-constantan junctions embedded in each probe cable. The lowermost junction is positioned inside the gradient sensor housing at the top of the probe. The reference junction for each cable is inside the electronics housing and is mounted in an isothermal block with a platinum resistance thermometer (the reference thermometer). The thermocouple circuit is diagramatically shown in figure 1.

The accuracy of the thermocouple measurements has special significance for interpreting the subsurface temperature profiles at the Apollo 17 site. Therefore certain features of the thermocouple measurement, which affect the accuracy, should be described. Firstly only the chromel - constantan junction TC1 inside the topmost gradient is coupled with the reference junction during a measurement sequence. The other junctions TC2, TC3 and TC4 are coupled with TC1 so that, in effect, TC1 becomes the reference junction and the top gradient sensor becomes the reference thermometer. Since the temperatures of TC3 and TC4 are much closer to that of TC1 than to that of the thermometer in the electronics box the calibration errors are reduced by this technique. Secondly, the placement of junction TC1 inside the gradient sensor permits a direct comparison between the two sensors on the Moon. Thus an in situ calibration of the thermocouple circuit against the much more accurate gradient sensor is carried out.

Conductivity experiments are made using 1000-ohm heaters that surround each of the gradient sensor housings. The experiments can be operated in either of two modes by energizing the heaters at 0.002 W or 0.5 W depending on the conductivity of the surrounding regolith. Because of the low conductivity

of lunar material at Taurus Littrow, only experiments using the lower power have been made on the Apollo 17 experiment. After initiation, power is left on for 36 or more hours and the temperature rise of the sensor beneath the heater is precisely measured by the appropriate bridge. A more detailed description of the operation of the heat flow experiment can be found in ref. 11.

Deployment of the Experiment at Taurus Littrow

The heat flow experiment is deployed as part of the Apollo Lunar Surface Experiments Package (ALSEP) and is located about 200 m west of the LM landing site. The electronics housing is located about 9 m north of the ALSEP central station and the two probes are emplanted approximately 5.5 m on either side of the electronics housing on approximately an E - W line. The ALSEP site is on a local topographic high, perhaps an inter-crater ridge between two wide but shallow depressions north and southeast of the site. The two probes are emplanted near the rim of the shallow northern depression.

The borehole for probe #1 was drilled east of the electronics housing to a depth of 2.54 m, and the probe was inserted to the maximum possible depth, 2.36 m. The rim of a small, relatively recent crater about 2 m in diameter and 0.3 m deep lies about 1 m northwest of this borehole. One of the thermocouples, TC12, is in a portion of the cable exposed above the surface. This portion of the cable, which is covered by a black sleeve, is oriented nearly N - S and is tipped up toward the south about 15° relative to the surface.

Probe #2 is buried in a borehole drilled west of the electronics housing to a depth of 2.55 m. The rim of a 3 m crater is about 2 m northwest of this probe site. Thermocouple TC22 is exposed above the surface, aligned nearly N-S and is almost level relative to the surface.

Summary of the Theory Relevant to the Lunar Heat Flow Measurement

In this section we will review the important aspects of heat transfer that are essential to interpretation of our temperature and conductivity measurements. For the reader primarily interested in the experiment's results this section may be skipped and used for reference only. The discussion will be summary in nature and for more detailed description, the reader is referred to references 10 and 12.

The Initial Cool Down of the Probe; Estimates of Thermal Conductivity of the Regolith and Equilibrium Temperatures

When the borestem is drilled into the soil and the probe inserted, they are at temperatures considerably higher than their subsurface surroundings. These higher temperatures result from the temperature of these components above the surface before emplacement and heat generated during drilling. Because of the complexity of the drilling process, it is very difficult to estimate the amount of heat dissipated and its distribution along the borestem. We know from measurements made within minutes after the probes were inserted that the probe is about 40 to 50K warmer than the surrounding undisturbed lunar soil. Because of the very low thermal conductivity of the lunar soil, this heat is dissipated very slowly. Even after 45 days some of the thermometers indicate continued cooling.

In general, the rate of equilibration of each probe sensor to the surrounding lunar medium depends on a number of different parameters, including thermal and geometrical properties of the probe - borestem system, thermal properties of the adjacent lunar medium, the thermal contact between the borestem and adjacent zone of disrupted lunar material and the total heat energy excess of the system upon completion of drilling. For long times ($t > 20$ hr) after the

probes are inserted, however, the probe sensor temperatures above equilibrium depend essentially on just two quantities, the total initial energy excess per unit length of the system, ΔE, and the thermal conductivity of the adjacent regolith, K_m :

$$T_p(t) - T_\infty = \Delta E/4\pi K_m t \qquad \text{(Eq. 2)}$$

where $T_p(t)$ = a probe sensor temperature at time t since emplacement
and T_∞ = the equilibrium sensor temperature.

The form of equation 2 has been verified by finite difference models as well as an analytical solution appropriate to a simplified distribution of ΔE between the probe and borestem. The analytical solution, which takes the form of equation 2 for long times, is described in detail in the appendix of section 11 of the Apollo 15 Preliminary Science Report (ref. 10).

Estimates of the regolith conductivity, K_m, can be made from the long time cool-down data using /equation 2 once a value for ΔE is assumed. Because of the uncertainties of the contribution of the drilling process to the total excess heat energy, two different assumptions have been made in regard to the ΔE term: first, that drill-heating effects are negligible and that all excess heat energy initially resides in the probe and borestem. The probe and borestem are assumed to be at the same initial temperature, T_0, following drilling, as measured by the probe sensors. For this assumption the initial energy excess can then be expressed simply as:

$$\Delta E = (S_p + S_b)\,(T_0 - T_\infty) \qquad \text{(Eq. 3)}$$

where S_p and S_b are the heat capacities per unit length of the probe and borestem respectively. The resultant problem has an analytical solution which is used to determine regolith conductivity estimates from the cool-down data. The above assumptions constitute the "minimum initial energy" case.

As a maximum initial energy estimate, it was assumed that a 2.2 mm thickness of disrupted lunar material had received enough heat during the drilling process to attain an initial temperature equal to that of the probe and borestem. The 2.2 mm contact zone thickness was chosen to correlate with the difference in drill-bit radius and borestem radius. The subsequent cool-down problem was then solved, assuming radial heat dissipation, using a finite difference model. The curve matching procedure was carried out for times > 20 hr when all parameter effects, with the exception of k_m, are negligible; i.e., when equation 2 is valid.

Because of the form of equation 2, the probe equilibrium temperatures can be estimated quite accurately independent of initial conditions and k_m. By considering sensor temperatures T_{p1} and T_{p2} for times t_1 and t_2 > 50 hr, we may eliminate the unknown factor $\Delta E/4\pi k_m$ from equation 2 to obtain:

$$T_\infty = \frac{T_{p2} \cdot t_2 - T_{p1} \cdot t_1}{t_2 - t_1} \qquad \text{(Eq. 4)}$$

Equilibrium temperatures differences, measured by the platinum resistance bridges, can be calculated in a similar manner.

Heat-Activated Conductivity Measurements

Since all eight conductivity measurements were made with a heater power of .002 W, this discussion will be confined to this mode of experiment. After the heater is energized, the temperature rise at the gradient sensor it encloses depends in a complex way on the thermal properties of nearby probe components, borestem and lunar material, as well as the contact zones between these elements. A detailed finite difference model of the conductivity experiment at each heater location is used to interpret the temperature history of the gradient sensor in terms of the conductivity of material external to the borestem. Numerical model computations, laboratory experiments and lunar experiments indicate that for times > 20 hrs the temperature rise, $\Delta T(t)$, is well defined by the simple relation:

$$\Delta T(t) = c_1 \ln(t) + c_2 \qquad \text{(Eq. 5)}$$

where c_1 and c_2 are constants. The form of equation 5 is the same as that for a heated infinite cylinder in an infinite homogeneous medium at long times; i.e. > 20 hr for a cylindrical source with a radius and heat capacity per unit length of the HFE probe - borestem system (ref. 13).

For an infinite cylindrical source

$$c_1 = Q/4\pi k_m \qquad \text{(Eq. 6)}$$

where Q is the power per unit length in W/cm. Thus c_1 depends solely on the heater power per unit length and conductivity. The constant c_1 can be easily determined since it is the slope of the temperature rise curve when

plotted versus ln t; therefore cylindrical sources are often used as a practical technique for measuring conductivity.

Conductivity is determined from lunar experiments by comparing observed slopes on a logarithmic time scale with values of c_1 calculated with the finite difference models. Parametric studies, in which certain thermal properties are varied singly in the numerical model, show that for times > 20 hr c_1 is very nearly insensitive to: changes in ρc of the surrounding medium, changes in borestem conductance and changes in the thermal links between the probe and borestem and the borestem and lunar medium. However, c_1 is sensitive to changes in conductance in the probe body which can alter the flow of heat from the heater axially along the probe. Assumptions of thermal properties in the numerical models that influence axial heat transfer along the probe are probably the largest source of error in the conductivity determinations.

The similarity in performance of the lunar conductivity experiment and an infinite cylindrical source is principally due to the relatively efficient flow of heat axially along the borestem. Even though the probe heater is very short, 1.9 cm, it heats a section of borestem that is long compared to the borestem diameter. For times > 20 hr the isotherms in the surrounding medium are roughly cylindrical in the vicinity of the heater as is shown in figure 2. The numerical computations also show that the experiment is most sensitive to lunar material within about 5 cm of the borestem wall.

The effective conductance of the contact zone has a very pronounced effect on the magnitude of the sensor temperature rise at any given time.

Since k_m can be determined independently the conductance of the contact zone is the principal remaining unknown parameter, and can be determined by matching observed and theoretical temperature curves for times > 0.5 hr.

Variations in Surface Temperature and its Effect at Depth

Lunar surface temperatures vary nearly 300K from just before lunar dawn to lunar noon. This variation induces subsurface variations that propagate downward as thermal waves. For a homogeneous medium of diffusivity α with a sinusoidal variation, $A_0 \cos \omega t$ at the surface, the temperature at a given depth, z, is given by

$$T(t, z) = A_0 e^{-\delta z} \cos(\omega t - \delta z) \qquad \text{(Eq. 7)}$$

where A_0 is the amplitude of the surface variation (degrees), ω the angular frequency (rad/sec) (2.5×10^{-6} for the diurnal variation and 2×10^{-7} for the annual variation), and $\delta = \sqrt{\frac{\omega}{2\alpha}}$ (cm^{-1}). (Eq. 8)

Equation 7 indicates that the variation decreases in amplitude by a factor e^{-1} and is delayed in phase one radian for every δ^{-1} centimeters of depth.

Propagation of surface temperature variations into the lunar regolith is more complex for a number of reasons. Firstly, the surface variation is not a simple sinusoid but contains significant higher harmonics. Secondly, thermal properties vary significantly with depth; and thirdly, radiative transfer, which depends on T^3, plays an important role in the upper few centimeters of the lunar soil. It is necessary to resort to numerical calculations which include these complications to determine the

expected temperature variations in the subsurface. In figure 3 the peak-to-peak attenuation and phase lag of the diurnal variation is shown as a function of depth for the conductivity profile at the Apollo 17 heat flow site. The upper part of the conductivity profile is derived from surface temperature measurements which are described in a later section of this report. Notice that for depths greater than a few centimeters the amplitude decreases in a simple exponential fashion as evidenced by the nearly straight line on a semilog scale. Similarly the phase lag shows a nearly linear increase with depth below a few centimeters. Thus the simple relation of equation 7 would nearly apply below these depths.

The temperature at lunar noon varies throughout the year due to the varying distance of the Earth - Moon system from the Sun. The noon temperature increases about 6K from aphelion to perihelion. The mean temperature, i.e., surface temperature averaged over a lunation, varies about 3K throughout a year. Although the amplitude of the annual cycle is a hundredth of the diurnal variation, the decay constant δ is $\sqrt{12}$ times smaller; consequently, annual variations penetrate deeper and induce significant heat flows to depths of a few meters and must be considered in interpretation of the experiment's results. The attenuation of amplitude and increase in phase lag for the annual wave is shown in figure 3 as a function of depth. Annual wave effects shown in figure 3 are based on the conductivity profile at Hadley Rille.

From figure 3 it can be seen that temperature fluctuations due to the diurnal cycle become virtually undetectable at depths > 100 cm and would have had little effect on heat flow below this depth before the probe and borestem were emplaced. Once the borestem is emplanted in the regolith,

its higher conductivity and radiative transfer inside the borestem will enhance the propagation of thermal waves downward. However, thermometers at 130 cm below the surface do not detect any temperature variation during a lunation cycle.

Corrections for the Shunting Effects of the Borestem and Probe

The axial conductance of the epoxy borestem is considerably higher than a vertical column of lunar soil of equal cross section. This fact, combined with the finite length of the borestem, results in some shunting of the steady-state heat flow through the borestem to the surface. Certain short sections of the borestem such as the bit and joints are made of titanium or steel and sizable disturbances occur near these parts. A second related effect results from the fact that the probes are radiatively coupled to the borestem walls and have a small axial conductance. This causes the probe bridges to read slightly smaller temperature differences than points on the borestem immediately adjacent to sensors.

These effects can be estimated by simplified analytical models and by laboratory experiments; both methods were used in our earlier analysis of Apollo 15 results. However, for the Apollo 17 analysis and the refined Apollo 15 results presented in this report, we have resorted to a numerical model of the probe in a medium in which heat is flowing parallel to the probe axis. The numerical model besides being more detailed also allows examination of certain combined effects that are hard to estimate with analytical models.

The numerical model computations show that the borestem and probe disturbances to the steady-state heat flow are small. In the extreme case the temperature difference across a probe section is 7% lower than the tempera-

ture difference across the same vertical distance interval far from the borestem. The numerical model has been used to apply corrections to all probe observations.

RESULTS

Subsurface Temperatures

The heat flow experiment was turned on while probe #2 was being inserted into the borestem and temperatures were recorded only minutes after drilling was complete. These temperatures ranged from 295K to 301K. The early cooling histories of probe #1 indicate similar initial temperatures. Subsequent to emplacement the probes cool toward the undisturbed regolith temperatures. Figure 4 shows the temperature histories of all sensors deeper than 65 cm for the first 45 days. After 45 days some sensors are continuing to cool; however, the expected future decrease is probably less than the error of absolute temperature measurement.

The equilibrium temperature differences and absolute temperatures of each sensor are listed in Table 2. The correction for the steady-state disturbance of the heat flow by the borestem and probe system is applied to temperature data listed under the headings "corrected temperature difference" and "corrected temperature." The appropriate corrections of the temperature difference due to the annual thermal wave during January 1973 are listed in the far right-hand column, but they have not been applied because they are based on the conductivity profile at Hadley Rille. Note that the largest correction is about -4%.

Temperature measurements of the thermocouples TC14 and TC24 are also shown in figure 4. Some randomly sampled representative points are

shown and the solid curve is fitted by eye to show the trend. The standard deviation of the points around the smoothed curve is about 0.3°C during the day and about half that value during the night. The values shown are calculated by subtracting the temperature at TC1 from that at TC4 and adding the result to the temperature at the top gradient sensor.

Comparison of the temperatures measured by TC11 and TC21 with those at the top gradient sensors show relatively large errors in absolute temperature measurement. The errors are shown in Table 3 below. The source of these errors has been traced to copper - kovar (Cu/Ko) junctions in each thermocouple circuit that are mounted on circuit boards in the electronics housing. The errors are proportional to temperature differences between the Cu/Ko junctions, so that the errors in TC11 and TC21 are direct measures of this temperature difference and can be used to estimate errors at all junctions. The larger errors during the night result from larger temperature gradients across the Cu/Ko junctions at night, and the larger errors at probe #2 junctions are caused by a greater distance between the Cu/Ko juntions in the probe #2 circuit. A preliminary analysis of EMF's produced by Cu/Ko junctions was used to calculate the corrections that should be applied to the data in figure 4. These corrections virtually erase the apparent variation between night and day. The corrections have been applied to the data compiled in Table 2. The uncertainty of determining these corrections is estimated as $\pm$0.4°C. Studies of the accuracies of the thermocouple measurements are continuing.

The values given in Table 2 represent the mean of the last 30 days of observation. The amplitude of the diurnal variation at this depth

cannot be determined with the present accuracy of the data, ±0.5 K.

In figure 5 the equilibrium temperatures are plotted as a function of depth. Temperatures along the body of probe #1 show a steady decrease in gradient with depth. The gradient decreases from .016 in the depth range 130 to 177 cm to .012 K/cm in the range 185 to 233 cm. This decrease is principally due to a general increase in conductivity of the regolith over the interval of measurement. The thermocouple temperature indicates a gradient of .013 K/cm from 66 to 130 cm; however the accuracy of this measurement is poor.

At probe #2 the probe thermometers (131 to 234 cm) indicate a rather uniform gradient of 0.0078 ./cm, whereas the gradient between 67 and 131 cm is 0.021 K/cm, a change by a factor of about 3. This large variation of gradient can only be partially accounted for by the variation of conductivity of the regolith immediately surrounding the borestem.

Apollo 15 Subsurface Temperatures

Subsurface temperatures measured at Hadley Rille below the depth disturbed by diurnal variations were reported in the "Apollo15 Preliminary Science Report" without correction for the annual wave. In addition, corrections for the borestem and probe disturbance were derived from much simpler models than those discussed in this report. Temperatures measured at longer times after probe insertion are now available and they allow a more accurate determination of equilibrium temperatures. The temperatures and temperature differences at four sensors on probe #1 at Hadley

Rille are presented in Table 4. More accurate corrections for the borestem disturbance and a correction for the annual wave effect have been applied. These measurements will be the basis for a slightly revised heat flow value.

Conductivity Estimates from Cool-Down Analysis

Because of the uncertainties in the total heat energy associated with drilling, two cases assuming different initial conditions have been examined. These cases have been described in the preceding section on theory. Results derived assuming initial borestem and contact zone temperatures equal to the initial probe sensor temperature are listed in Table 5 under the heading "With Drill Heating Effects." Conductivity estimates derived assuming that only the borestem and probe were initially at elevated temperatures are listed under the heading "Without Drill Heating Effects." The two cases are considered to be bracketing assumptions of the actual initial conditions. Cool-down conductivity estimates were made for each of the eight sensors along each probe. Additionally, cool-down analyses were performed assuming drill heating effects for the thermocouples located 65 cm above each probe.

The large noise on the thermocouple data limits the accuracy of conductivities deduced from their cooling history. Deductions of the conductivity at depths from 3 to 15 cm below the surface, which will be discussed later in this report, give values of about 1.2×10^{-4} W/cm-k. Based on these results at shallow depths we estimate the conductivity lies in the range 1.0 to 1.6×10^{-4} W/cm-k at 66 cm. This range is indicated in figure 5.

It can be seen by comparison with the more accurate heater-activated conductivity determinations discussed in the next section that drill heating effects cannot be neglected if reliable conductivity information is to be extracted from the cool-down data. When substantial drill heating effects are included in the cool-down analyses, conductivity determinations as well as variations with depth agree well with the heater-activated conductivity experiment results. The cool-down conductivity estimates are particularly valuable in interpolating between the more accurate heater-activated conductivity determinations.

Heater-Activated Conductivity Experiments

Conductivity experiments at each of the eight heater locations have been carried out. Figure 6 shows the sensor temperature rise history together with theoretical curves for one such experiment. The conductivities k_m and contact conductances H_2 are given in Table 6. These results are shown in figure 5 together with the cool-down estimates with drill heating effects. It is clear that the conductivity does not vary in any simple way with depth.

There is a rough correlation between drill penetration rate during borestem drilling and the measured conductivity. The more resistant layers where the drill penetrated slowly correspond to depths where higher conductivity is observed. The more resistant layers likely correspond to more compacted regolith materials or possibly to a higher concentration of centimeter size rock fragments. Either of these phenomenon can increase the bulk conductivity.

The relatively high conductivity measured at 130 cm on probe #1 lies within a zone from 80 to 130 cm where penetration was slow. Directly below this layer, drilling rates were relatively high and the conductivity values are correspondingly lower. These correlations are used to interpolate values between discrete measurements. In figure 5 the solid line which passes through the heater-activated conductivity values represents a layered model of conductivity in the regolith based in part on penetration rates and in part on cool-down estimates. At probe #2, some of the drilling operation was not visually monitored so that correlations with conductivity cannot be made during the unmonitored period which includes about half the depth range where the probes are emplaced.

One interesting feature of these conductivity results is a rather large difference between the conductivity profiles at probe #1 and probe #2. It is possible that layers as defined by conductivity have some dip relative to the surface. For example, the high conductivity layer at 100 cm at probe #1 could correspond to the high conductivity layer between 170 and 230 cm at probe #2.

The contact conductance, H_2, arises from low conductivity material lying in a disturbed zone just outside the borestem. We estimate this zone to be 2.2 mm thick. The conductivity, K_c, of material in the contact zone is given by

$$K_c = H_2 \cdot [b + 1/2\ \Delta r] \ln \left(\frac{b + \Delta r}{b} \right) . \qquad \text{(Eq. 9)}$$

See figure 2 for definition of parameters in this equation. As an example for H_2 = 1.4 x 10^{-4} W/cm^2-K, K_c = 3.0 x 10^{-5} W/cm-K. This value of conductivity is about a factor of 6 less than the surrounding regolith.

Apollo 15 Results

Six conductivity experiments using a heater power of 0.002 W were run on Apollo 15 probes. The analyses of three of these measurements were not described in the "Apollo 15 Prelimin Science Report" because it was very difficult to separate changes due eater turn-on from large diurnal variations in temperature. Subsequently, two of the measurements have been repeated at times in the lunation when the rate of temperature change at the heater location was minimal. In addition, diurnal temperature variation from preceding and succeeding lunations are available to help interpolate trends during the time that the heater is on. Lastly, some refinements have been made in the finite difference models of the conductivity experiments. The newer models indicate small adjustments in our previously published values. The revised Apollo 15 conductivity values at each heater location are given in Table 6.

Heat Flow

The magnitude of the vertical component of heat flow in the regolith can be calculated from the temperature and conductivity profiles in figure 5. Over each depth interval z_1 to z_2

$$F_z = K_{ave} \frac{\Delta T_{z_1-z_2}}{z_2-z_1} \qquad \text{(Eq. 10)}$$

where $\Delta T_{z_1-z_2}$ is the corrected temperature difference listed in Tables 2 and 4, and K_{ave} is the average conductivity in the depth interval z_1-z_2 calculated from the layered models in figure 5.

Gradients, average conductivities and heat flows calculated from Apollo 15 and Apollo 17 results are presented in Table 7. Notice that the bottom line of Table 7 for Apollo 17 probes #1 and #2 presents heat flow data over the entire depth range of temperature measurement. At probe #1 the most representative value of heat flow is thought to be that determined by the probe data, 2.8×10^{-6} W/cm^2. At probe #2 the measurement is possibly disturbed as will be discussed below and the most representative value is that calculated using data between 67 and 234 cm, 2.5×10^{-6} W/cm^2. The heat flow calculated over the interval 91-138 cm is felt to be the best value from the Apollo 15 measurements.

At the Apollo 17 probe #1 site the heat flow is quite uniform over the entire depth range. The variation falls well within the estimated error of measurement. Probe #2 results show a uniform heat flow along the length of the probe but heat flow between 67 and 131 cm is 70% greater. The large change in gradient is only partly compensated for by an increase in conductivity with depth. The overall heat flow, 2.5×10^{-6} W/cm^2 , is in fair agreement with the probe #1 value 2.8×10^{-6} W/cm^2.

DISCUSSION OF HEAT FLOW RESULTS

The Probe #2 Measurement

The change in heat flow at probe #2 by a factor slightly less than 2 over the depth range 67 to 234 cm is most reasonably explained by refraction of heat flow in the vicinity of a large buried boulder. A

relatively large number of rocks are strewn over the ALSEP area. Lunar basalts have conductivities of about 1.2 to 1.8 x 10^{-2} W/cm-K at 250K (ref.15). These values are 60 to 90 times the conductivity of the fine-grained regolith material. Thus large blocks of solid rock in the subsurface can result in significant shunting of heat flow.

To illustrate the shunting effect, the distortion of heat flow lines and isotherms around and through a square of material having 60X the conductivity of a surrounding infinite medium is shown in figure 7. The model is two-dimensional and symmetric about the left-hand margin of the figure. One significant feature of the model is that very little effect is felt at distances > 1/2 the width of the rock. Thus heat flow measurements would have to be made quite close to a rock, < 1/4 the width, to detect a disturbance as large as that at probe #2. On the other hand, probe #2 must be more than 5 cm from a rock in order for the rock not to have a detectable effect on the heater-activated conductivity experiments.

If probe #2 were located relative to a large subsurface boulder in a zone defined by the dashed rectangle in figure 7, a temperature profile similar to that observed would result. Other features such as the slightly higher absolute temperatures measured by probe #2 relative to probe #1 at all depths would also be explained. It should be noted that to explain the rather sudden change in gradient shown in figure 5, a rather sharp cornered rock is required.

If the vertical gradient were calculated using the temperature difference between points (a) and (b) in figure 7, the result would not be much different from the vertical gradient far from the rock. This is be-

cause the measurement interval is large enough to span the zone of dilation of isotherms adjacent to the rock and the compensating zone of compression of isotherms above it. If the same is true for probe #2, then the gradient determined by using temperature points at 67 and 234 cm should be close to the regional value. The fact that the average gradient at probe #2 is in close agreement with results of probe #1, which is thought to be free of such disturbances, supports this possibility. The results of probe #1 should be regarded as the more representative value of heat flow at Taurus Littrow.

The Effects of Topography:

Detailed assessment of the effects of topography on the Taurus Littrow measurement have not been completed in time for this report. However, some idea of the magnitude of expected disturbances can be made based on very simplified terrain models. On the Moon there are two important effects of topography: 1) Surface relief causes a distortion of subsurface isotherms to conform to the surface temperature distribution. Consequently a lowering of regional heat flow is generally found over features that are convex up and an augmentation of heat flow over concave up features. 2) Because the mean surface temperature depends on a radiative balance of solar flux, radiation to space and reradiation from the surrounding lunar surface, lunar topography has a significant effect on the surface temperature distribution. In general, depressions such as craters will have slightly elevated mean temperature because of the decreased view of the crater floor to space and reradiation from other parts of the crater (ref. 16). On the other hand a north-facing slope such as that of the South Massif would have a lower mean temperature because of

the relatively large angle of incidence of solar rays throughout the lunar day.

Craters of all sizes greater than 1 m in diameter that are within a distance of one crater diameter could have a measurable effect on the heat flow measurement. For example, the small craters near probes #1 and #2 must be considered as well as the 600 m crater called Cameiot about 600 m to the east of the ALSEP site. Most of these craters have an aspect ratio, diameter over depth, of about 6 to 1. The dominant effect of such craters is to increase heat flow in areas just outside the rim due to the slightly higher mean surface temperature inside. Finite difference models show that the excess heat flow falls off very rapidly with distance from the crater rim. At one crater radius from the rim of a crater whose floor is warmer by 3K than the surrounding flat surface, heat flow is increased - .1 W/cm^2. Since the heat flow probes are one or more radii away from the rims of all craters of interest, the combined effect of all craters would be small. An estimate of .3 W/cm^2 or 10% would be conservative. The important result is that a negative correction must be applied to the observed values to compensate for nearby craters.

The valley floor at Taurus Littrow aside from craters is relatively smooth and only the mountain ranges north and south of the site would have significant effects. The effect of the massifs can be estimated using a method developed by Lachenbruch (ref. 17). The valley at Taurus Littrow is modeled as a flat-floored trough in an otherwise flat surface. The walls of the trough have uniform slopes equal to the average slopes of the north and south massifs measured from topographic maps. Lachenbruch has published tables which permit an estimate of the effect on heat flow of

such sloping surfaces intersecting horizontal planes. Based on this model the topographic effect of the massifs will cause a +20% increase in heat flow at the ALSEP site. This estimate is maximal since it assumes that the trend of the ridges extends infinitely at their maximum elevation. The effect of the South Massif in particular is overestimated because the ridge does not extend very far to the southeast of the ALSEP site.

Lastly, the valley at Taurus Littrow would have a slightly greater mean temperature (~ 1 - 2K) than the surrounding regions because it behaves radiatively like a crater. The flow of heat from the warmer valley floor to the surface outside the bounding massifs would tend to decrease the heat flow in the valley. This effect has not been quantitatively estimated at this time. It may be significant and would tend to counterbalance the positive effects already described.

In summary, our preliminary analysis of the effect of topography on the Apollo 17 measurement indicates that a negative correction estimated at 15 to 25%, should be applied to this observation. However, we feel that we should await a more detailed and careful analysis before assuming that effects of topography result in a significant difference between the heat flow measurements at the Taurus Littrow and Hadley Rille sites.

Possible correlation with surface radioactivity

As described above, a correction for the gross effects of topography of about -20% might be applicable to observed heat flow at Taurus Littrow, which would result in a value about 25% less than that measured at Hadley Rille. Because the difference depends on the topographic correction, its

significance may be questionable. However, taken at face value there is a correlation between the heat flow at the two sites and the surface radioactivity, as measured by the Apollo 15 gamma ray spectrometer (ref. 18). Relatively high thorium abundances were observed over the southeast corner of Mare Imbrium and appreciably smaller abundances over the southeast corner of Serenitatis. The gamma ray spectrometer is sensitive only to isotopes in the most superficial layer. This tentative correlation with the heat flow measurement, which detects the integrated effects of radiogenic heating to depths on the order of ~ 300 km, indicates the surficial variations may extend to depth. It further suggests that the variation of surface radioactivity may be the best available indicator of the variation of heat flow over the lunar surface. We want to reemphasize these conclusions must await a more thorough analysis of topographic effects.

Comparison with Earth-Based Microwave Measurements

Prior to the in situ measurements of Apollo 15 and 17, estimates of the lunar heat flow have been made based on centimeter wavelength observations of the Moon's natural emission. (See, for example, references 7 - 9). As is well-known, beyond the infrared, the lunar regolith becomes increasingly transparent at longer wavelengths. Thus, observations at longer wavelengths yield temperature information at increasing depths into the lunar regolith. For wavelengths greater than about 5 cm, the effective emitting layer is far enough below the lunar surface that no variation in apparent brightness temperature over a lunation can be detected. However, an increase in brightness temperature with increasing wavelength has been observed. A plot of these measurements is given in ref. 9. Between 5 and 20 cm, a nearly linear increase

of brightness temperature, $T_b(\lambda)$, with wavelength, λ, yields an average spectral gradient of $\partial T_b/\partial\lambda = 0.8K/cm$. To interpret the spectral temperature gradient in terms of a heat flow, one must estimate the electrical properties, as well as the thermal conductivity, k, of the effective emitting layer for the 5 - 20 cm waves. In particular, the characteristic penetration depth of an electromagnetic wave, $\ell_e(\lambda)$, must be known as a function of wavelength.

Tikhonova and Troitskii (ref. 9) used simplified models of thermal and electrical property profiles to explain the microwave data over the spectral range 5 - 50 cm. Their resultant inferred heat flow values of $2.9 - 4.0 \times 10^{-6}$ W/cm are in remarkable accord with the in situ Apollo measurements, considering the approximations and assumptions necessary to the remote determination. In particular, the electrical and thermal parameters were estimated from observations only applicable to depths characterized by diurnal temperature variations. The assumption that near surface parameter values apply to meter depths could lead to significant errors in the interpretation of the observed spectral gradient. Electrical property determinations based on remote radar measurements as well as measurements on returned lunar samples must be used to interpret the measured spectral gradient in terms of a thermal gradient. If the electrical and thermal properties of the regolith are considered homogeneous for depths greater than about 70 cm, and extend at least 5 - 10 m, the thermal temperature gradient can be expressed in terms of the spectral gradient by the following equation:

$$\frac{\partial T}{\partial z} = \frac{\lambda \partial T_b/\partial\lambda}{(1-R)\ell_e} \qquad \text{(Eq. 11)}$$

where R is the appropriate centimeter wave reflection coefficient for the lunar surface - space interface.

For very low electrical conductivities as are found in the lunar regolith, the electromagnetic penetration depth, $\ell_e(\lambda)$, may be written for the centimeter wave spectral region as:

$$\ell_e(\lambda) = \lambda/(2\pi\sqrt{\epsilon}\ \tan\ \Delta) \qquad \text{(Eq. 12)}$$

where ϵ is the dielectric constant and tan Δ the loss tangent at centimeter wavelengths.

The average temperature gradient measured in situ at the Apollo 15 and 17 sites, 0.017 K/m, would produce the observed spectral gradient if $\sqrt{\epsilon}$ tan $\Delta \simeq .003$, assuming R = 0.05. The feasibility of such a value for $\sqrt{\epsilon}$ tan Δ is supported by direct surface observations of Weaver in the 0.4 to 3 cm wavelength range (ref. 19). Direct measurements of returned Apollo samples over a wide range of frequencies indicate a dielectric constant for the regolith material in the range 2.2 - 3.2 that is nearly frequency independent. However, loss tangent measurements yield values in the range 0.0004 - 0.01, and are frequency dependent (ref. 20, 21, 22). Additional electrical property measurements and refined analysis of the existing data on regolith samples must be made before the thermal gradient measured in situ can be supported on a Moon-wide basis by the spectral gradient observations.

The Representativeness of the Two Heat Flow Measurements

The regional geological settings of Hadley Rille and Taurus Littrow are quite similar. Both are located on lava-flooded embayments at the edge of mascon basins. If the heat flow is influenced by structural or compositional anomalies unique to this type of region, they would affect both measurements. To that extent they would not be representative of global flux from the moon. On the other hand, the possible compatibility of our results with the microwave emission spectral gradient between 5 and 20 cm wavelength lends support to the possibility that local anomalies at the two sites are not large.

Despite the reservations set down in the previous paragraphs, the existing data concerning heat flow from the lunar interior indicates that a significant area of the Moon is characterized by a flux of between 2.5 and 3.0 $\mu w/cm^2$. Numerous thermal history calculations have shown that the contribution of initial heat (e.g. that gained during accretion) to the present surface flux is relatively small (ref. 10,23) even if the Moon were molten throughout initially. Some scientists have suggested that at the present time the Moon is thermally atsteady state (e.g. ref. 24). In either case, it follows that a predominant part of the surface flux, 2.0 to 3.0 $\mu w/cm^2$, must result from radioactive isotopes in the Moon. The geochemical data is convincing that most of these isotopes are concentrated in the outer layers of the Moon. In addition, the abundances indicated by the heat flow values would require that the heat sources be near the surface to prevent melting in the outer several hundred kilometers.

The radiogenic heat production per cm^3 of rock can be expressed in terms of the abundance of uranium since the ratios of the other two im-

portant long-lived, heat-generating isotopes, ^{40}K and ^{232}Th, to uranium is well established and quite uniform in the lunar samples. The heat production per unit volume at the present time in W/cm^3 is about 0.71 times the uranium abundance in ppm (e.g. ref. 23 and 25). If most of the uranium is concentrated within 300 km of the surface, so that it contributes to the present flux, then the total lunar uranium abundances required to contribute 2.0 to 3.0 $\mu W/cm^2$ to the heat flow is about .05 to .075 ppm. These abundances are much higher than those of chondrites and significantly higher than estimates of the Earth's total abundance of about .03 ppm (ref. 4).

SURFACE TEMPERATURES DEDUCED FROM THERMOCOUPLE MEASUREMENTS

At each of the two heat flow holes, one of the thermocouples is embedded in a section of the cable which is approximately 15 cm from the top of the borestem and suspended above the lunar surface (see fig. 8). These thermocouples are in radiative balance with the lunar surface, the solar flux and space and hence provide a measurement of the surface brightness temperature throughout the lunation. The flux balance equation governing the thermocouple temperature is:

$$2\pi a_c dl\, \epsilon_c \sigma T_c^4 = 2\pi a_c dl\, F_{c-m}\, \epsilon_m\, \alpha_{cir}\, \sigma\, T_m^4 + 2 a_c dl\, S\, \alpha_{cs} \sqrt{1-p^2} + 2\pi a_c dl\, SA\, \alpha_{cs}\, F_{c-m} \cos\lambda \sin\phi \quad \text{(Eq. 13)}$$

where: T_c = thermocouple temperature

T_m = lunar surface brightness temperature

a_c = radius of thermocouple cable

dl = elemental length of cable

ϵ_c = infrared emissivity of cable

α_{cir} = infrared absorptivity of cable

α_{cs} = absorptivity of cable to solar flux

F_{c-m} = view factor of cable to the lunar surface, including the surrounding mountains

P = cosine of the angle between the sun line and the cable axis, a function of cable orientation and lunar phase angle

λ = selenographic latitude at Taurus Littrow

ϕ = lunar phase angle measured from local sunrise

ϵ_m = infrared emissivity of the lunar surface $\cong 1.0$

S = the mean solar constant = .1352 W/cm^2

A = the lunar albedo = 0.08

σ = the Stefan-Boltzmann constant

The first term on the right-hand side of equation 13 represents flux into the cable element from the lunar surface; the second term represents direct flux from the sun; the third term represents solar energy reflected diffusely from the lunar surface and impinging on the cable.

The radiative properties of the cable, ϵ_c, α_{clr}, α_{cs} were determined by laboratory measurement prior to the Apollo 17 mission. The cable orientations for both probe locations were determined from ALSEP photographs.

Solving equation 13 for the surface brightness temperature yields:

$$T_m = \left[\frac{\epsilon_c \sigma T_c^4 - (S/\pi)\alpha_{cs}\sqrt{1-\rho^2} - SA F_{c-m} \cos\lambda \sin\phi}{F_{c-m}\,\epsilon_m \alpha_{clr}\,\sigma} \right]^{1/4} \quad \text{(Eq. 14)}$$

During the lunar night, using $\epsilon_m = 1$ and $\epsilon_c = \alpha_{clr}$, equation 14 reduces to

$$T_m = \left[\frac{T_c^4}{F_{c-m}} \right]^{1/4} \quad \text{(Eq. 15)}$$

Equations 14 and 15 assume that the surrounding mountains at Taurus Littrow are at the same temperature as the surface throughout the lunation. The deviation from this assumption, especially during the lunar day, may be quite large. However, both of the thermocouples have view factors to the mountains about 1/12 of their view to the surface. Thus, even large anomalous temperatures on the slopes of surrounding mountains will produce only negligible errors in the surface temperature determination.

Shown in figure 9 is a full lunation plot of deduced lunar surface brightness temperatures at Taurus Littrow. Vertical bars represent estimated error bounds. The daytime temperatures were determined solely from the temperature data of the exposed probe #2 thermocouple for two reasons. First, the orientation of the thermocouple at probe #1 was much more difficult to obtain from the photographs; second, the probe #1

thermocouple appeared to have a more substantial view of the radiation shield atop the borestem; the radiation shield is a highly reflective square of aluminized mylar which could add a substantial unknown factor to equation 14.

The nighttime temperatures are not subject to the errors due to uncertainties of the cable orientations and the data shown is an average of the two thermocouple reductions. Nighttime surface temperatures deduced from each of the two above-surface thermocouples differed by no more than 2K throughout the lunar night. The data gaps near sunset and immediately following sunrise correspond to times of rapid temperature changes. During these periods, equation 14 loses its validity as the finite time constant of the thermocouple cable must be taken into account.

From the data of figure 9, a mean surface temperature of 216K (±5K) was calculated for the Taurus Littrow site, indicating a mean temperature rise of ~ 39K between the surface and the top probe sensors. Only a small part of this mean temperature rise (no more than 5K) can be accounted for by the measured heat flow. The mean temperature gradient is due mainly to the contribution of radiative heat transfer within the highly porous dust layer about 2 - 3 cm thick at the surface. During the warm lunar day heat is transferred more effectively into the lunar surface than it can be transferred out during the cold lunar night. To conserve net flux over a lunation, a mean temperature gradient is established, mainly confined to the porous surface layer. A similar phenomenon was observed at the Apollo 15 site, where a mean temperature rise of 45K was measured between the surface and the top probe sensor.

(The value of 35K reported earlier (ref. 10 has been revised to include the effect of the occlusion of the early morning sun at Hadley Rille due to local topography as well as refinements in the thermocouple-to-surface temperature reduction calculation.) The total rise in mean temperature actually takes place almost entirely over the first few centimeters.

The temperature dependence of the diurnal heat transfer in the near surface layer can be examined quantitatively by postulating an effective thermal conductivity which is a function of temperature:

$$k(T) = k_c + k_r \cdot T^3 \qquad \text{(Eq. 16)}$$

The functional form of / equation 16 has been verified experimentally for silicate powders in vacuum (ref.26). Cremers and Birkebak have also found the conductivity of returned lunar fines to fit a functional relationship of the form of equation 16(ref.27). The parameter R_{350} which equals $K_r \cdot 350^3/K_c$ first used by Linsky in examining this phenomenon (ref.28),represents a measure of the radiative contribution to the heat transfer in the upper few centimeters. By using one-dimensional models of the lunar regolith, one finds that R_{350} must be within the range 1.7 - 2.2 for the Apollo 17 site and between 2.5 and 3.0 for the Apollo 15 site to produce the observed mean temperature gradients. The range of values for the Apollo 17 site correspond closely to the value of 1.48 obtained by Cremers and Birkebak for returned Apollo 12 samples (ref. 27). Similar measurements on Apollo 11 samples yielded R_{350} values approximately equal to 0.5. It is important to note, however, that even very slight disturbances to the in situ configuration of the porous lunar fines

may have large effects on their thermal properties. In any case, the fact that a large mean temperature gradient has been observed at both lunar heat flow sites, separated by 700 km , strongly indicates that a porous layer in which radiative heat transfer plays a dominant role is a prevalent feature of the lunar surface, at least in the mare regions.

It is fortunate that our more accurate surface temperature determinations are made during the lunar night for it is the post-sunset surface cool-down data which is most strongly constrained by the thermal properties within the top 5 - 10 cm of the surface. Figure 10 shows on expanded scale the reduced lunar surface nighttime temperatures at the Apollo 15 and Apollo 17 sites. The solid curves represent best fitting computer models of the thermal properties of the upper 15 cm of regolith at each site. The density and mean conductivity profiles used to produce the theoretical curves are shown in the inset figure. (Mean conductivity is the effective conductivity at a given depth at the mean temperature of that depth.) The density profile used for the Apollo 15 site is based on inferences drawn from drill core penetration rates and surface disturbance due to astronaut activity reported by J. Mitchell (personal communication) of the Apollo 15 soil mechanics team. The density profile for the Apollo 17 site was determined from preliminary examination of returned core tube samples (D. Carrier, personal communication). In both the Apollo 15 and 17 models the heat capacity as a function of temperature was taken from Robie et al. (ref. 29) data on returned Apollo 11 samples. In both models, a low conductivity layer of about 2 cm thickness is required to fit the steep drop in surface temperature

immediately following sunset. The Apollo 15 model then requires a steep, but not discontinuous, rise in conductivity with depth down to 5 cm to produce the increased flattening of the cool-down curve through the lunar night. The Apollo 17 model, however, requires a very sharp rise in conductivity at a depth of about 2 cm to produce the abrupt flattening of the cool-down curve at about 190° phase angle. The subsequent increase in conductivity with depth is slight enough so that the Apollo 17 model may be considered essentially a 2-layer model. The large jump in conductivity at 2 cm is also supported by the preliminary density profile which indicates a fairly high density quite close to the surface. The Apollo 15 density profile, on the other hand, supports the possibility that a substantial conductivity gradient exists over the upper 30 cm of the regolith.

It is important to emphasize that the most critical surface temperature data required for the purpose of determining thermal regolith profiles is that during the 10 - 30 hours immediately following sunset. Surface temperature data during this period have been the most difficult to obtain from remote infrared brightness scans. The level and steepness of the cool-down data immediately following sunset is controlled almost entirely by the thermal properties of the upper 2 cm. If the very early nighttime data is not sufficiently accurate to constrain the thermal properties of the upper 2 - 3 cm of dust layer within $\pm$30%, then subsequent attempts to determine deeper conductivity values unambiguously from the flattened part of the cool-down curve will not be possible. For example, the broken line curve of figure 10 fits the nighttime data after 192° phase well within the error bands of the data. However,

discrepancies in the early post-sunset fit produced by different conductivities within the upper 2 cm lead to discrepancies up to a factor of 2 in conductivity determinations for depths below 2 cm. (See curve 17a in inset of fig. 10.)

CONCLUSIONS

With this last Apollo mission two heat flow measurements have been successfully made on the lunar surface. Both measurement sites are in similar regional settings in the northeast quadrant of the Moon. Taurus Littrow and Hadley Rille sites are located in embayments in the mountainous rims of the Imbrium and Serenitatis mascon basins which have been flooded by mare-type basalts.

Surface brightness temperatures were calculated from the temperature of thermocouples suspended several centimeters above the lunar surface. The mean surface temperature at Hadley Rille throughout a lunation cycle is 207 K. The mean temperature increases with depth very rapidly in the upper few centimeters and is about 252 K at a depth of 90 cm. The main reason for this increase of 45 K is the predominant role of radiative heat transfer in the loosely packed upper layer. During the lunar night the surface temperature at Hadley Rille falls to 93 K. From the cool-down history after sunset we have deduced that the upper 2 cm of the regolith is characterized by a conductivity of 1.5×10^{-5} W/cm-°K. Below this depth the conductivity increases rapidly and probably in a continuous manner until it reaches values of about 1.5×10^{-4} W/cm°K at depths where the probes are emplaced.

At Taurus Littrow the mean surface temperature is 216 K and, as in the case of Hadley Rille, increases a few tens of degrees in the upper 2 cm so that at a depth of 67 cm a mean temperature of 254 K is measured. The minimum temperature just before lunar dawn is 103 K, 10°K higher than Hadley Rille. This higher temperature is primarily due to the existence of a relatively high conductivity layer at a depth 2 cm below the surface. From the point of view of thermal properties the regolith at Taurus Littrow can be described as two layers: an upper 2 cm loosely-packed layer of very low conductivity(1.5×10^{-5} W/cm-K) in which heat transfer by radiation predominates and a lower layer with much higher conductivity (>1.2×10^{-4} W/cm-K) and higher density (1.8 - 2.0 gm/cm^3).

Subsurface temperature and conductivity measurements at depths below 90 cm, where the large diurnal variations are negligibly small, indicate a steady state heat flow through the surface at Hadley Rille of 3.1×10^{-6} W/cm^2 and 2.8×10^{-6} W/cm^2 at Taurus Littrow with an estimated error of $\pm$20%. These fluxes are deduced from average temperature gradients in the regolith between 1.3 and 1.7 K/m and an average conductivity in the range 1.7×10^{-4} to 2.0×10^{-4} W/cm-K. Conductivity generally increases with depth in the regolith although some layering, with high conductivity materials overlying lower conductivity materials, is found at both sites (see Table 6). A conductivity value of nearly 3×10^{-4} W/cm-K was measured at the bottom of probe #1 at the Apollo 17 site. Thermal gradients decrease with depth in some cases in response to the increase in conductivity. At Taurus Littrow probe site #2 a large decrease in gradient with depth is possibly attributable to a large subsurface boulder in close proximity to the probe.

The heat flows at both sites are to some extent affected by local topography. Preliminary estimates indicate a correction of -15 to -25% may be applicable to the Taurus Littrow values as a result of the adjacent massifs. However, a more refined analysis is required.

The heat flow measured at the two sites is approximately 1/2 of the Earth's average heat flow (6.3×10^{-6} W/cm^2). If these two values are representative of the Moon as a whole, then a heat flow of 1/2 the Earth's requires a heat production per unit mass for the Moon's interior over twice that of the Earth. This statement assumes both planetary bodies are near steady state so that total surface heat loss is nearly equal to the present interior heat production.

Since the long-lived radio isotopes of ^{40}K, ^{235}U, ^{238}U and ^{232}Th are the principal source of heat in the Earth and Moon, the heat flow results imply a two to three fold enrichment of uranium in the Moon relative to the Earth. Lunar samples show that the abundance of potassium relative to uranium is 1/3 to 1/4 that of the Earth so that in the Moon uranium is the main contributor to internal heating. These isotopes must be concentrated in the outer 100 to 200 km of the Moon to avoid extensive melting at shallow depth at present.

Re-interpretation of Earth-based measurements of microwave brightness temperatures using the new data on regolith thermal and electrical properties will be important in determining the representativeness of the in situ lunar heat flow measurements. Further more-refined microwave observations of the Moon, especially narrower beamed measurements over discrete portions of the lunar disc, would be valuable in determining possible variations of heat flow over the lunar surface.

ACKNOWLEDGMENTS

The development of the Heat Flow Experiment and research at Columbia University was supported by NASA contract NAS 9-6037. The development and testing of instrumentation was carried out by Bendix Aerospace Systems Division assisted in many essential areas by Arthur D. Little, Inc., Gulton Industries Inc. and the Rosemount Engineering Company. The Lunar Surface Drill was developed by the Martin Marietta Corporation. We wish to thank Kenneth Peters for help in much of the numerical analysis. Dr. Robert Jastrow granted generous use of the Goddard Institute for Space Studies' computer facility. The encouragement and advice of Maurice Ewing, Sydney Clark and Alfred Wechsler are gratefully acknowledged.

REFERENCES

1. Lee, W. H. K. and S. Uyeda, Chapter 6: Review of Heat Flow Data, in Terrestrial Heat Flow, W. H. K. Lee, Ed., 1965, Geophys. Monograph #8, American Geophysical Union, pp. 68-190.
2. Urey, H. C., Proceedings National Academy of Science, U. S. 42, 1956, p. 889.
3. Gast, P. W., Limitations on the Composition of the Upper Mantle, J. Geophys. Res., Vol. 65, 1960, pp. 1287-1297.
4. Wasserburg, G. J., G. J. F. MacDonald, F. Hoyle and W. A. Fowler, Relative Contributions of Uranium, Thorium and Potassium to Heat Production in the Earth, Science, Vol. 143, 1964, pp. 465-467.
5. Langseth, Jr., M. G., and R. P. Von Herzen, Chapter 9: Heat Flow through the Floor of the World Oceans, in The Sea, Vol. 4, Part 1, A. E. Maxwell, Ed., 1971, pp. 299-352.
6. Latham, G. V., M. Ewing, F. Press, G. Sutton, J. Dorman, Y. Nakamura, N. Toksoz, D. Lammlein, F. Duennebier, Section 9: Passive Seismic Experiment, Apollo 16 Preliminary Science Report, NASA SP-315, 1972, pp. 9-1 - 9-29.
7. Baldwin, J. E., Thermal Radiation from the Moon and the Heat Flow through the Lunar Surface, Royal Astronomical Society Monthly Notice 122, 1961, pp. 513-522.
8. Krotikov, V. D. and V. S. Troitskii, Detecting Heat Flow from the Moon, Soviet Astronomy, Vol. 7, No. 6, 1964, pp. 822-826.
9. Tikhonova, T. V. and V. S. Troitskii, Effect of Heat from within the Moon on its Radio Emission for the Case of Lunar Properties which Vary with Depth, Soviet Astronomy, Vol. 13, No. 1, 1969, pp. 120-128.

10. Langseth, Jr., M. G., S. P. Clark, Jr., J. L. Chute, Jr., S. J. Keihm and A. E. Wechsler, Section 11: Heat-Flow Experiment, Apollo 15 Preliminary Science Report, 1972, pp. 11-1 - 11-22.

11. Smith, B. D., The Lunar Heat Flow Experiment, Bendix Technical Journal Vol. 4, No. 2, 1971, pp. 64 - 79.

12. Langseth, Jr., M. G., E. M. Drake, D. Nathanson and J. A. Fountain, Chapter 2c: Development of an In Situ Thermal Conductivity Measurement for the Lunar Heat Flow Experiment, in Thermal Characteristics of the Moon, John W. Lucas, Ed., AIAA Progress in Astronautics and Aeronautics Series, Vol. 28, 1972, The MIT Press, Cambridge, pp.169-204.

13. Jaeger, J. C., Conduction of Heat in an Infinite Region Bounded Internally by a Circular Cylinder of a Perfect Conductor, Australian J. Phys., Vol. 9, 1956, pp. 167 - 179.

14. Keihm, S. J., J. L. Chute, K. Peters and M. G. Langseth, Jr., Apollo 15 Measurement of Lunar Surface Brightness Temperatures: Thermal Conductivity of the Upper 1 - 1/2 Meters of Regolith, Earth and Planetary Science Letters, (publication date to be known soon).

15. Horai, K., G. Simmons, H. Kanamori, D. Wones, Thermal Diffisivity and Conductivity of Lunar Material, Science, Vol. 167, No. 3918, 1970, p. 730.

16. Buhl, D., W. J. Welch and D. G. Rea, Anomalous Cooling of a Cratered Lunar Surface, J. Geophys. Res., Vol. 73, No. 24, 1968, pp. 7593 - 7608.

17. Lachenbruch, A. H., Rapid Estimation of the Topographic Disturbance to Superficial Thermal Gradients, Rev. Geophys., Vol. 6, No. 3, 1968, pp. 365 - 400.

18. Metzger, A. E., J. I. Trombka, L. E. Peterson, R. C. Reedy and J. R. Arnold, Lunar Surface Radioactivity: Preliminary Results of the Apollo 15 and Apollo 16 Gamma-Ray Spectrometer Experiments, Science, Vol. 179, No. 4075, 1973, pp. 800 - 803.

19. Weaver, H., The Interpretation of Thermal Emissivity from the Moon, in Solar System Radio Astronomy, ed. J. Aarons, 1965, Plenum Press, New York, p. 295.

20. Gold, T., B. T. O'Leary and M. Campbell, Some Physical Properties of Apollo 12 Lunar Samples, Proceedings of the Second Lunar Science Conference, Geochemica et Cosmochemica Acta, Supplement II, Vol. 3, 1971, pp. 2173 - 2184.

21. Katsube,T. J. and L. S. Collett, Electrical Properties of Apollo 11 and Apollo 12 Lunar Samples, Proceedings of the Second Lunar Science Conference, Geochemica and Cosmochemica Acta, Supplement II, Vol. 3, 1971, pp. 2367 - 2379.

22. Strangway, D. W., W. B. Chapman, G. R. Olhoeft and J. Carnes, Electrical Properties of Lunar Soil Dependences on Frequency, Temperature and Moisture, Earth and Planetary Science Letters, Vol. 16, 1972, pp. 275 - 281.

23. Hanks, T. C. and D. L. Anderson, Origin, Evolution and Present State of the Moon,, Phys. of Earth and Planetary Interiors, Vol. 5, 1972,pp. 409-425.

24. Turcotte, D. L., A. T. Hsui, K. E. Torrance and E. R. Oxburgh, Thermal Structure of the Moon, J. Geophys. Res., Vol. 77, No. 35, 1972, pp. 6931 - 6939.

25. Hays, J. F., Radioactive Heat Sources in the Lunar Interior, Phys. Earth Plant. Interiors, Vol. 5, 1971, pp. 1 - 8.

26. Watson, K. I., Thermal Conductivity Measurements of Selected Silicate Powders in Vacuum from 150 - 350 K, II. An Interpretation of the Moon's Eclipse and Lunation Cooling Curve as Observed Through the Earth's Atmosphere from 8 - 14 Microns, Ph. D. Thesis, California Institute of Technology, Pasadena, 1964.

27. Cremers, C. J. and R. C. Birkebak, Thermal Conductivity of Fines from Apollo 12, Proceedings of the Second Lunar Science Conference, Vol. 3, 1971, MIT Press, Cambridge, pp. 2311 - 2315.

28. Linsky, J. L., Models of the Lunar Surface Including Temperature Dependent Thermal Properties, Icarus, Vol. 5, 1966, pp. 606 - 634.

29. Robie, R. A., B. S. Hemingway and W. H. Wilson, Specific Heats of Lunar Surface Materials from 90 to 350 Degrees Kelvin, Science, Vol. 167, 1970, pp. 749 - 750.

TABLE 1. HEAT FLOW EXPERIMENT TEMPERATURE MEASUREMENTS

Thermometer	Temperature Difference, K		Absolute Temperature, K	
	Range	Accuracy	Range	Accuracy
Gradient Bridge[1] (Platinum Resistance)	±2/±20	±0.001/±0.01	190-270	±0.05
Ring Bridge (Platinum Resistance)	±2	±0.002	190-270	±0.05
Cable[2] Thermocouples	-	-	70-400	±0.5
Reference Thermometer (Platinum Resistance)	-	-	253-363	±0.01

[1]Gradient-bridge temperature difference measurements are made at 2 sensitivities with a ratio of 10 to 1.

[2]The stated accuracy applies when the top gradient sensor of each probe is used as the reference thermometer, and temperature differences between the junction and the top gradient sensor are less than 10 K. About 1/2 the stated error is due to uncertainties in determining the correction for the copper/kovar junctions, which are in the thermocouple circuit.

TABLE 2: APOLLO 17 HFE SUBSURFACE TEMPERATURE DATA

TEMPERATURE DIFFERENCE MEASUREMENTS

	BRIDGE	INTERVAL (cm)	EQUIL. TEMP. DIFF.[1] (K)	CORR. TEMP. DIFF.[2] (K)	ANNUAL WAVE CORRECTION (K)
PROBE 1	DTG11	130-177	0.707	0.755	-0.027
	DTR11	139-168	0.435	0.467	-0.018
	DTG12	185-233	0.533	0.559	-0.001
	DTR12	194-224	0.322	0.326	<.001
PROBE 2	DTG21	131-178	0.370	0.390	-0.027
	DTR21	140-169	0.218	0.223	-0.018
	DTG22	186-234	0.336	0.359	-0.001
	DTR22	195-225	0.206	0.212	<.001

1 The error associated with extrapolating to equilibrium temperature differences is ± .003K.

2 The uncertainty introduced by these corrections is estimated to be ± 2%.

ABSOLUTE TEMPERATURE MEASUREMENTS

	SENSOR TYPE	DEPTH cm	EQUIL. TEMP.[3] (K)	CORR. TEMP.[4] (K)
PROBE 1	THERMOCOUPLE TC4	66	254.2	254.2
	PLATINUM RESIST.	130	255.06	255.02
	" "	139	255.19	255.17
	" "	168	255.62	255.64
	" "	177	255.76	255.78
	" "	185	255.91	255.91
	" "	194	256.03	256.04
	" "	224	256.36	256.37
	" "	233	256.44	256.47
PROBE 2	THERMOCOUPLE TC4	67	254.7	254.7
	PLATINUM RESIST.	131	256.07	256.05
	" "	140	256.09	256.09
	" "	169	256.31	256.31
	" "	178	256.44	256.44
	" "	186	256.48	256.48
	" "	195	256.52	256.51
	" "	225	256.73	256.73
	" "	234	256.82	256.84

3 The accuracy of extrapolated absolute temperatures is ±0.05 K.

4 The correction for the annual wave to be applied to the thermocouple is + 0.04 K.

TABLE 3: THERMOCOUPLE ERRORS AND CORRECTIONS

	ERROR (TC1 - TOP GRADIENT SENSOR), K	
SENSOR	LUNAR DAY	LUNAR NIGHT
TC11	+1.1	+1.9
TC21	+1.4	+2.5

	ESTIMATED CORRECTIONS*	
SENSOR	LUNAR DAY	LUNAR NIGHT
TC14	+0.4	+0.7
TC24	+0.6	+1.2

*The uncertainty in determining these corrections is estimated as $\pm$0.4°K.

TABLE 4: APOLLO 15 HFE SUBSURFACE TEMPERATURE DATA

TEMPERATURE DIFFERENCE MEASUREMENTS

PROBE 1

BRIDGE	INTERVAL cm	EQUIL. TEMP. DIFF. (K)	CORR. TEMP. DIFF. (K) 1	ANNUAL WAVE CORRECTION (K)
DTG12	91-138	0.803	0.833	-0.37
DTR12	100-129	0.484	0.479	-0.28

1 The effect of the annual wave on day 272, 1971 has been removed

ABSOLUTE TEMPERATURE MEASUREMENTS

PROBE 1

SENSOR TYPE	DEPTH (cm)	EQUIL. TEMP. (K)	CORR. TEMPERATURE (K)
PLATINUM RESISTANCE	91	252.20	252.16
" "	100	252.33	252.33
" "	129	252.81	252.81
" "	138	253.00	253.01

TABLE 5: CONDUCTIVITIES FROM COOL-DOWN HISTORIES

SENSOR DEPTH	HEATER LOCATION	CONDUCTIVITY ($W \times 10^{-4}$/cm-K) WITH DRILL HEATING EFFECTS	CONDUCTIVITY ($W \times 10^{-4}$/cm-K) WITHOUT DRILL HEATING EFFECTS
	PROBE 1		
66		1.0	-
130	H11	2.3	1.3
139		1.9	1.1
168		1.9	1.1
177	H12	2.0	1.0
185	H13	1.9	1.1
194		2.1	1.1
224		2.8	1.4
233	H14	2.7	1.6
	PROBE 2		
67		1.0	-
131	H21	2.0	1.2
140		2.0	1.1
169		2.4	1.3
178	H22	2.7	1.7
186	H23	2.9	1.7
195		2.7	1.5
225		2.8	1.5
234	H24	2.5	1.5

TABLE 6: RESULTS OF HFE CONDUCTIVITY EXPERIMENTS

APOLLO 17

HEATER LOCATION	DEPTH (cm)	CONDUCTIVITY[1] ($W \times 10^{-4}$/cm-K)	CONTACT CONDUCTANCE[2] ($W \times 10^{-4}/cm^2$-K)
		PROBE 1	
H11	130	2.50	1.4
H12	177	1.72	1.6
H13	185	1.79	1.4
H14	233	2.95	1.2
		PROBE 2	
H21	131	2.06	1.6
H22	178	2.36	1.1
H23	186	2.64	1.5
H24	234	2.24	2.3

APOLLO 15

HEATER LOCATION	DEPTH (cm)	CONDUCTIVITY ($W \times 10^{-4}$/cm-K)	CONTACT CONDUCTANCE ($W \times 10^{-4}/cm^2$-K)
		PROBE 1	
H11	35	1.41	0.8
H12	83	2.11	0.8
H13	91	1.60	0.9
H14	138	2.50	1.0
		PROBE 2	
H23	49	1.46	0.5
H24[3]	96	2.43	0.6

[1] The estimated error of conductivity measurement is $\pm$15%.

[2] Estimated error is $\pm$20%. In the theoretical model the thickness of the contact zone is 2 mm.

[3] It is very probable that a section of broken borestem lies just outside this location so that the uncertainty of this measurement is very large.

TABLE 7: HEAT FLOW DATA

DEPTH INTERVAL (cm)	TEMPERATURE GRADIENT (K/cm)	AVERAGE CONDUCTIVITY ($W \times 10^{-4}$/cm-K)	HEAT FLOW ($W \times 10^{-6}/cm^2$)
		APOLLO 17	
		PROBE 1	
66-130	0.013	1.6	2.1
130-177	0.0158	1.79	2.83
139-168	0.0163	1.72	2.80
185-233	0.0118	2.39	2.81
194-224	0.0113	2.48	2.81
66-224	0.014	1.8	2.5
		PROBE 2	
67-131	0.021	1.5	3.1
131-178	0.0082	2.26	1.86
140-169	0.0078	2.30	1.79
186-234	0.0076	2.50	1.89
195-225	0.0074	2.53	1.87
67-225	0.013	2.0	2.5
		APOLLO 15	
		PROBE 1	
91-138	0.0175	1.78	3.11
100-129	0.0166	1.68	2.82

FIGURE CAPTIONS

1. At top is a drawing of a heat flow probe. At left bottom is a simplified schematic of a typical platinum resistance bridge circuit and on the right the thermocouple circuit.
2. The geometry of the probe, borestem, contact zone and lunar regolith in the vicinity of a conductivity experiment. The dashed lines show surfaces of equal temperature rise in degrees K after the heater has been on for 36 hours. The model parameters are Km = 2.4×10^{-4} W/cm-K and $H_2 = 1.5 \times 10^{-4}$ W/cm^2-K.
3. The attenuation of the peak-to-peak amplitude of the diurnal and annual temperature with depth in the regolith is shown at the left. The δ's are the effective decay constants deeper than 20 cm. At the right the phase lag with depth is shown. The values of λ are the wavelengths of the thermal wave below 20 cm. The model used for the diurnal variation is from Apollo 17 data. See the last section of this paper. The annual curves are calculated from a Hadley Rille thermal properties model (ref. 14).
4. Temperature histories of all sensors 65 cm or deeper at probes #1 and #2. The short pulses appearing on some of the sensor traces result from heater initiation for conductivity experiments. The numbers on each curve refer to the depths below the surface. The lowermost curves on each plot are TC4 thermocouple measurements. Some representative data points from the thermocouples are shown to indicate the scatter of these measurements. Temperatures shown are calculated by subtracting TC1 values from those of TC4 and adding them to the top gradient sensor temperature. Corrections given in Table 3 have not been added.

5. Equilibrium temperatures, conductivities and heat flows measured by the Apollo 17 probes. The open circles on the conductivity plot are calculated from cool-down curves assuming maximum drilling energy and the solid circles are heater-activated experiment results. The solid line represents a layered model used for calculating heat flow. In the heat flow figure the solid lines give heat flow over the three largest intervals. The dashed line is the average heat flow between 66 and 234 cm. At the far left the geometry of the probe in the subsurface is shown.

6. Temperature rise during a conductivity experiment (solid dots) is compared with a theoretical curve derived from a model with k_m = 2.7 x 10^{-4} W/cm-K and H_2 = 1.5 x 10^{-4} W/cm^2-K. In the inset the temperature rise for times greater than 1000 minutes is shown on an expanded scale plotted against the logarithm of time. The observed data is compared with two bracketing theoretical curves. The reduced conductivity is 2.64 W/cm-K.

7. The effect of a square of material on vertical heat flow (shaded area) which has a conductivity 60 times that of the surrounding material, shown by the distortion of isotherms and flow lines. These results are based on a finite difference model computation.

8. Photograph of probe #2 borestem protruding from the lunar surface. The Heat Flow Experiment housing is in the background. The thermocouple is in the black portion of cable about 10 cm from the top of the stem.

9. Surface temperatures determined from thermocouple measu... Vertical bars are estimates of the error limits.

10. Temperatures during the lunar night at Apollo 17 (solid dots) and Apollo 15 (open circles). Vertical bars are estimated errors. The continuous curves are theoretical curves derived from the thermal property models shown in the inset.

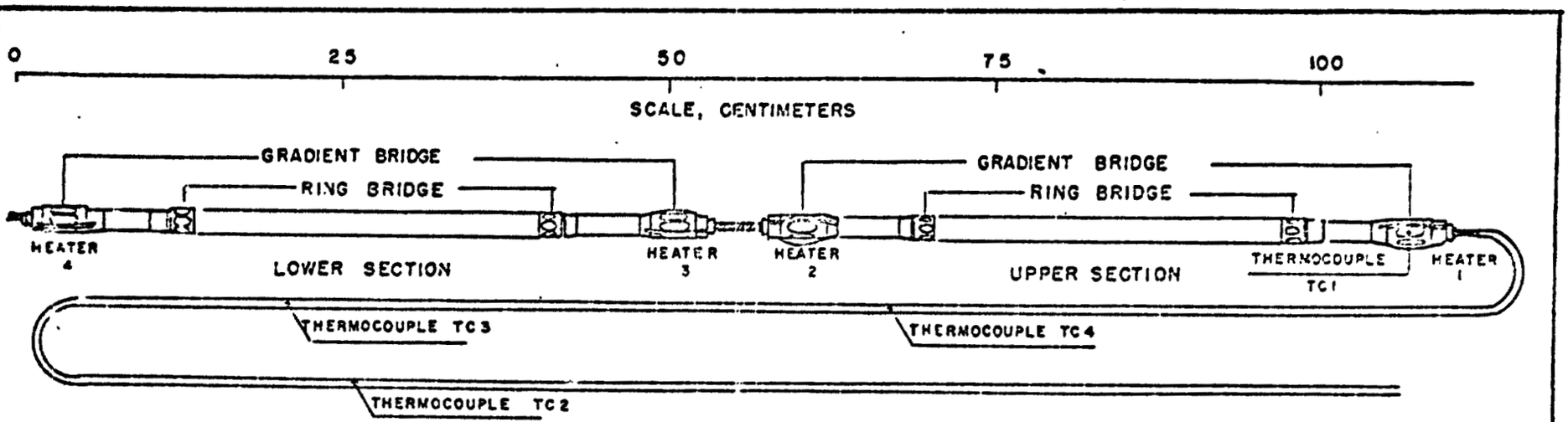

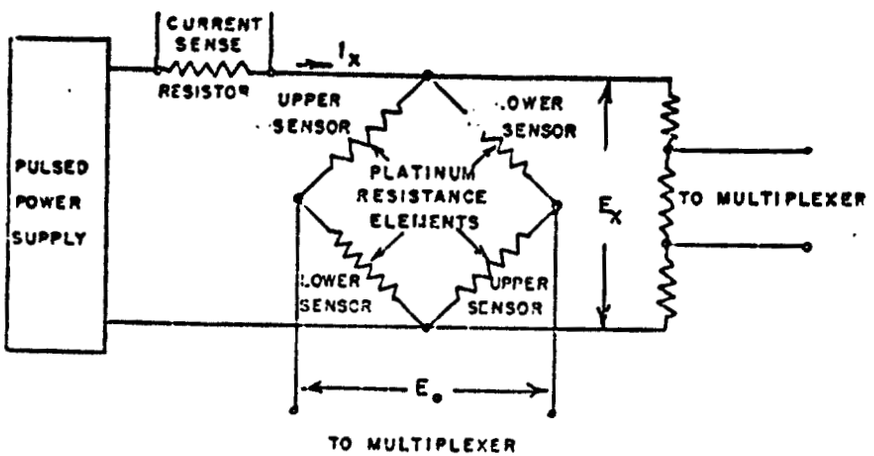

SCHEMATIC OF HFE PLATINUM RESISTANCE BRIDGE

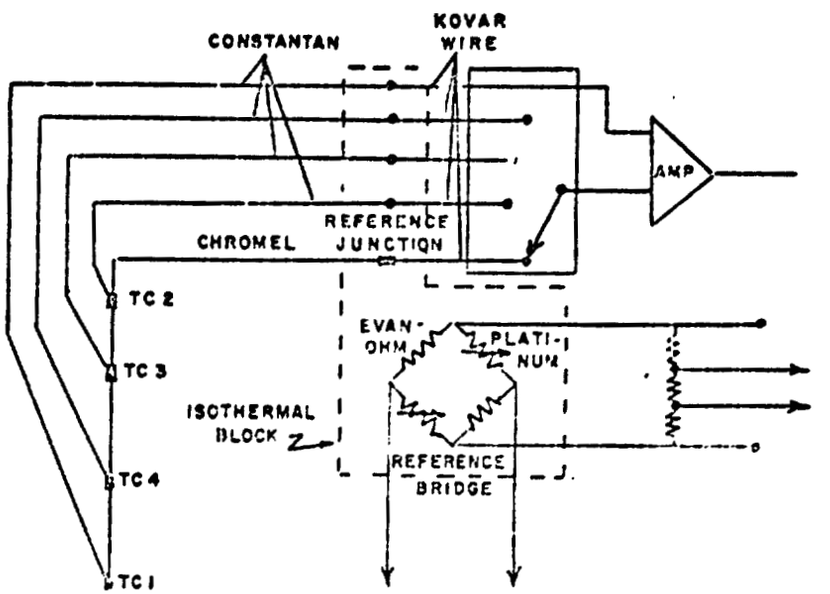

SCHEMATIC OF THERMOCOUPLE CIRCUIT

Figure 2 THE PSR Apollo 17

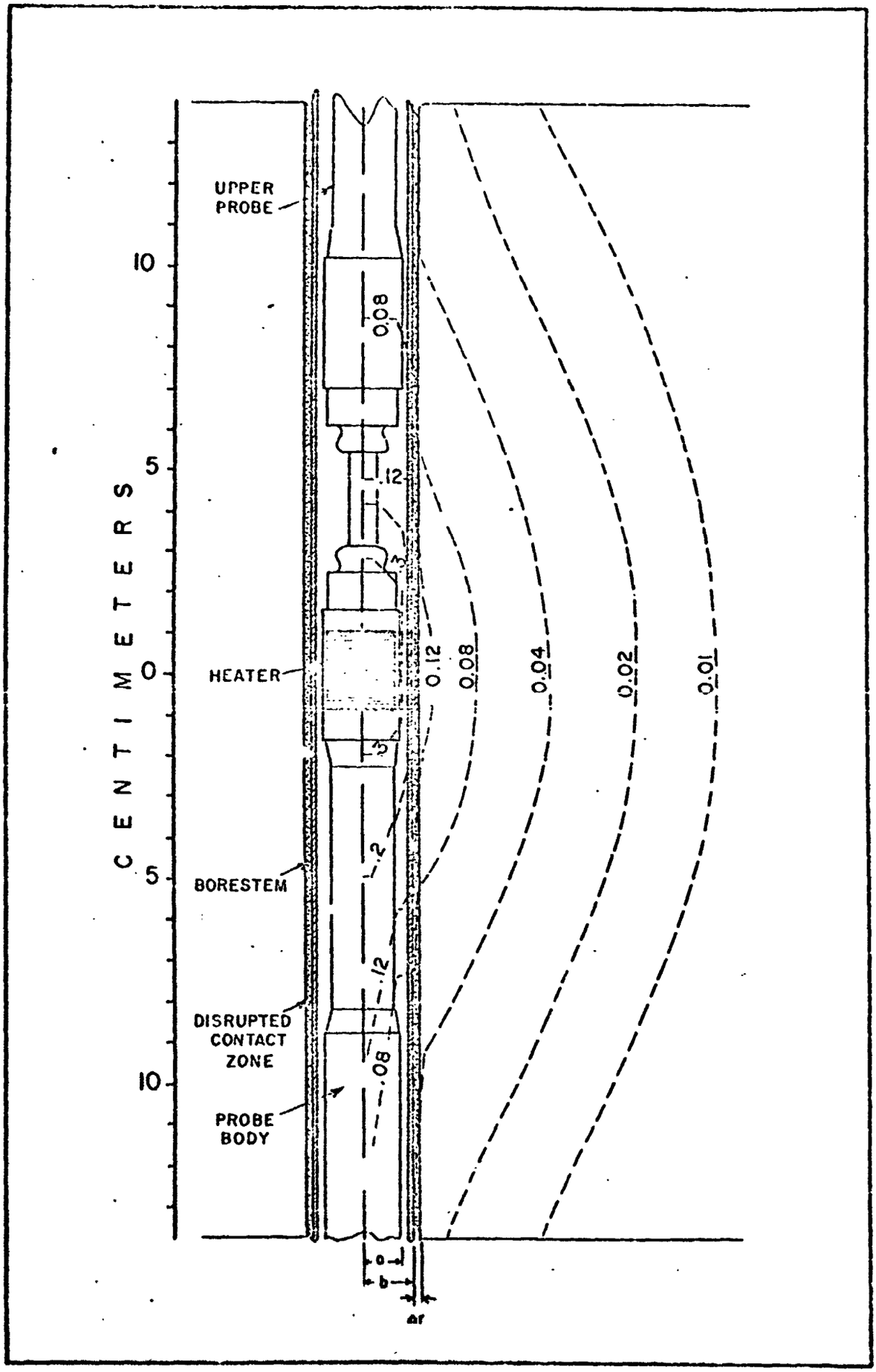

HFE
Apollo 17 PSR

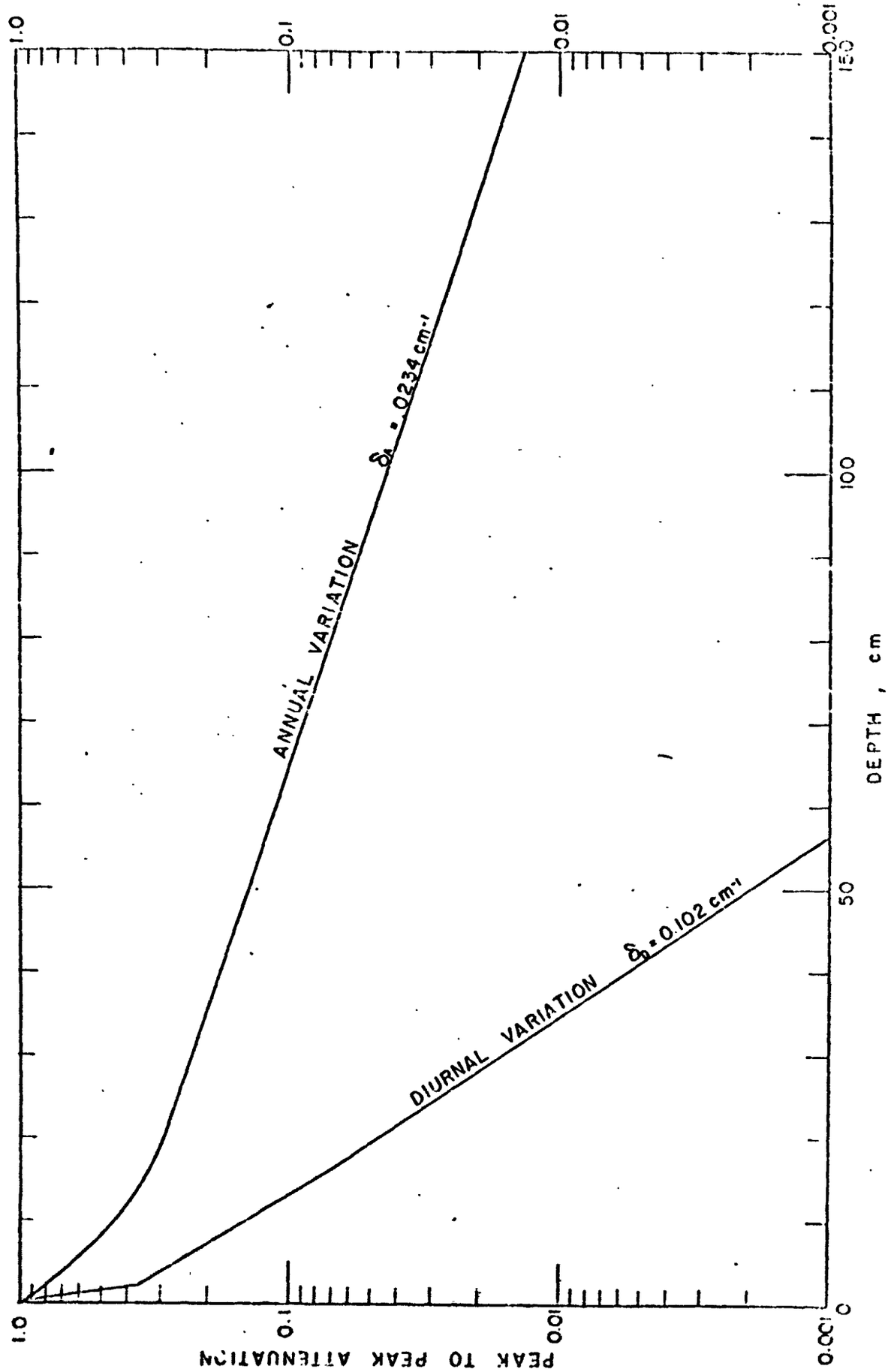

Figure 3 (rigi
HFE
Apollo 17 PSR

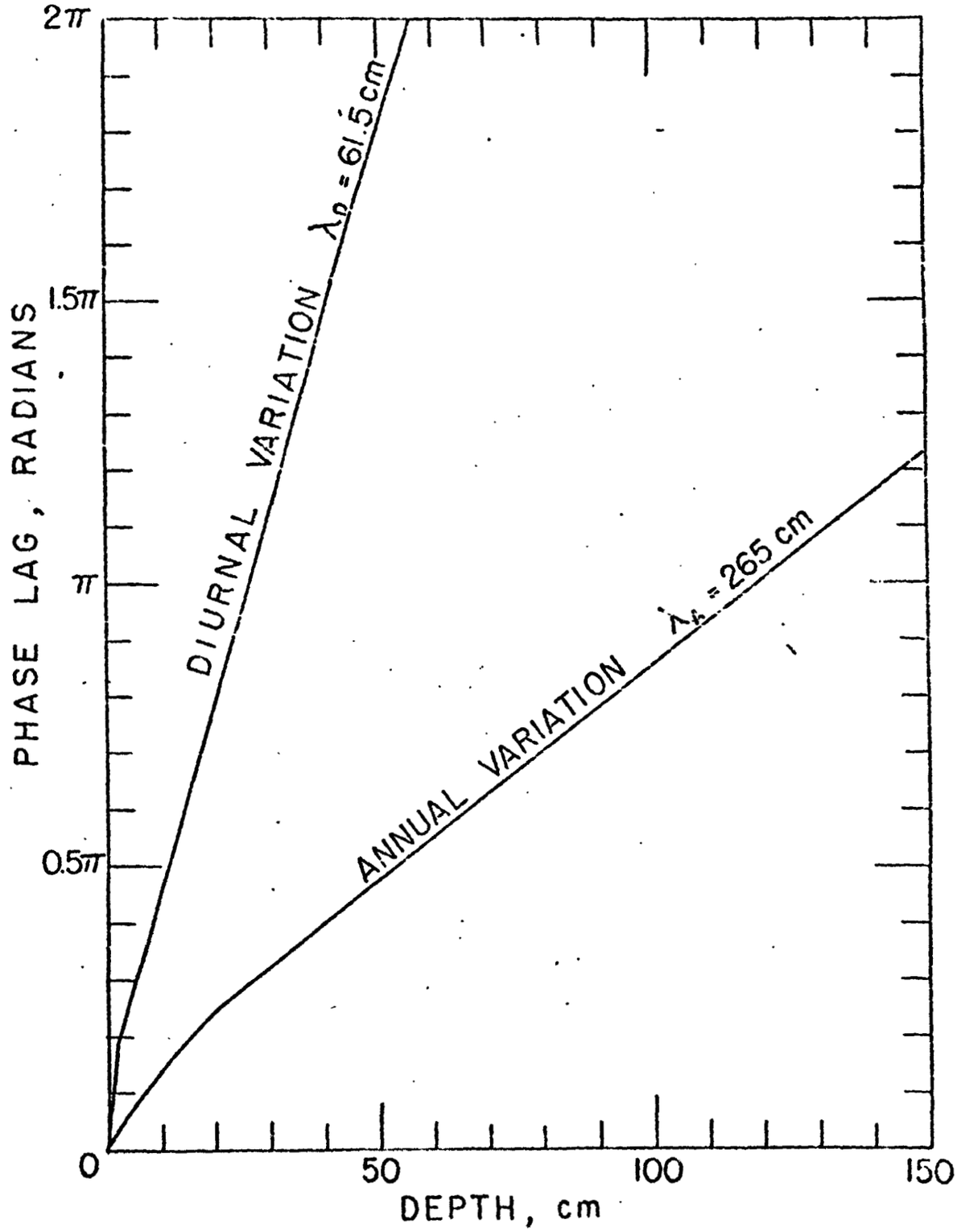

Figure 4 (top)
HFE Apollo 17 PSR

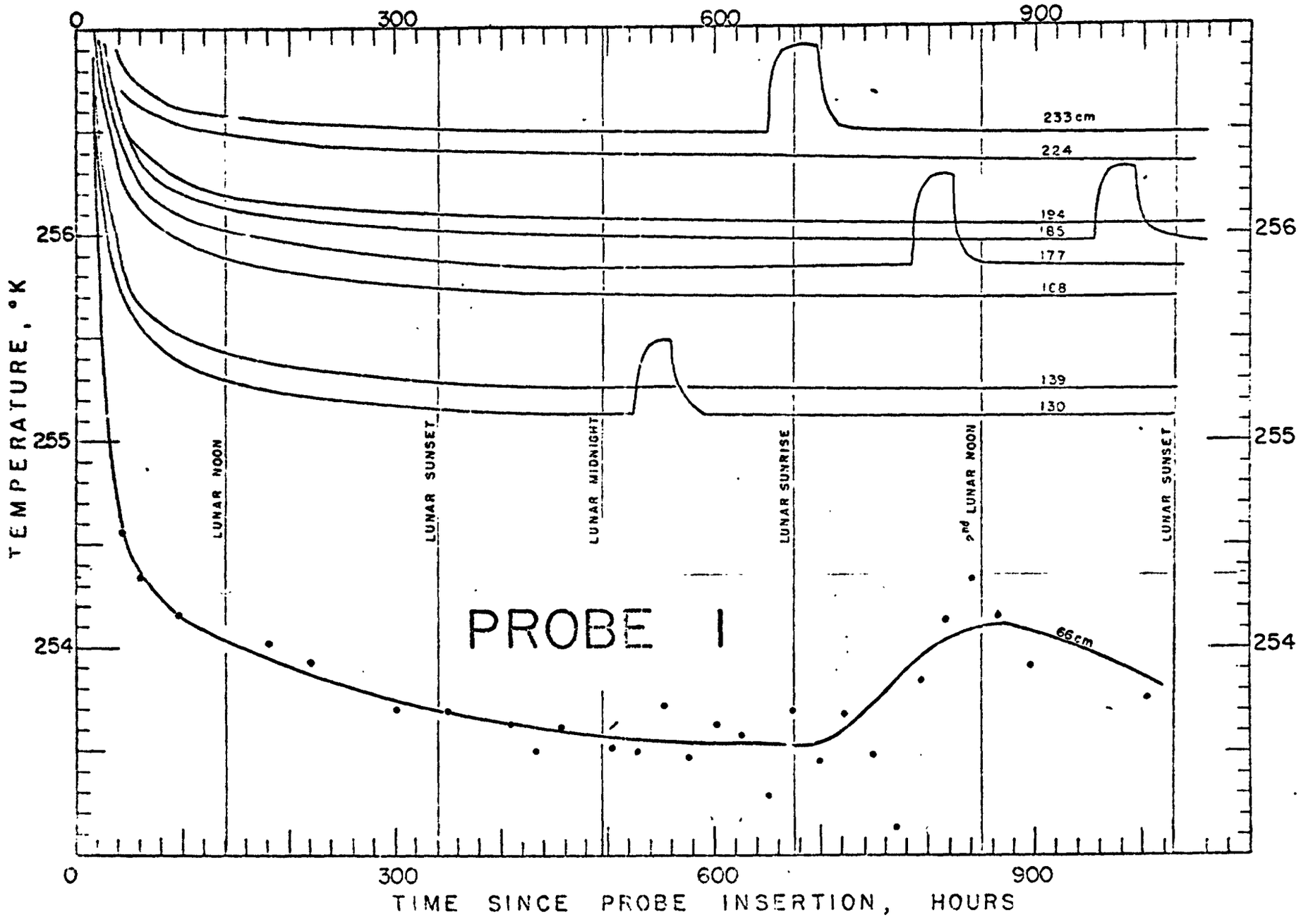

Figure 4 (bott
HFE- PSR APOLL

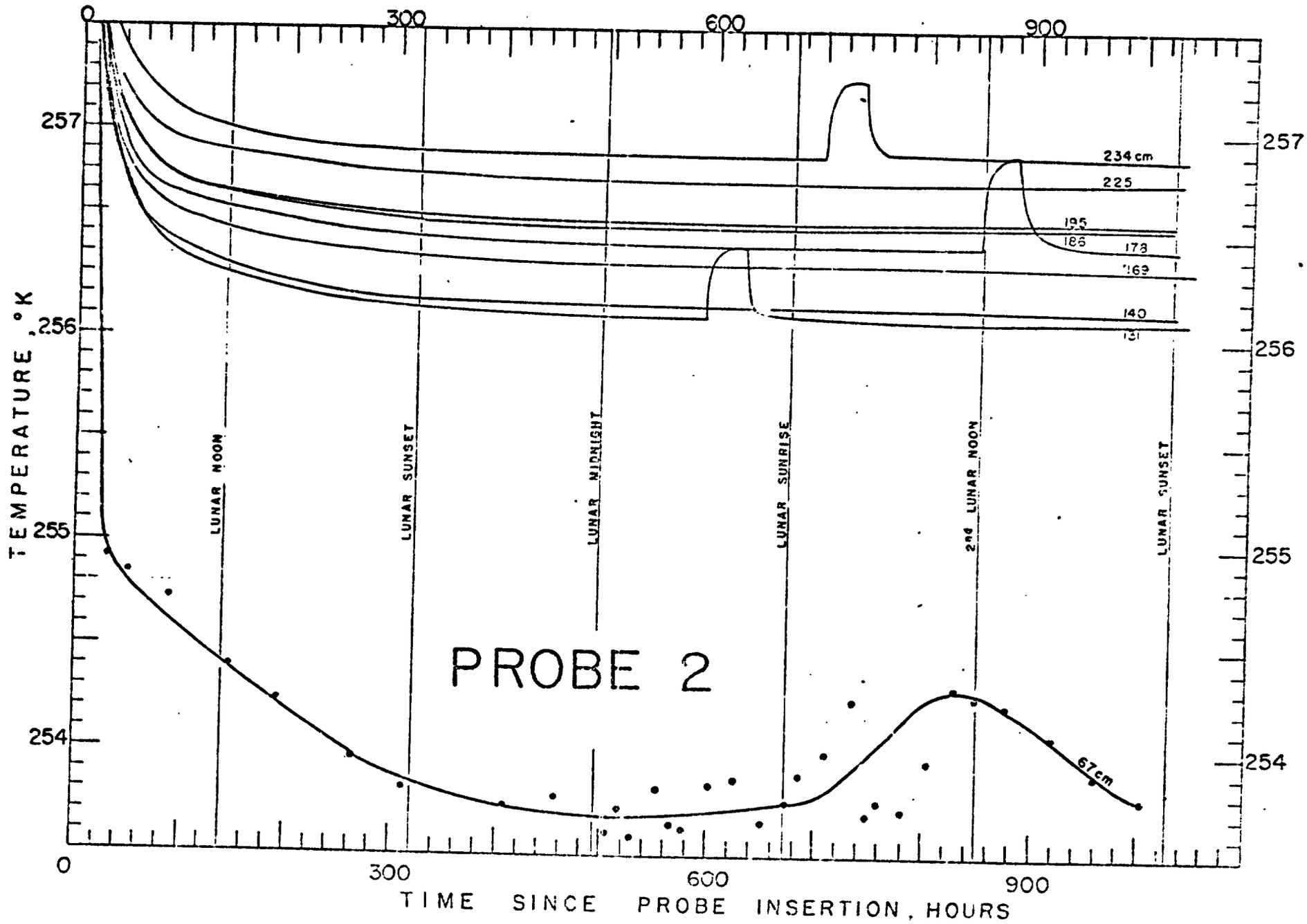

Figure 5 (top)
HFE PSR Apollo 17

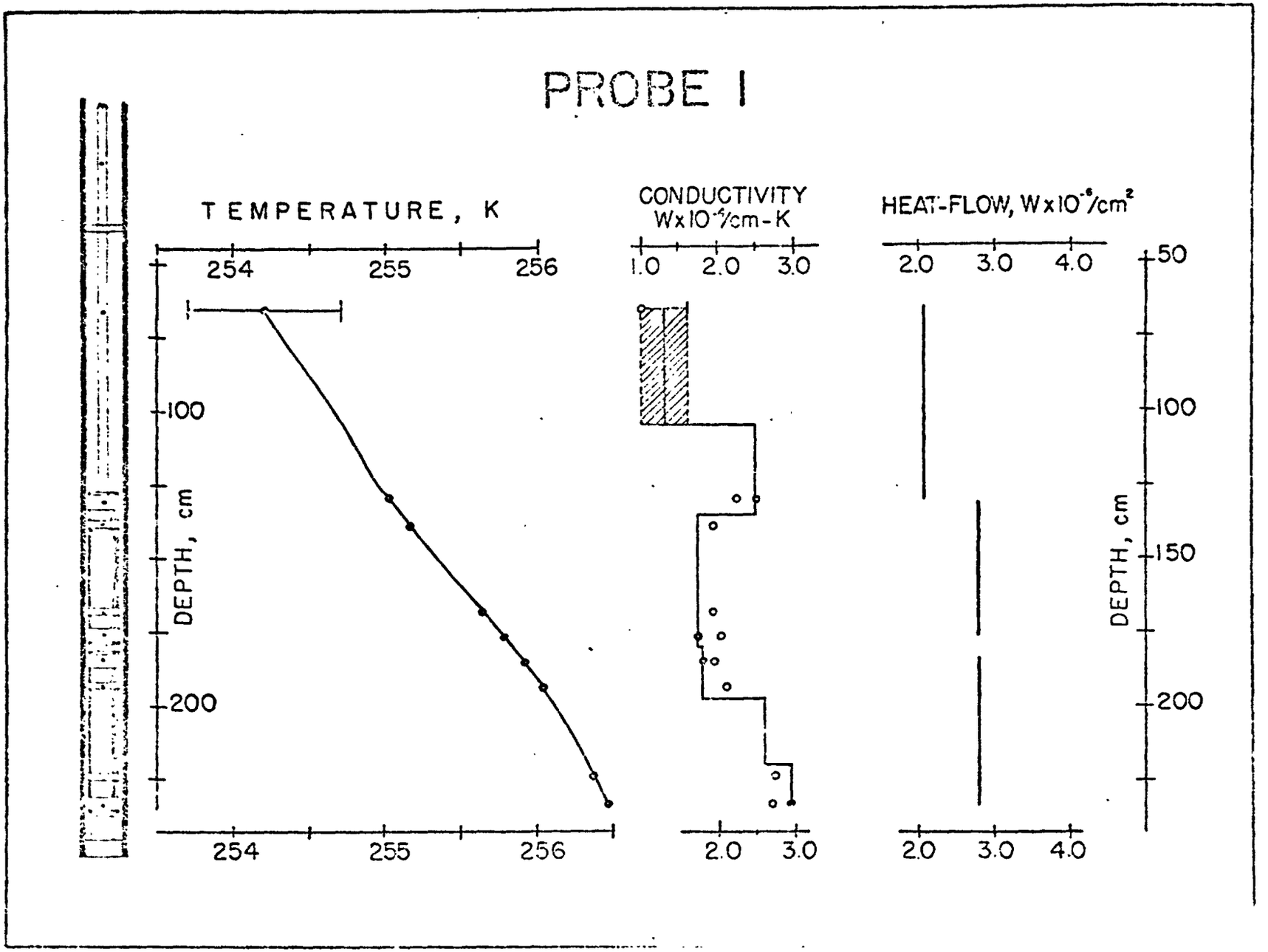

Figure 5 (bottom)
HFE PSR Apollo 17

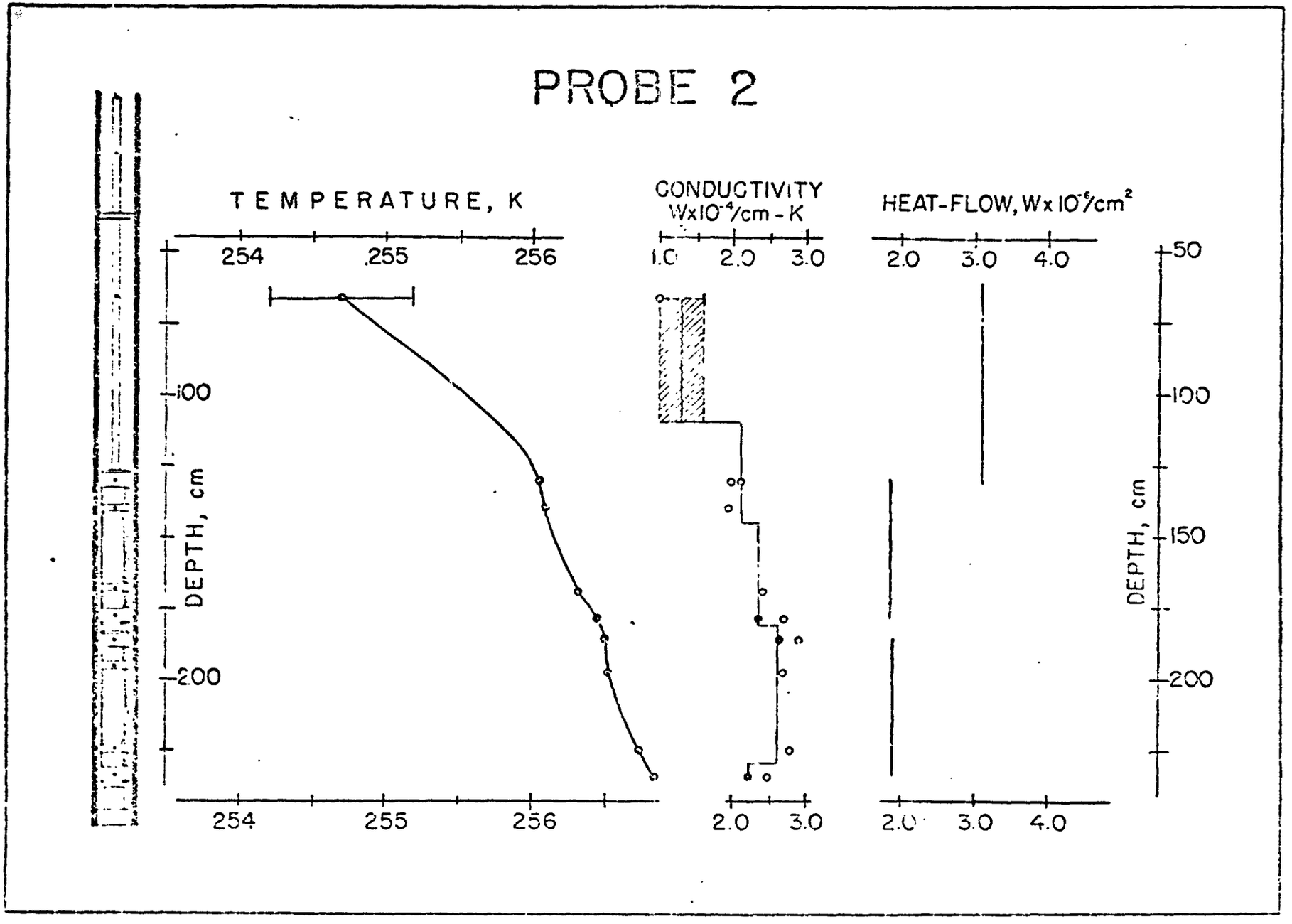

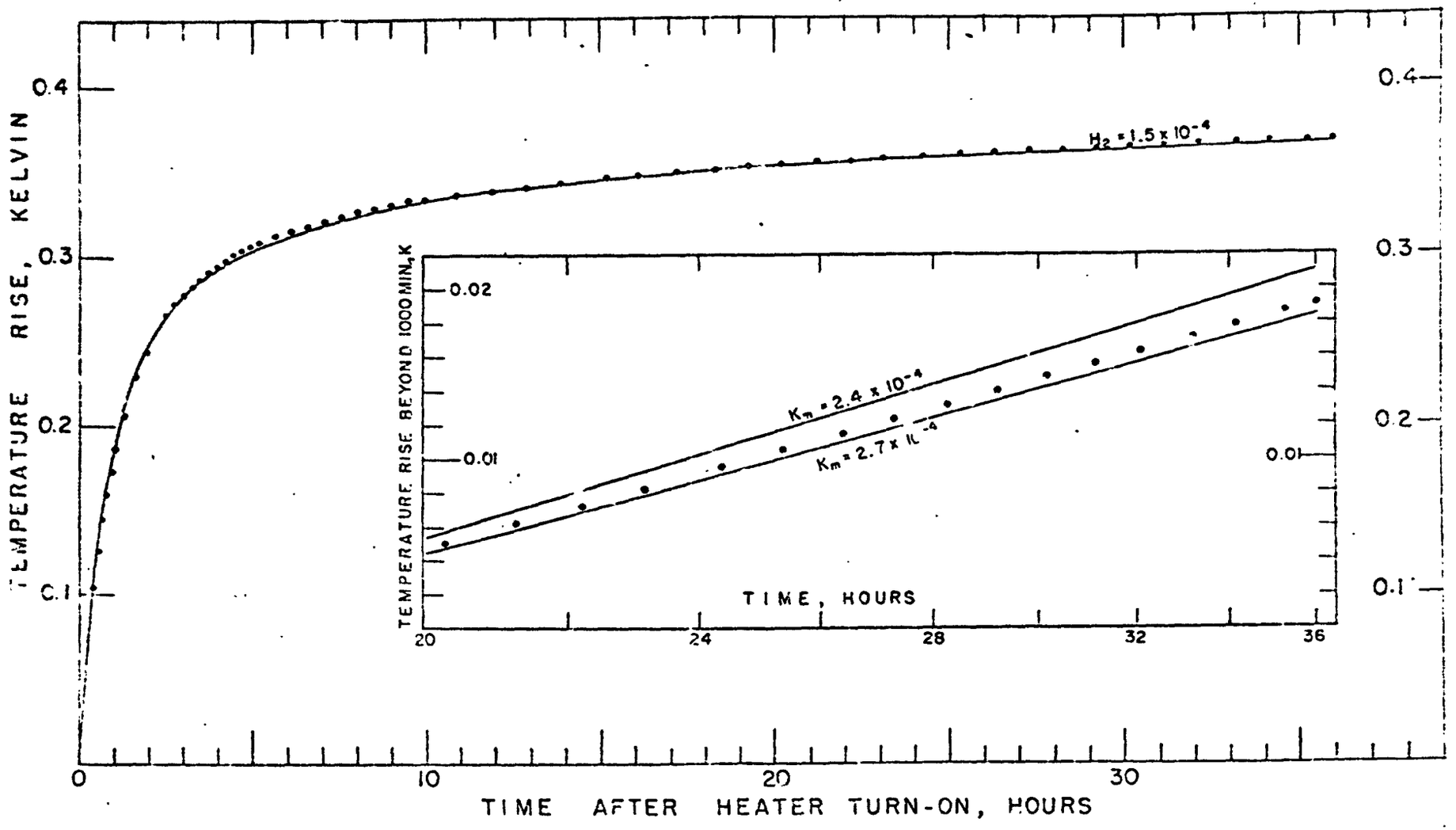
TEMPERATURE RISE, KELVIN
0.4
0.3
0.2
0.1
0
10
20
30
TIME AFTER HEATER TURN-ON, HOURS
$H_2 = 1.5 \times 10^{-4}$
TEMPERATURE RISE BEYOND 1000 MIN, K
0.02
0.01
$K_m = 2.4 \times 10^{-4}$
$K_m = 2.7 \times 10^{-4}$
TIME, HOURS
20
24
28
32
36

Figure 7
HFE PSR Apollo 17

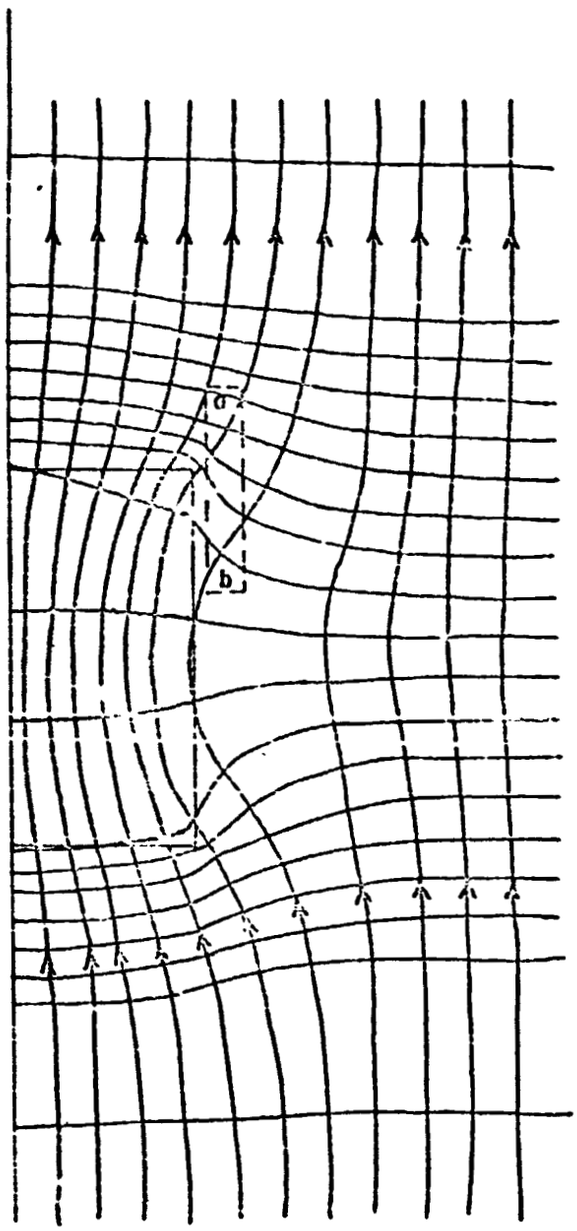

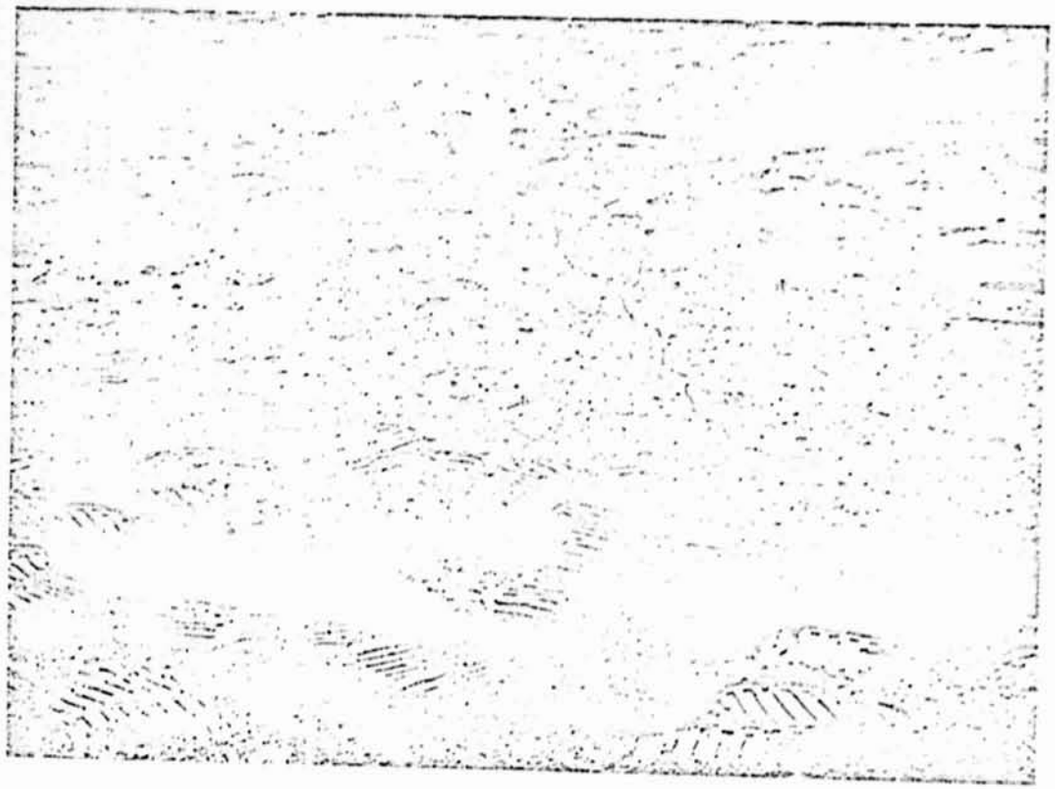

Figure 8
HFE PSR A17

Figure 9 IIFE PSR Apollo 17

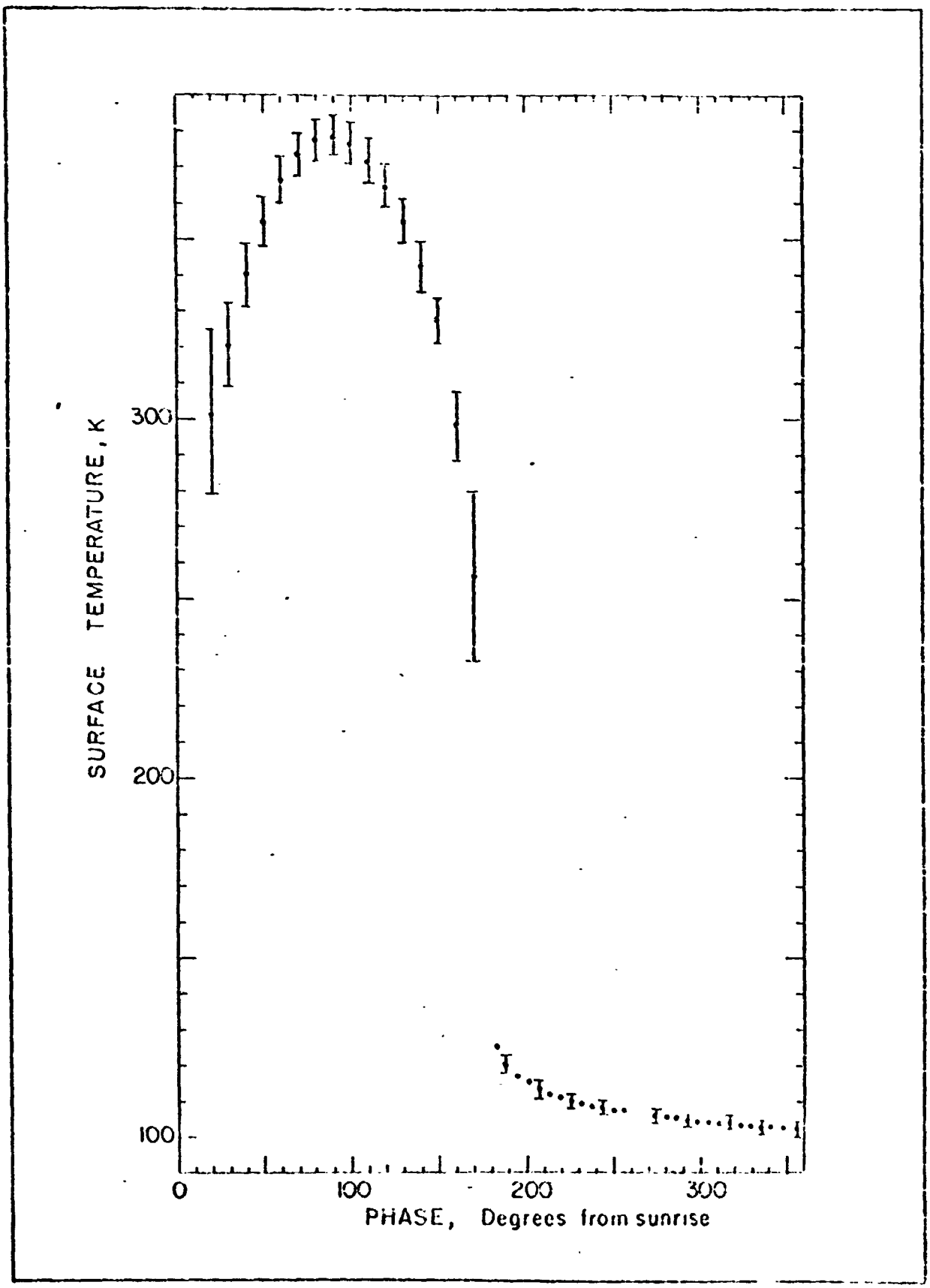

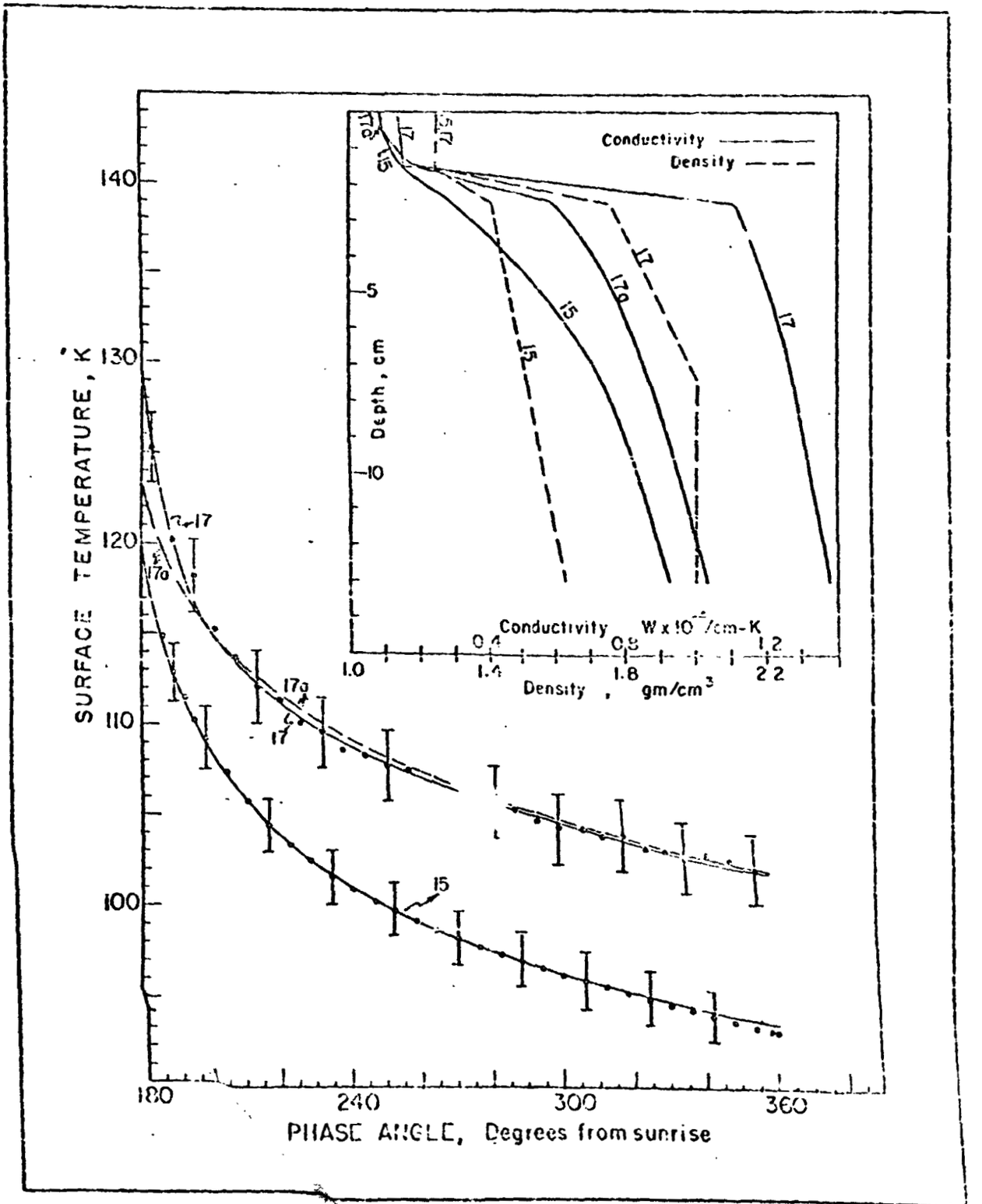
SURFACE TEMPERATURE, K
140
130
120
110
100
180
240
300
360
PHASE ANGLE, Degrees from sunrise
17a
17
15
Conductivity
Density
Depth, cm
-5
-10
Conductivity W x 10⁻⁴ /cm-K
0.4
0.8
1.2
1.0
1.4
1.8
2.2
Density, gm/cm³